MECHANISTIC MODELING OF BITUMINOUS MORTARS TO PREDICT PERFORMANCE OF ASPHALT MIXTURES CONTAINING RAP

Dissertation

submitted to and approved by the

Department of Architecture, Civil Engineering and Environmental Sciences
University of Braunschweig – Institute of Technology

and the

Department of Civil and Environmental Engineering
University of Florence

in candidacy for the degree of a
Doktor-Ingenieurin (Dr.-Ing.) /
Dottore di Ricerca in Civil and Environmental Engineering

by
Chiara Riccardi
born 05/01/1987
from Viareggio (LU), Italy

Submitted on	21.02.2017
Oral examination on	08.05.2017
Professorial advisors	Prof. Massimo Losa Prof. Michael P. Wistuba

2017

Abstract

In last decades the use of Reclaimed Asphalt Pavement (RAP) materials in asphalt mixtures has seen a significant expansion for economical and environmental reasons. Nevertheless, there are still two important issues which have not been effectively solved: the first regards the characterization of the aged binder contained in RAP; the second concerns the ability to predict the performance of asphalt mixture composed with high RAP content.

Regarding the first problem, the current methods are based on extraction and recovery of the RAP binder using solvents; however, these methods are not fully accurate since they can alter the rheological properties of the binder. For this reason, in the present work, a new procedure to back-calculate the rheological properties of the aged binder contained in RAP materials and of the blends composed with fresh and RAP binder, was developed. This is based on DSR tests performed on mortars, composed by mixing the fine fraction of the RAP aggregate with virgin binder. Using the Nielsen model, specifically adapted to asphalt mortars' case and the Voigt model, the rheological properties of RAP binder can be back-calculated from mortars tests. The present procedure has two advantages: the aged binder contained in RAP is tested as it is after the milling process, avoiding any further treatments, while the testing campaign is centered on the mortar phase, which is one of the most important phases governing the properties of the mixtures and, therefore, the performance of asphalt pavements.

Regarding the second problem, a multi-scale approach based on rheological model (2 Spring, 2 Parabolic Elements, 1 Dashpot, 2S2P1D model) and on empirical models (Hirsh e Witczak models) was developed to predict the rheological properties of asphalt mixture containing RAP materials, starting from tests on asphalt mortars and taking into account the grading of the aggregates and the volumetric composition of the mixtures.

This methodology allows to make reliable previsions for both the problems addressed, as demonstrated by the results of the validation tests carried out in this doctoral thesis. In addition, the present research provides innovative solutions to address some of the issues which are currently of particular importance for the purposes of extending the use of RAP material in the production of asphalt mixture.

Key words: RAP, mortar, blend, rheology, Nielsen model, Voigt model, 2S2P1D model, Hirsh model, Witczak model.

Abstract

Nell'ultimo ventennio si è assistito a un rapido incremento dell'utilizzo di materiale fresato nelle pavimentazioni stradali dovuto in parte al risparmio economico derivante dall'utilizzo di questo materiale e in parte ai vantaggi ambientali. Tuttavia, esistono ancora due importanti problematiche alle quali non è stata data una risposta efficace: la prima riguarda la caratterizzazione del bitume invecchiato contenuto nel fresato; la seconda riguarda la possibilità di prevedere le prestazioni delle miscele confezionate utilizzando elevate quantità di fresato.

Con riferimento alla prima problematica, i metodi attualmente disponibili sono basati sull'estrazione e sul recupero del bitume contenuto nel fresato per mezzo di solventi. Tali metodi presentano però vari problemi connessi al fatto che l'estrazione e il recupero del bitume può alterarne le proprietà reologiche. Per questo motivo, nel presente lavoro, si è sviluppata una nuova procedura che permette di eseguire un retrocalcolo delle proprietà reologiche del bitume invecchiato e dei blends, composti da bitume invecchiato e bitume vergine, partendo da test su malte composte miscelando la parte fine degli aggregati del fresato e il bitume vergine; utilizzando il modello di Nielsen, appositamente adattato al caso di materiali bituminosi, e il modello di Voigt si riesce a determinare le suddette proprietà reologiche utilizzando i risultati dei test eseguiti sulle malte. Ciò ha un duplice beneficio: da una parte è possibile caratterizzare il bitume invecchiato contenuto nel fresato nelle stesse condizioni di lavoro in cui si trova all'interno della pavimentazione, evitando che subisca ulteriori trattamenti, dall'altra si possono eseguire le prove di caratterizzazione su una delle fasi che maggiormente governano le proprietà delle miscele in conglomerato bituminoso e che quindi regolano le performance delle pavimentazioni.

Con riferimento alla seconda problematica, è stata sviluppata una procedura di modellazione multiscala, basata sia su modelli reologici (2 Spring, 2 Parabolic Elements, 1 Dashpot, 2S2P1D model) sia su modelli empirici (Hirsh e Witczak models), che permette di prevedere il comportamento reologico delle miscele in conglomerato bituminoso, contenenti materiale fresato, partendo direttamente dai risultati di prove eseguite sulle malte e tenendo conto della composizione granulometrica degli aggregati e di quella volumetrica delle miscele.

La metodologia messa a punto consente di ottenere previsioni affidabili per entrambe le problematiche affrontate, come dimostrato dai risultati delle prove di validazione eseguite nell'ambito della tesi, e di fornire una soluzione innovativa ad alcune questioni che risultano attualmente di particolare rilievo ai fini della estesa utilizzazione del fresato per il confezionamento dei conglomerati bituminosi.

Parole chiave: fresato, mortar, blend, reologia, modello di Nielsen, modello di Voigt, modello 2S2P1D, modello di Hirsh, modello di Witczak.

Abstract

In den vergangenen Jahrzehnten hat der Einsatz von Ausbauasphalt beziehungsweise Reclaimed Aspalt Pavement (RAP) in Asphaltmischgut aus ökonomischen und ökologischen Gründen eine deutliche Ausweitung erfahren. Jedoch gibt es bezüglich zwei wichtiger Aspekte, noch keine effektiven Lösungsansätze: Der erste Aspekt ist die Charakterisierung des im RAP enthaltenen gealterten Bitumens; Der zweite Aspekt betrifft die Prognose der Gebrauchseigenschaften von von Asphalt mit einem hohen Zugabeanteil von RAP.

Hinsichtlich des ersten Problems beruhen die derzeitigen Verfahren auf der Extraktion und Wiedergewinnung des RAP-Bindemittels unter Verwendung von Lösemitteln; Diese Verfahren sind jedoch nicht hinreichend genau, da sie die rheologischen Eigenschaften des Bindemittels verändern können. Aus diesem Grund wurde in der vorliegenden Arbeit ein neues Verfahren zur Rückrechnung der rheologischen Eigenschaften des in RAP-Materialien enthaltenen gealterten Bindemittels und der Verschneidung des frischen und des RAP-Bindemittels entwickelt. Dieses Verfahren basiert auf DSR-Analytik, die an Asphaltmörteln durchgeführt wurde. Die Asphaltmörtel wurden aus deraus der feinen Anteile des RAP und frischem Bindemittel zusammengesetzt. Auf Basis des Voigt-Modells in Kombination mit dem Nielsen-Modell, das speziell bezüglich der Asphaltmörteleigenschaften angepasst wurde, können die rheologischen Eigenschaften des RAP-Bindemittels aus den Ergebnissen der DSR-Analytik zurückberechnet werden. Das vorliegende Verfahren bietet zwei Vorteile: Das im RAP enthaltene gealterte Bindemittel kann direkt nach dem Fräsvorgang getestet werden ohne weitere Konditionierung. Weiterhin konzentrieren sich die Untersuchungen an der Asphaltmörtelphase, welche maßgebenden Einfluss auf die Asphaltmischguteigenschaften und den resultierenden Gebrauchseigenschaften hat.

In Bezug auf das zweite Problem wurde ein Mehrskalen Modell angewandt, das auf einem rheologischen Modell (2 Spring (Federn), 2 Parabolische Elemente, 1 Dämpfer, 2S2P1D Modell) und auf empirischen Modellen (Hirsh e Witczak Modelle) basiert, um die rheologischen Eigenschaften des Asphalts zu prognostizieren. Die Eingangsparameter des Mehrskalen Modells werden mittels DSR-Analytik am Asphaltmörtel unter Berücksichtigung der Korngrößenverteilung und der volumetrischen Zusammensetzung bestimmt.

Die Validierungsergebnisse dieser Arbeit zeigen, dass dieentwickelte Methodik eine zuverlässige Prognose der angesprochenen Aspekte ermöglicht. Darüber hinaus bieten die referierten Ergebnisse innovative Lösungsansätze , um die Verwendung von RAP in der Asphaltmischgutproduktion zu maximieren.

Schlüsselwörter: RAP, Asphaltmörtel, Rheologie, Nielsen Modell, Voigt Modell, 2S2P1D Modell, Hirsh Modell, Witczak Modell.

Acknowledgements

I would like to express my gratitude towards a number of individuals who have helped make this research possible. First, my two advisors, Prof. Massimo Losa and Prof. Michael Wistuba, which gave me the possibility to do this incredible experience that really changes my life. Thanks for guiding and supporting me during these three years, also in the tough moments.

I would like to thank Dr. Augusto Cannone Falchetto for his precious support and help.

I would like to thank Prof. Pietro Leandri and Ing. Patrizia Rocchio for their advices and encouragement during the years.

I would like to thank all the ISBS team for helping me with the huge amounts of laboratory tests, and also for their support during my stay in Braunschweig.

I would like to thank all my friends (the old and the new one) with whom I share many of the joys and challenges of these three years.

I would like to thank my family for their love, support, and constant encouragement over the years. In particular, I would like to thank my brother for always staying close to me even if he was physically far away.

Lastly, and most importantly, I would like to thank my future husband, Gaspare, for his love, support, and patience throughout this process, without which I most certainly would not have succeeded.

Finally, I would like to thank and dedicate this thesis to my mother, Giovanna. Although it has been years since you have passed, I still take your teaching and your dreams with me, every day.

Index

Chapter 1

1. Introduction

1.1 Context

In the last decades, the use of Reclaimed Asphalt Pavement (RAP) materials in asphalt mixtures has seen a significant expansion due to the increase of materials costs, and to a deeper understanding for a more environmentally oriented construction process (Kennedy et al., 1998; Holtz and Eighmy, 2000, McGraw et al., 2010; Wistuba et al., 2012; Radenberg et al., 2012, Cannone Falchetto et al., 2012). The use of RAP can increase the sustainability of asphalt pavements by reducing the use of new asphalt binder and virgin aggregates and by limiting material disposal (Hansen and Copeland, 2014).

Despite the massive use of RAP in the production of asphalt pavement, an accurate estimation of the rheological properties of the aged binder contained in RAP materials is still a challenge. In literature phenomenological and theoretical relations are available for evaluating performance of asphalt mixtures starting from binder properties. Yet, relevant problems arise when these approaches are used for RAP that are related mainly to difficulties in determining properties of the aged RAP binder.

Current methodologies used to determine properties of the RAP binder are based on the extraction and recovery method, as specified in EN 12694, EN12697 and in AASHTO T164, but many research studies (Stroup-Gardiner and Nelson, 2000; Ma and Zhang, 2008; Ma and Huang, 2008) consistently showed that this method is not accurate for many reasons: 1) it alters the binder properties; 2) the solvent extraction produces binder hardening, as shown by Kondrath, 2009 and Burr et al., 1991. Further concerns are associated to the presence of residual solvent after recovery and to the further aging of binder during the heating process. For example, researches indicated even 0.5% residual solvent could cause a 50% decrease in viscosity (Peterson et al., 2000).

These problems considering, its difficult to predict reliably mixture performance from properties of the blend of fresh and RAP binders, and, therefore, its difficult to determine the maximum percentage of RAP, without elaborate asphalt mixture testing, that can be added into a mixture without compromising its rheological and mechanical performance.

1.2 Objective

In order to overcome the limitations listed in the previous section, this thesis focuses on an analytical forward and inverse modeling with the aim of predicting RAP-modified asphalt materials performance across the different material phases. Asphalt mixture is commonly modeled as a composite material consisting of three constituents: air voids, asphalt binder and aggregate of different size and shape. In

the past and more recently, different research efforts have conventionally identified a number of phases within asphalt mixture: asphalt mastic, mortar, fine aggregate matrix (FAM). In particular, asphalt mastic contains fillers ranging from 1μm to 75μm in a binder matrix; mortar containing fine aggregate particles from 75μm to 150μm in a mastic matrix (Arshadi et al., 2014); and FAM are composed of fine aggregate particles smaller than 1.18 mm or 2.36 mm, depending on the Nominal Maximum Aggregate Size (NMAS) of the mixture (Underwood et al., 2013), in a mortar matrix. The goal of the present thesis is achieved through the possibility of experimentally measuring the properties of binders, mortars and mixtures, while avoiding extraction and recovery of the RAP binder, and by rheological modeling the interrelation between the different material phases (a detailed explanation of the methodology is presented in the following section).

This approach will be validated through a preliminary investigation of different mechanical properties for limited types of material factor-level combinations (such as particles content, binder type, RAP source, aging levels).

The research plan consists in the development of a new procedure, that is based on a multi-phase approach, for predicting the mechanical properties of asphalt mixture, such as Complex modulus E^* and phase angle δ, from those of binders and mortars; particularly, these latter are composed of a selected fine fraction of RAP (passing the 0.15 mm sieve) and fresh binder. Based on this procedure, the extraction and recovery method is avoided, and the RAP binder contained in the selected fraction of the RAP can be used directly for testing, avoiding any further type of treatment (solvent extraction, oxidation). Moreover, tests on asphalt mixtures samples that are costly and time consuming, can be avoided or considerably reduced.

The proposed procedure can be used also in the inverse mode for determining properties of binders directly from tests on mortars; by this way, existing models, specifically adapted, can be used directly to predict the mechanical properties of mixtures from binder properties avoiding the extraction and recovery of the RAP binder.

1.3 Overview of the methodology

The methodology used in the present study is summarized in the flow chart of Figure 1; letter E identifies the existing models while letter N indicates the newly proposed linking relationships between the different material phases, which are addressed in this thesis.

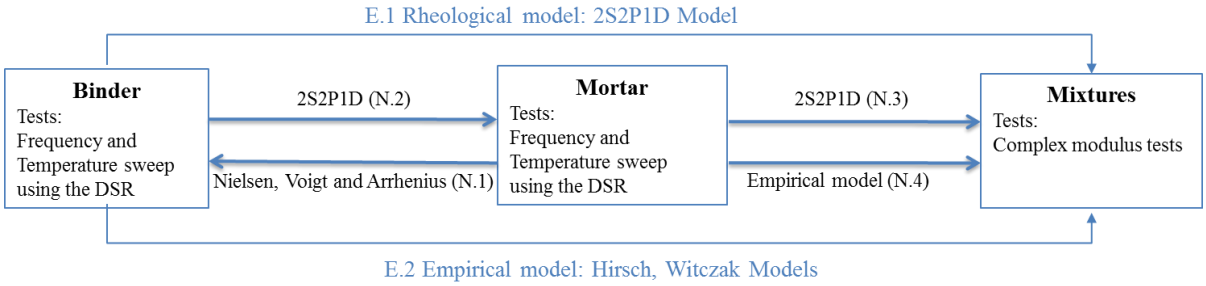

E: Existing model; N: New proposed links between the different material phases.

Fig.1 *Research methodology*

Specifically, as shown in Figure 1, two different approaches can be used to determine the mechanical properties of mixtures: one based on rheological models and one relying on empirical models.

The rheological 2S2P1D (2 Springs, 2 Parabolic elements, 1 Dashpot) model, developed by Di Benedetto et al., 2004, links the mechanical properties of mixtures to those of binders (E.1 in Figure 1). In the present study, the use of this model will be extended to the prediction of the rheological properties of mortar from those of binder and to the estimation of the response of mixture from that of mortar (link N.1, N.3 in Figure 1). At the same time, the variation of the characteristic time as function of RAP binder percentage will be analyzed, since this 2S2P1D model parameter governs the temperature dependency and representing the time needed for the system to relax. Furthermore, a link between the characteristic time of the mixture and its volumetric composition will be sought.

Two additional models, the empirical Witczak and micro-mechanical Hirsch models (E.2 in Figure 1) (Bari et al., 2006; Christensen et al., 2003), which allow predicting the complex modulus of mixtures from those of binders, will be used. In the present work, the Witczak model (Bari et al., 2006) will be calibrated in order to predict complex modulus of mixtures from those of the corresponding mortars replacing the traditional binder data input (N.3 in Figure 1).

Moreover, a new procedure for estimating binder properties by performing tests on mortar will be developed. This procedure is based on the enhancement of the Nielsen model (Lewis and Nielsen 1970, Riccardi et al., 2016), which takes into account the stiffening effect of aggregate particles at low frequencies and high temperatures, coupled with the use of the Voigt model.

1.4 Innovative Aspects

The innovative aspects introduced in the present thesis are summarized hereafter:

1. To develop a new procedure for estimating the rheological properties of RAP binder and of the bituminous blends, composed by fresh and RAP binder, from tests on asphalt mortars and

implement a new procedure to estimate the Performance Grade (PG) of these binders based on the Master curves;

2. To develop new approaches, based on the rheological properties of binders and mortars, for estimating the maximum amount or RAP that can be added into a mixture without compromising its performance;
3. To extend the 2S2P1D model to predict the mechanical properties of mortars from those of binders as well as to predict the properties of asphalt mixtures from those of mortars containing RAP materials;
4. To modify a phenomenological model in order to estimate rheological properties of asphalt mixtures containing RAP materials starting from those of asphalt mortars.

1.5 Practical application of the procedure

The procedure based on the Nielsen and Voigt models can be used to back-calculate the master curves of the bituminous blends composed with fresh and RAP binder and of the RAP binder itself. From the obtained master curves the high, intermediate and low critical temperatures can be determined and then, using the blending chart, the maximum percentage of RAP that can be added to a mixture without compromising its performance can be calculated.

On the other hand, the multiscale procedure can be used to predict the complex modulus and the phase angle of mixture containing RAP, starting from tests on the corresponding asphalt mortars. These predicted values of the mixture can be used as input in the Mechanistic-Empirical Pavement Design Guide (MEPDG) (AASHTO MEPDG-1, 2008) in order to examine the responses such as stress, strain and deflection of asphalt pavements.

The MEPDG is a pavement design and performance predicting method, developed by the National Cooperative Highway Research Program (NCHRP) in 2002, that using detailed traffic loading, material properties, and environmental data, allows to compute the pavement response and to predict the incremental damage over time.

The MEPDG was adopted as a pavement design guide by the American Association of State Highway and Transportation Officials (AASHTO) in April, 2011 and in order to use this procedure, pavement engineers need a quick, easy and accurate method for obtaining dynamic modulus value avoiding laboratory dynamic modulus tests on mixtures. In fact, these tests on mixtures requires a series of expensive sampling and testing equipment, experienced laboratory personnel, and a relative long waiting time before knowing the results. Therefore, the proposed procedure to back-calculate the dynamic modulus of mixtures composed with RAP materials, starting from tests on the corresponding asphalt mortars, is an efficiently alternative method to time consuming and costly tests on asphalt mixture.

Chapter 2

2. Literature review

The literature review is focused on some models existing in literature and that will be modified or adapted in order to achieve the specific aims of the thesis.

2.1 Existing models

E.1 2S2P1D Model

The 2S2P1D (2 Springs, 2 Parabolic elements, 1 Dashpot) is a rheological model that represents a modification of the Huet-Sayegh model (Sayegh, 1965) proposed by the research team of ENTPE/France (Olard & Di Benedetto, 2003; Olard, 2003; Di Benedetto, Olard, Sauzéat, & Delaporte, 2004; Pouget, Sauzéat, Di Benedetto, Olard, 2010; Tiouajni, Di Benedetto, Sauzéat, Pouget, 2011). It includes a linear dashpot in series with two parabolic elements and with the spring of stiffness G_∞- G_0 assembled in parallel with a second spring (G_0) (Figure 2).

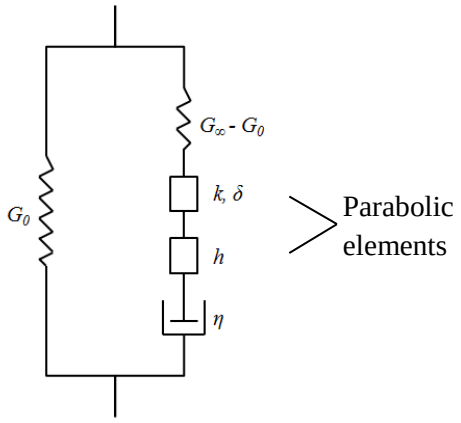

Fig.2 *2S2P1D model*

At reference temperature, the 2S2P1D model expression for complex modulus is given by:

$$G^*(i\omega\tau) = G_0 + \frac{G_\infty - G_0}{1+\delta(i\omega\tau)^{-k} + (i\omega\tau)^{-h} + (i\omega\beta\tau)^{-1}} \quad [1]$$

Where i is the complex number defined by i^2=-1; ω is the angular frequency such that ω= 2πf_r and f_r is the reduced frequency; k and h are exponents such as 0<k<h<1; δ is a constant; G_0 is the shear modulus when $\omega\rightarrow$0; G_∞ is the glassy shear modulus when $\omega\rightarrow\infty$; η is the Newtonian viscosity such

that $\eta = (G_\infty - G_0)\beta\tau$; β is a constant; τ is the characteristic time (function of temperature), based on the Time-Temperature Superposition Principle (TTSP):

$$\tau(T) = a_T \cdot \tau_0 \quad [2]$$

where a_T is the shift factor at temperature T; $\tau_0 = \tau(T_0)$ determined at the reference temperature T_0.

The shift factor at a specific temperature T, $a_T(T)$, can be obtained using the Williams-Landel-Ferry (WFL) Equation for bituminous materials:

$$\log a_t(T) = -\frac{c_1(T-T_0)}{c_2+(T-T_0)} \quad [3]$$

where C_1 and C_2 are empirical constants.

In more details, as shown in Figure 3, parameter h controls the slope at low values of G', while k governs the slope at high values of G' in the Cole- Cole diagram. δ is associated to the slope at the low temperatures/high frequencies in the master curve of the complex modulus and the height of the maximum point in the Cole- Cole diagram, while β is linked to the slope at high temperatures/low frequencies.

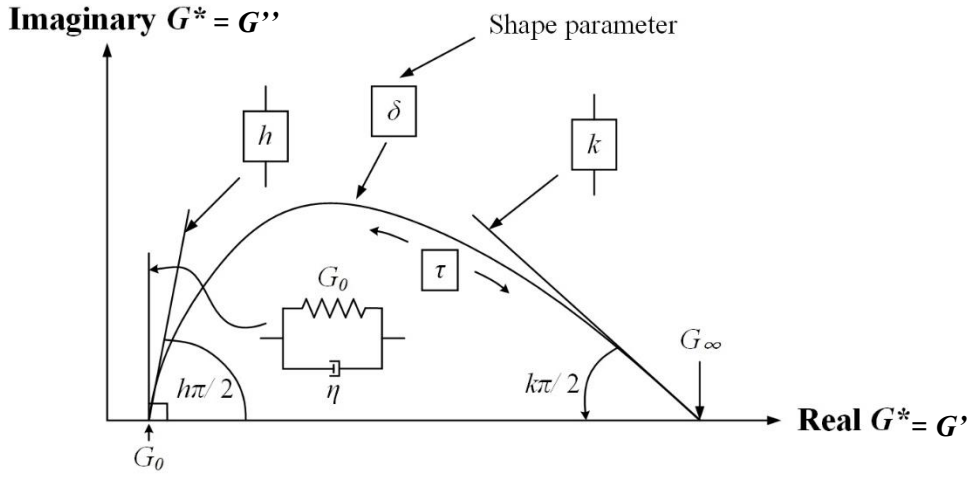

Fig. 3 *Visualization of the parameters of the 2S2P1D model.*

Therefore, seven constants (G_0, G_∞, δ, k, h, β and τ) are needed to entirely determine the linear viscoelastic behavior of a specific material at a given temperature. For asphalt binders the experimental static modulus is close to zero and can be assumed as negligible; hence, the number of constants can be reduced to six.

The great advantage of this model is that it is valid for any bituminous material (binder, mortar, mixture) and the constants δ, k, h are the same for binder and the corresponding mortars and mixtures.

In literature the relationship between binder and mixture can be found in Olard and Di Benedetto, 2003; Di Benedetto et al., 2004 through the characteristic time parameter:

$$\tau_{mix} = 10^{\alpha}\tau_{binder}(T) \quad [4]$$

where α is found by fitting the experimental results and it probably depends on mix design and ageing during mixing.

Writing Equation 1 for the binder and mixture, the following expressions are obtained:

$$G^*_{binder}(i\omega\tau_{binder}) = G_{0\,binder} + \frac{G_{\infty binder} - G_{0binder}}{1+\delta(i\omega\tau_{binder})^{-k}+(i\omega\tau_{binder})^{-h}+(i\omega\beta\tau_{binder})^{-1}} \quad [5]$$

$$G^*_{mix}(i\omega\tau_{mix}) = G_{0\,mix} + \frac{G_{\infty mix} - G_{0mix}}{1+\delta(i\omega\tau_{mix})^{-k}+(i\omega\tau_{mix})^{-h}+(i\omega\beta\tau_{mix})^{-1}} \quad [6]$$

Therefore, combining Equation 1, 5 and 6 and considering that δ, k, h, β are the same for the binder and the corresponding mixture, the following relationship between the mixture complex modulus and the binder one can be obtained:

$$G^*_{mix}(\omega, T) = G_{0mix} + (G^*_{binder}(10^{\alpha}\omega, T) - G_{obinder})\frac{G_{\infty mix} - G_{0mix}}{G_{\infty binder} - G_{0binder}} \quad [7]$$

This equation corresponds to a negative translation along the real axis, a homothetic expansion from the origin plus a positive translation of the binder curve in the Cole-Cole plane as depicted in Figure 4.

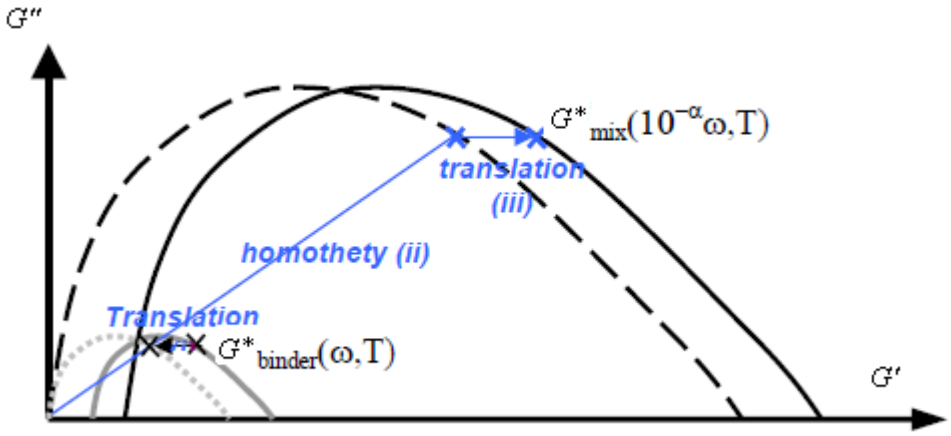

Fig.4 *Prediction of the mixture modulus from binder one in the Cole-Cole plane*

Equation 7 is known as Shift-Homothety-Shift in time-Shift (SHStS) transformation, developed by Olard & Di Benedetto, 2003; Di Benedetto et al., 2004.

E.2 Empirical Models to determine the complex modulus of mixtures from the complex modulus of binders

In literature a lot of empirical models were developed to predict the complex modulus of asphalt mixtures from the complex modulus of the binder; two of the most widely utilized and accepted models are those developed by Christensen et al., 2003 (Hirsch model) and by Bari & Witczak, 2006 under the NCHRP 1-40D project (Witczak 1-40D model). It is important to note that the performance of this type of model varies with the type of asphalt mixtures and other volumetric properties.

E.2.1 Hirsch model

The Hirsch model is a semi-empirical method to predict the asphalt mixture modulus. The effective response is obtained by assembling the different elements composing the mixture in series and in parallel as shown in Figure 5. In literature, different versions of the Hirsch model can be found; in the present work, we focus on the version of Christensen et al. 2003, that allows to predict the modulus of Hot Mix Asphalt (HMA), $|E^*|$, from the shear modulus of the binder, $|G^*|$, and from the volumetric properties of the mix as shown in Equation 8:

$$|E^*| = P_c\left[E_{agg}V_{agg} + 3|G^*|_b(V_b)\right] + (1 - P_c)\left[\frac{V_{agg}}{E_{agg}} + \frac{(1-V_{agg})^2}{3\,|G^*|_b V_b}\right]^{-1} \quad [8]$$

$$P_C = \frac{\left(20+\frac{VFA\cdot 3|G^*|_b}{VMA}\right)^{0.58}}{650+\left(\frac{VFA\cdot 3|G^*|_b}{VMA}\right)^{0.58}} \quad [9]$$

where $|E^*|$ is the dynamic modulus of the asphalt mixture (psi), E_{agg}, V_{agg} are the modulus and volume fraction of the aggregate, $|G^*|_b$, V_b are the dynamic shear modulus (psi) and the volume fraction of the binder, P_c is the contact volume and it is an empirical factor that determines the amount of parallel or series elements in the mixtures, VMA is the void content in mineral aggregates (%), VFA is the volume of voids in aggregates filled with binder (%), V_a is the air void content (%).

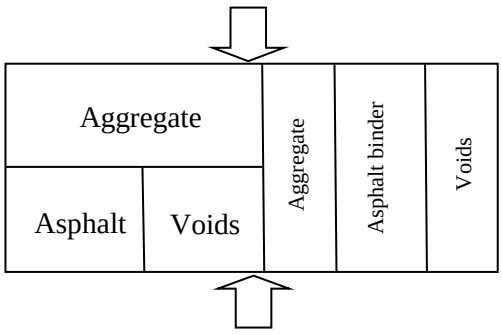

Fig.5 *Semi-Empirical Model proposed by Christensen et al., 2003.*

E.2.2 Witczak 1-40D model

The Witczak 1-40D model, expressed by Equation 10 is able to predict the asphalt mixture stiffness over a range of temperatures, loading rates, and aging conditions using the dynamic shear modulus ($|G_b^*|$) and phase angle (δ_b) of binder as input parameters.

$$\log|E^*| = -0.349 + 0.754\,|G_b^*|(6.65 - 0.032\rho_{200} + 0.0027\,(\rho_{200})^2 + 0.011\rho_4 - 0.0001(\rho_4)^2 + \\ +0.006\,\rho_{38} - 0.00014(\rho_{38})^2 - 0.08V_a - 1.06\left(\frac{V_{beff}}{V_{beff}+V_a}\right) + \\ + \frac{2.56+0.03\,V_a+0.71\left(\frac{V_{beff}}{V_{beff}+V_a}\right)+0.012\rho_{38}-0.0001(\rho_{38})^2-0.01\rho_{34}}{1+e^{(-0.7814-05785\log(|G_b^*|)+0.8834\log(\delta_b))}} \qquad [10]$$

Where $|E^*|$ is the dynamic modulus of mixture (psi), $|G_b^*|$ is the dynamic shear modulus of binder (psi), ρ_{200} is the percentage passing #200 sieve (75 μm), ρ_4 is the cumulative percentage retained on #4 sieve (4.75 mm), ρ_{38} is the cumulative percentage retained on 3/8 in sieve (9.5 mm), ρ_{34} is the cumulative percentage retained on 3/4 in sieve (19 mm), V_a are the air voids (% by volume), V_{beff} is the effective binder content, δ_b is the binder phase angle.

E.3 Nielsen model

The Nielsen model is a rheological model that takes into account the variation of the rheological behavior of a matrix due to aggregation of particles, degree of particle dispersion and particle size; it is able to predict the stiffening effect of filler considering the physical-chemical reinforcing effects.

The original formulation of the Nielsen model (Lewis and Nielsen, 1970a; 1970b), adapted to the specific case of bituminous mortars, is expressed by equation [11]:

$$\frac{G_m^*}{G_b^*} = \frac{1+A\cdot B\cdot V_p}{1-B\cdot\Psi\cdot V_p} \qquad [11]$$

Where:

G_m^* is the complex modulus of the mortar (composed by fine aggregate particles and binder);
G_b^* is the complex modulus of the binder;
V_p is the volume fraction of fine aggregate particles calculated as the ratio of the particle volume over the composite (mortar) volume in percentage.
A, B and ψ are dimensionless model parameters that are explained in detail in the following.
A is a constant that is equal to:

$$A = K_E - 1 \qquad [12]$$

Where K_E is the generalized Einstein coefficient that is an indicator of the physical chemical contribution to stiffening; it represents the stiffening rate of composites as a function of particles

addition, and by this way, it includes in the equation an interaction factor between particles and suspension (Shashidhar and Romero, 1998).

For spherical particles in dilute suspension, having a perfect interface (no slippage) between particles and matrix, K_E is 2.5 as derived by Einstein (Einstein, 1906); when K_E is 1.0, there is no bond between particles and binder. As K_E increases, there is more of a stiffening effect with the addition of particles.

The agglomeration of particles increases the Einstein coefficient; for large agglomerates with spherical particles in cubic packing, the Einstein coefficient approaches 4.77; for particles in random packing it would be 6.76.

Particles that are elongated ellipsoids or are rod like in shape also increase the Einstein coefficient. The expected value of K_E as a function of the axial ratio of the ellipsoids or rods, for the case of randomly oriented particles, such as would occur at very low rates of shear, can be found in literature (Nielsen, Landel, 1994). High rates of shear orient the rods and decrease the effective value of the Einstein coefficient (Shashidhar and Romero, 1998).

In the case of shear modulus with spherical fillers, the value of *A* for any Poisson's ratio of the matrix, ν_b, is:

$$A = \frac{7-5\nu_b}{8-10\nu_b} \quad [13]$$

B accounts for the relative moduli of particles and binder phases and it is equal to:

$$B = \frac{G_p/G_b^* - 1}{G_p/G_b^* + A} \quad [14]$$

where G_p is the modulus of particles.

The coefficient ψ in Equation [11] is given by Equation [15]:

$$\psi = 1 + \frac{1-\varphi}{\varphi^2} V_p \quad [15]$$

where φ is the maximum volumetric packing fraction. It is the maximum amount of particles that can be added to the matrix without the appearance of air voids; it denotes the volume-filling contribution to stiffening and different methods can be employed to determine its value. Some of them measure the maximum volumetric packing fraction in air. Since it is related to the voids in the compacted filler, it can be estimated by using the Rigden Voids apparatus. φ is calculated as the ratio between the true and the apparent volume of the particles. Theoretically, the maximum value of φ is 0.74 for spheres in hexagonal close packing, or 0.524 in cubic packing (Nielsen, Landel, 1994). Experimentally, particles pack randomly unless great care is taken to achieve such regular orientation. For random close packing, the theoretical value of φ is equal to 0.632 whilst the experimental one is equal to 0.63. Therefore, the maximum volumetric packing fraction varies with particle shape and state of

agglomeration. Typical values for different packing of spheres and aligned rods can be found in literature (Nielsen, Landel, 1994).

Several researchers have noted however that different fillers stiffen any binder to a different extent (Dukatz and Anderson, 1980; Anderson et al., 1982; Shashidar and Romero, 1998) and this has been a limitation to the approach of measuring the filler properties in air. Crucially, voids in the compacted filler are measured in air and do not account for interactions between the binder and the filler in the mastic. Interactions of fillers in different binder types may lead to changes in different ways. For example φ may differ in different binder as a result of different levels of dispersion of the filler, or alternatively the filler may cause changes in the viscosity of the liquid phase as a result of restructuring, physic-chemical changes or other such effects. Therefore, it would be better to estimate φ with settling test in asphalt.

By fitting Equation 11 to experimental data, the parameters A and ψ and therefore K_E and φ can be estimated.

In order to better understand the significance of K_E and φ on stiffening potential, the stiffening ratio is plotted versus the volume fraction of the particles varying φ and keeping K_E constant, as shown in Figure 6.

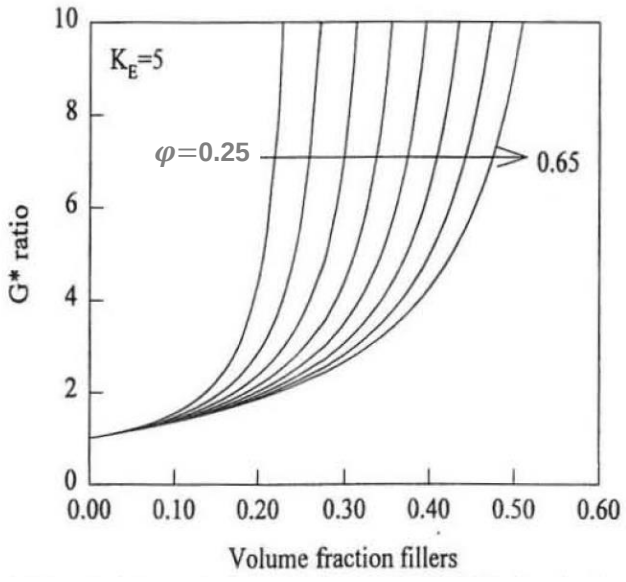

Fig.6 *Effect of variation of φ on stiffening ratio, while keeping K_E constant (Shashidhar et al.,1999).*

The parameter φ acts as a vertical asymptote to the curves. In fact, at $V_p = \varphi$ the particles touch one another. Mortar with V_p greater than φ is not possible, since under these conditions there will be three different material phases (fine particles, asphalt and air voids) and in such a case the Nielsen Model cannot be applied. On the other hand, plotting the stiffness curves varying K_E and keeping φ constant,

as shown in Figure 7, an increase of the slope of the curves as K_E increases can be observed. Thus, this parameter is an indicator of the rate of increase of stiffness with addition of filler particles.

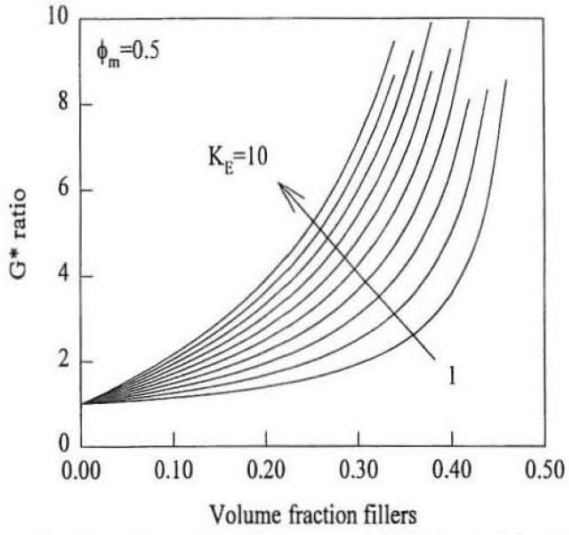

Fig.7 *Effect of variation of K_E on stiffening ratio, while keeping φ constant (Shashidhar et al., 1999).*

E.4 Voigt Model

The structure of the micro-mechanical Voigt model for a bi-phase composite material can be idealized as shown in Figure 8. The strain in each phase is the same and the equation of the model can be written as (Lakes, 2009):

$$G_c^* = G_1^* V_1 + G_2^* V_2 \qquad [16]$$

where G_c^*, G_1^*, G_2^* refer to the complex shear modulus of the composite, of phase 1 and phase 2 respectively; V_1 and V_2 are the volume fractions of phase 1 and phase 2 respectively, with the condition that $V_1+V_2=1$.

Fig. 8 *Idealized scheme of the Voigt composite: a) laminar; b) fibrous*

Taking the ratio of real (*G'*) and imaginary (*G''*) parts of the complex modulus, the loss tangent of the composite is given by (Lakes, 2009):

$$\tan\delta_c = \frac{V_1 \tan\delta_1 + V_2 \frac{G'_2}{G'_1} \tan\delta_2}{V_1 + \frac{G'_2}{G'_1} V_2} \qquad [17]$$

where tanδ_c, tanδ_1 and tanδ_2 are the loss tangent of the composite, of phase 1 and of phase 2, respectively; and G'_1 and G'_2 are the real parts of the complex modulus of phase 1 and 2, respectively.

E.5 Arrhenius Model

Arrhenius, 1887 proposed a mixing rule, expressed in Equation 18, to estimate the viscosity of a two components system, further validated for asphalt binders by Davison et al., 1994 as

$$\eta_{mix} = \frac{{\eta_A}^{\alpha} \cdot \eta_B}{{\eta_B}^{\alpha}} \quad [18]$$

where, η_{mix} is the viscosity of the bituminous blend, η_A and η_B are the viscosities of the two asphalt binders and α is the concentration of the binder A. Since there is a direct relationship between viscosity and stiffness changes, Equation 18 can be re-written for G^* as following:

$$G^*_{mix} = \frac{{G^*_A}^{\alpha} \cdot G^*_B}{{G^*_B}^{\alpha}} \quad [19]$$

2.2 Master Curves

In the present Section, two different models to plot the Master curves of the different asphalt material phases are reported.

2.2.1 Christensen Anderson Maresteanu (CAM) model

Master curves provide a fundamental rheological understanding of viscoelastic materials and allow estimating the mechanical properties over a wide range of temperature ad frequency that could be realized in the field, but that are not pratical to simulate in laboratories. In the present work, in order to plot the master curves of the complex modulus and of the phase angle, the model presented in NCHRP 459, 2001 was used. This is a universal model valid for binders, mortars and mixtures. It's composed of three equations:

$$G^* = G^*_e + \frac{G^*_g - G^*_e}{[1+(f_c/f'))^k]^{m_e/k}} \quad [20]$$

where:

$G^*_e = G^*(f \to 0)$ is the equilibrium complex modulus, G_e*=0 for binders; $G^*_g = G^*(f \to \infty)$ is the glass transition complex modulus; k and m_e are two dimensionless shape parameters; f_c is the location parameter with dimensions of frequency, where the G_g* and m_e asymptotes intercept; $f'_c = f_c(\frac{G^*_e}{G^*_g})^{1/m_e}$ is the frequency where the G_e* and m_e asymptotes intercept; f' is the reduced frequency, function of both temperature and strain.

Figure 9 illustrates the complex modulus master curve calculated as for Equation [20].

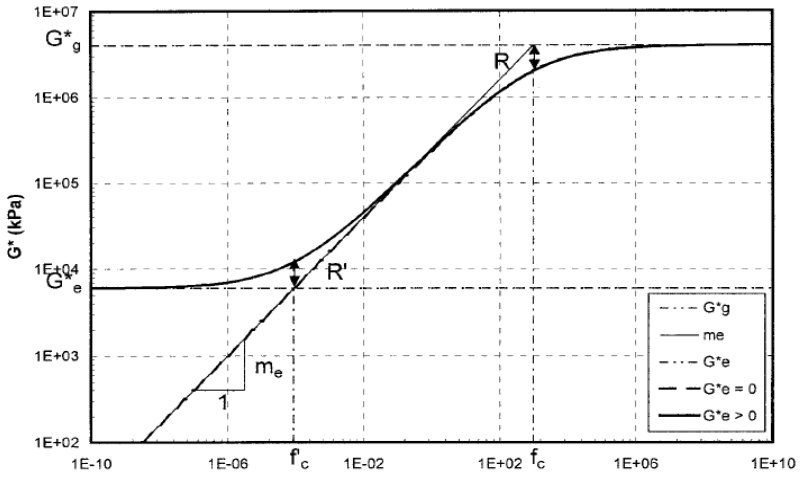

Fig. 9 *Typical representation of a Master Curve.*

These parameters allow to calculate the complex modulus and phase angle master curves by using the equations [20] and [21] respectively:

$$\delta = 90I - (90I - \delta_m)\left\{1 + \left[\frac{\log(f_d / f')}{R_d}\right]^2\right\}^{-m_d/2} \qquad [21]$$

where:

$$I = \begin{cases} 1 \; for \; mixtures \\ \begin{cases} 0 \; if \; f' > f_d \\ 1 \; if \; f' \leq f_d \end{cases} \end{cases} \quad for \; binders$$

The well-known Williams–Landel–Ferry (WLF) formulation is used in the model to express the temperature-shift factor a_T, as expressed in Equation 3.

This model can be used to plot the master curves of the complex shear modulus G^* and of the complex modulus E^*.

2.2.2 Sigmoidal model

Another model frequently used to plot the master curves of the mixtures is the sigmoidal model reported in Equation 22:

$$\log E^* = \delta + \frac{\alpha}{1 + e^{(\beta + \gamma \cdot \log f')}} \qquad [22]$$

Where δ is the minimum value of E^*, α is equal to $log\ E_{max}$-$log\ E_{min}$, β and γ are shape parameters and f' is the reduced frequency.

Chapter 3

3. Estimation of the rheological properties of RAP binders avoiding the extraction and recovery method

In this chapter, a new procedure to estimate the rheological properties of RAP binder and of bituminous blends composed with RAP binder, avoiding the extraction and recovery method is presented. Furthermore, a procedure to back-calculate the PG grade of these binders is introduced and two different methods to determine the maximum amount of RAP that can be added to a mixture without compromising its performance at low, intermediate and high temperature are proposed.

3.1 Development of a new procedure to estimate the RAP binder properties from results on mortar tests

In the present Section, a new procedure specifically developed in order to determine the rheological properties of the RAP binder and of the bituminous blends, composed of fresh and different RAP binder percentages, avoiding the extraction and recovery methods, is described. The procedure is based on the rheological Nielsen model (see Section E.3), specifically adapted in order to take into account the stiffening effect at low frequency and high temperature, and on the Voigt model (see Section E.4).

The proposed methodology is summarized in Figure 10 (Riccardi et al., 2016). First, mortars consisting of fresh binder mixed together with different volume fractions of a selected fine fraction of RAP (SRAP), that are the fine fraction of the RAP, passing sieve with an opening size of 0.15 mm, or with SRAP aggregate (called Burned Selected Reclaimed Asphalt Pavement, BSRAP) obtained by ignition, (particles size smaller than 150 μm) are produced (Ma et al., 2009, Riccardi et al., 2015 and 2016). Then, Dynamic Shear Rheometer (DSR) (AASHTO T315, 2012; EN 14770, 2012) tests are performed on SRAP and BSRAP mortars. Finally, in order to back-calculate the effective complex modulus and the phase angle of the blends of virgin and SRAP binders, a new approach based on the Nielsen model (Landel and Nielsen, 1993) for composite materials is used.

The original expression of the Nielsen model is specifically adapted to take into account the effect of low frequencies and high temperatures on the stiffening contribution of fine particles in the mortar. Once the rheological properties of the bituminous blends are calculated, the simple Voigt model can be used to determine the complex modulus and the phase angle of the RAP binder. The use of both

SRAP mortar and BSRAP mortar allows to clearly identifying the actual stiffening effect of the aggregates contained in the RAP material facilitating the identification of the model parameters.

The application of this approach using RAP with different binders is explained hereafter.

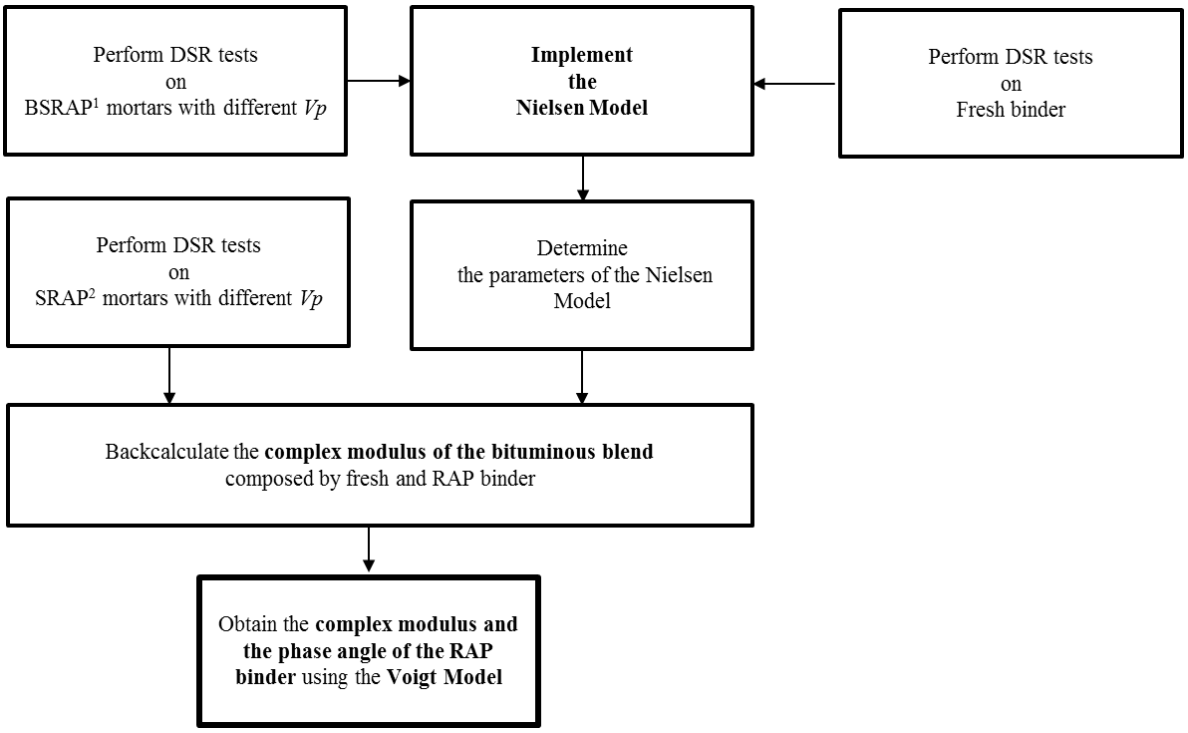

[1]*BSRAP: Burned Selected Reclaimed Asphalt Pavement*

[2]*SRAP: Selected Reclaimed Asphalt Pavement*

Fig. 10 *Research approach flow chart (Riccardi et al., 2016).*

3.1.1 Development of the Enhanced Nielsen model (N.1)

The original formulation of the Nielsen model (Equation 11) does not take into account the effect of frequency and temperature on the stiffening ratio $|G_m^*/G_b^*|$, between the complex modulus of the asphalt mortar and that of the asphalt binder. In fact, this model was used in the past at a single frequency and at a single temperature.

Performing temperature and frequency sweep tests on mortars and binders, the stiffening ratio $|G_m^*/G_b^*|$, was calculated and then plotted as function of frequency *f*, at a constant temperature T=20°C. In addition, $|G_m^*/G_b^*|$, was also computed with the Nielsen model, as it was used until now, and compared with the ratio obtained using the experimental data (Figure 11).

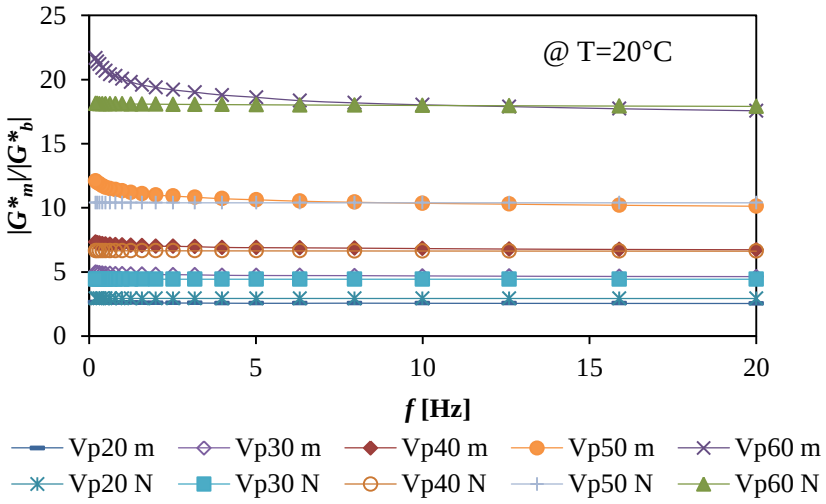

Fig. 11 *Stiffening ratio versus frequency for different SRAP particle volume fractions (V_p) in % (e.g. Vp20) and at T=20°C (m= measured value, N= Nielsen model calculated value).*

A stiffening increase for the experimental values can be observed especially at low frequency which corresponds to intermediate and high temperatures. In fact, at lower frequencies, the binder is softer and the relative stiffening effect of particles is more significant, if not dominant. In addition, such a stiffening effect depends also on the volumetric fraction of aggregate particles. Therefore, it is not surprising that a higher stiffening effect is observed for higher V_p= 60%, for which the aggregate skeleton may lead to significant interlocking phenomena.

In order to take into account this stiffening effect at lower frequencies, the Nielsen model needs to be adapted. Leandri et al., 2015, proposed to modify the Nielsen model adding a correction factor, which is a logarithmic function of the inverse of the testing frequency, but using this method the effects of temperature and frequency are taken into account separately and moreover the regression coefficients can vary depending on the fitting algorithm chosen and on the starting values of the coefficients. Therefore, in this work the Nielsen model in its original formulation was used, but the parameters A and φ were adapted.

In particular, the time-temperature superposition principle was used in order to consider the effect of temperature and frequency at the same time. The parameters A and φ were determined by non-linear curve fitting the shifted data at different volume content of fine aggregate particles to the Nielsen model, let the parameter A to vary with the reduced frequency, and imposing a single value for the parameter φ.

The parameter *A*, that depends on the Poisson's ratio, as shown in Equation 13, was found to decrease when the reduced frequency increases, in accordance to the trend of the complex Poisson's ratio versus the reduced frequency observed by Di Benedetto et al., 2010.

Moreover, the maximum volumetric packing fraction φ, was also calculated as the ratio between the maximum volumes of aggregate particles obtained using the Rigden Voids apparatus and the apparent volume of aggregate particles determined in accordance to EN 1097-7(2008). The average value of the particle maximum density ρ_{cp} was determined on three specimens of the compacted particles. Therefore, knowing the apparent density of the particles, the maximum volumetric packing fraction, φ, was estimated and it results in very close agreement with literature values (Nielsen, Landel, 1994). All the values of A and φ for the different materials used in the present work are reported in Section 3.1.3.

3.1.2 Description of materials and tests

One artificially aged and three real RAP sources (one from Italy, one from England and one from Germany) were used in the present study. The first one was used to develop and to validate the proposed procedure to estimate the RAP binder properties from those of asphalt mortars using the enhanced version of the Nielsen model in combination with the Voigt model; the other RAP sources were used to confirm the applicability of the procedure to real RAP sources.

The tests carried out included the characterization of the materials to be tested:

- Determination of the binder content of the fine fraction (passing #100 sieve with an opening size of 0.150 mm) of the RAP using the Soxhlet extractor method (EN 12697-1);
- Determination of the density of the fine fraction of the RAP in accordance to EN 1097-7;
- Determination of the Rigden Voids in accordance to EN 1097-4.

Once all the needed characteristics were known, two different types of mortars were produced:

- SRAP mortar composed by mixing different percentage of Selected fraction of RAP (SRAP) passing sieve with an opening size of 0.149 mm (V_p=35; 50%), shown in Figure 12 a, with fresh binder.
- Burned SRAP (BSRAP) mortars consisting of different percentages (V_p=20; 35; 50%) of fine fraction of the RAP aggregate extracted from the SRAP, shown in Figure 12 b, with fresh binder.

a)  b) 

Fig. 12 *a) Selected Reclaimed Asphalt Pavement (SRAP); b) Burned Selected Reclaimed Asphalt Pavement (BSRAP)*

This sieve (#100) size limit was selected to assure a consistent reliability of the test procedure. It is good practice to prepare DSR specimens with a gap (thickness) at least ten times larger than the actual maximum aggregate particle size (Liao et al., 2013); hence, larger aggregates were not considered, since this may potentially result in misleading measurements.

In Figure 13 all terms concerning the materials used in the present study are graphically represented. As shown, Burned Selected Reclaimed Asphalt Pavement (BSRAP) represents the aggregate extracted by ignition from SRAP (Ma et., al 2010). Combining BSRAP and fresh binder, BSRAP mortars are obtained, while mixing SRAP, composed of BSRAP and RAP binder, with fresh binder, SRAP mortars can be produced.

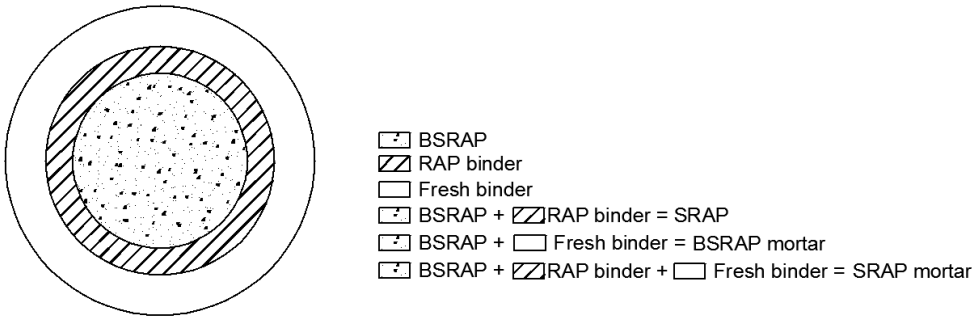

Fig. 13 *Scheme of the terms used in the present study.*

In more details SRAP and BSRAP mortars were produced in order to have the same aggregate skeleton considering the RAP binder that coats the aggregates, as part of the total binder (V_b) as represented in Figure 14.

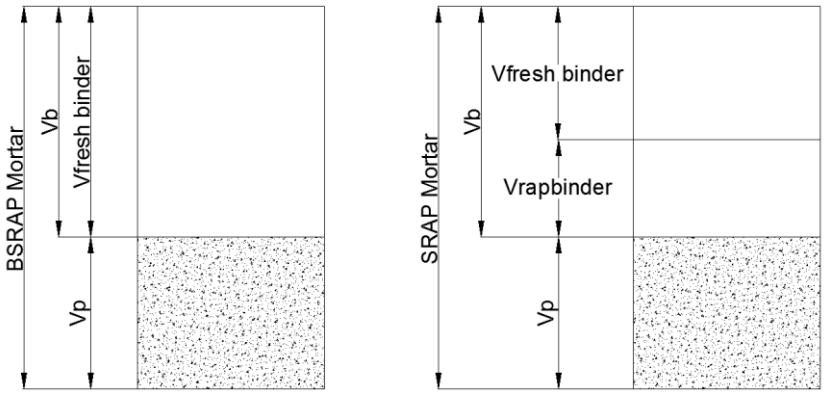

Fig. 14 *Volume distribution of mortars*

All the mortars and also the fresh binder were tested with the DSR in the classical configuration of parallel plate (AASHTO T 315, EN 14770) performing frequency and temperature sweep in order to measure the rheological properties and to plot the master curve of the complex modulus and of the phase angle. For each test and each material, three replicates were tested.

3.1.2.1 Artificial RAP source

An artificially aged binder was manufactured subjecting a 50/70 Pen grade binder to Rolling Thin Film Oven Test (RTFOT) (EN 12607-1) and 2 times on Pressure Aging Vessel (PAV) (EN 14769). Then this binder, called in the following "artificially RAP binder" was used to produce an artificial SRAP composed by the fine fraction (passing sieve with an opening size of 0.149 mm) of a sand mixed with the artificially aged binder.

The density of the fine fraction of the sand was determined in accordance to EN 1097-7 and the average between three determinations results 2.735 g/cm^3.

The composition of the artificial SRAP is reported in Table 1. The binder percentage by weight results 15.48% with respect to the aggregate.

Table 1. *Composition of the artificially SRAP*

	Fine fraction of sand	**Binder 50/70 aged**
Weight (g)	129.15	20.00
γ(g/cm^3)	2.735	1.025
Volume (cm^3)	47.23	19.51
%Volume	70.76	29.24

The fresh binder used was a 70/100 Pen grade.

Moreover two bituminous blends composed by the 70/100 Pen Grade and different percentages of the artificial RAP binder, that corresponds to 35 and 50 % of SRAP, were produced.

Frequency and temperature sweep tests using the DSR in the classical configuration of parallel plate with 8 mm diameter and 2 mm gap were performed on the following binders in order to determine the complex modulus and the phase angle master curves reported in the following:

- ✓ 70/100 Pen Grade
- ✓ 50/70 RTFO+2PAV aged
- ✓ Bituminous blends composed by 77.7% of 70/100 and 22.3% of 50/70 RTFO+2PAV; and by 58.7% of 70/100 and 41.3% of 50/70 RTFO+2PAV. These percentages of fresh 70/100 and aged 50/70 binders were used in order to recreate the same amount of fresh and RAP binder in

the SRAP mortars corresponding to 35 and 50% of SRAP, considering the SRAP contained 15.48% of aged binder.

Frequency and temperature sweep tests were also performed on artificial BSRAP and SRAP mortars. The strain amplitude used for the binders was 0.05% while for the mortars it was 0.005%. These values were chosen, after applying a strain amplitude, in order to keep the material response in the Linear Viscoelastic (LVE) domain. The master curves of the complex modulus and of the phase angle, determined as explained in Section 2.2, of the binders are reported in Figure 15 a and b respectively, and the master curves of the BSRAP and SRAP mortars are reported in Figure 16 and 17. The parameters of the master curves are reported in Annex 1. In Figure 15, the artificial RAP binder content of 22% and 41% by weight of total binder (virgin and RAP binder) corresponds to volume fraction of aggregate particles in mortars of 35% and 50% respectively.

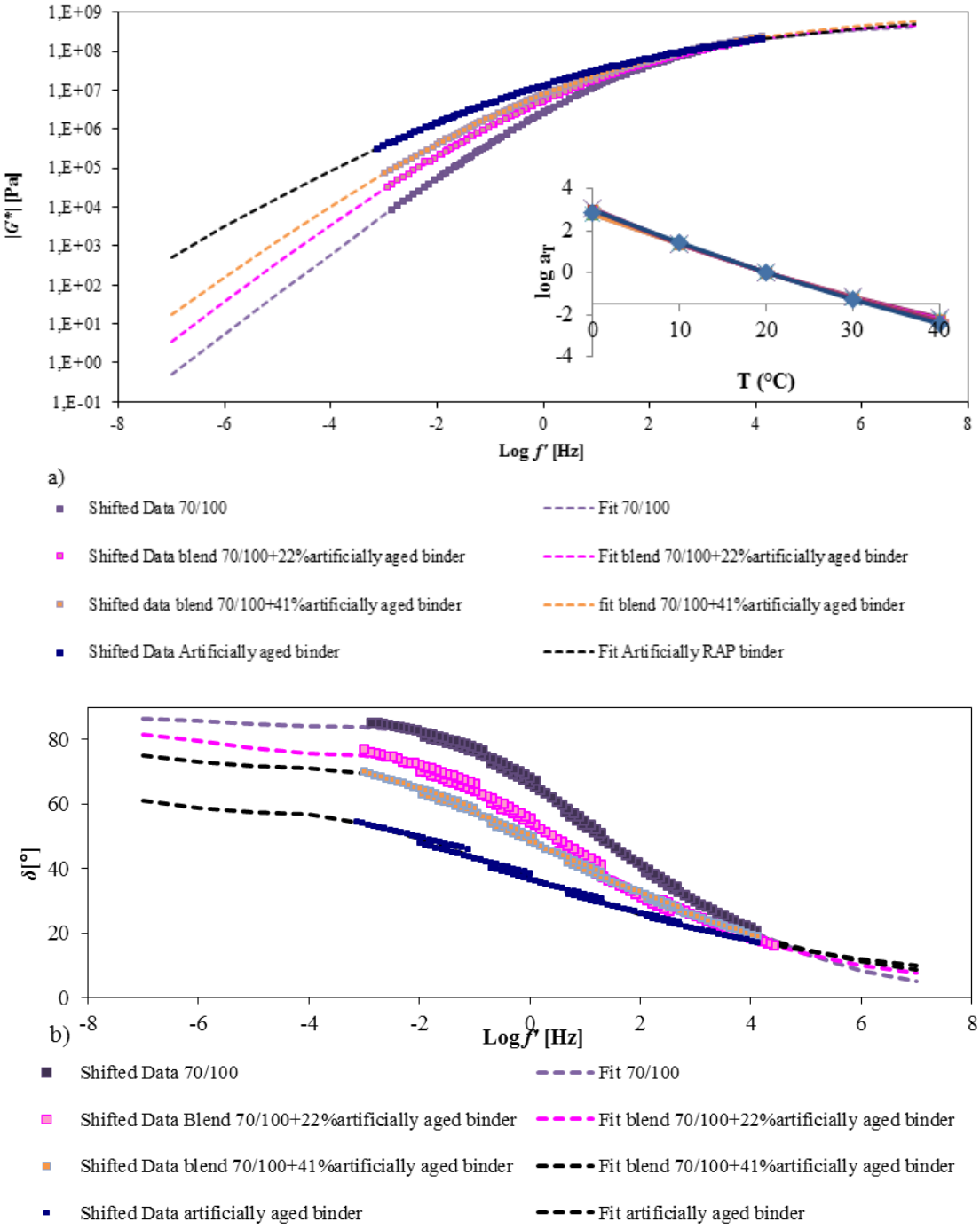

Fig. 15 *Master curves a) of the Complex modulus b) of the phase angle of the fresh binder, of the bituminous blends and of the artificial aged binder.*

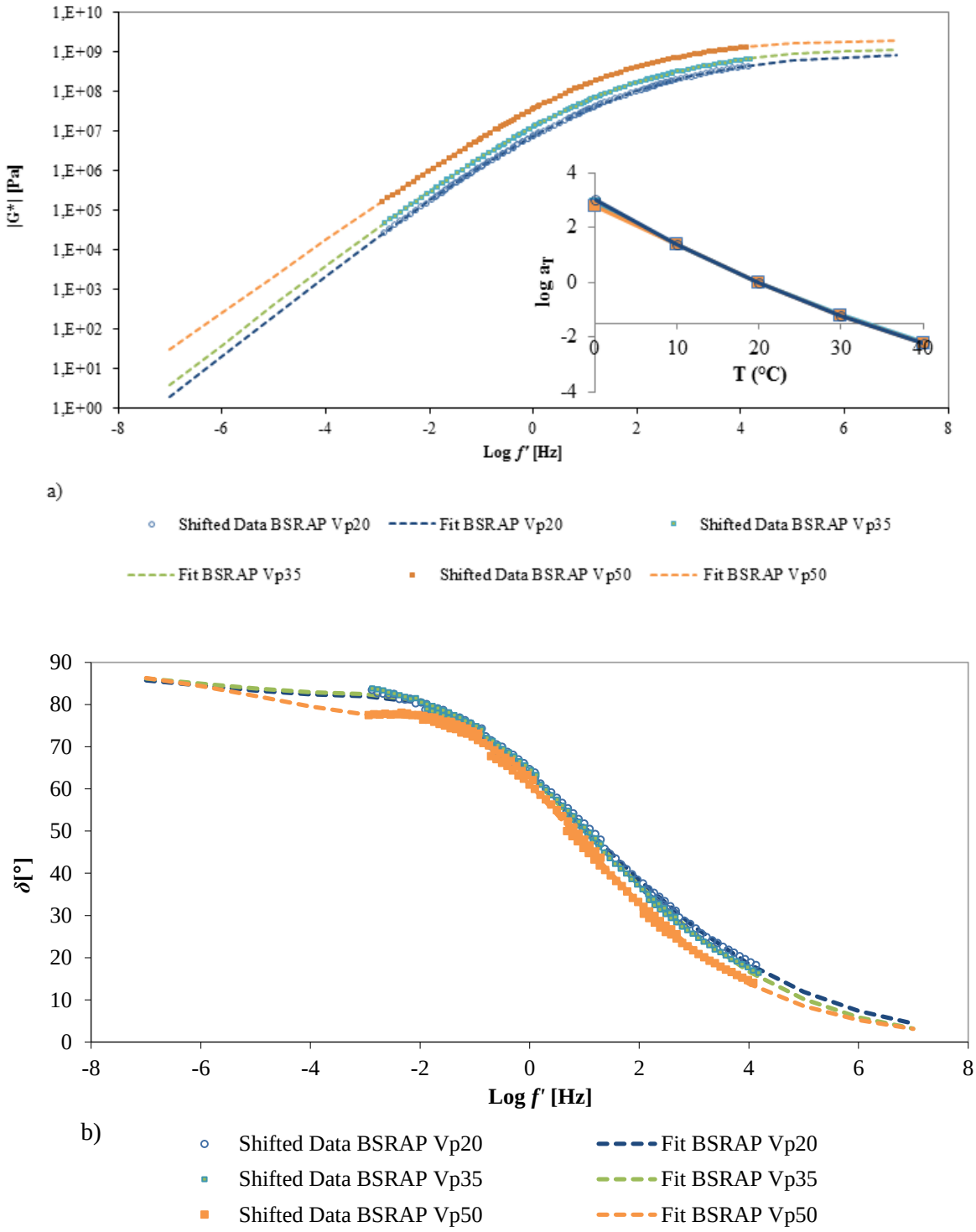

Fig. 16 *Master curves a) of the Complex modulus b) of the phase angle of the BSRAP mortars.*

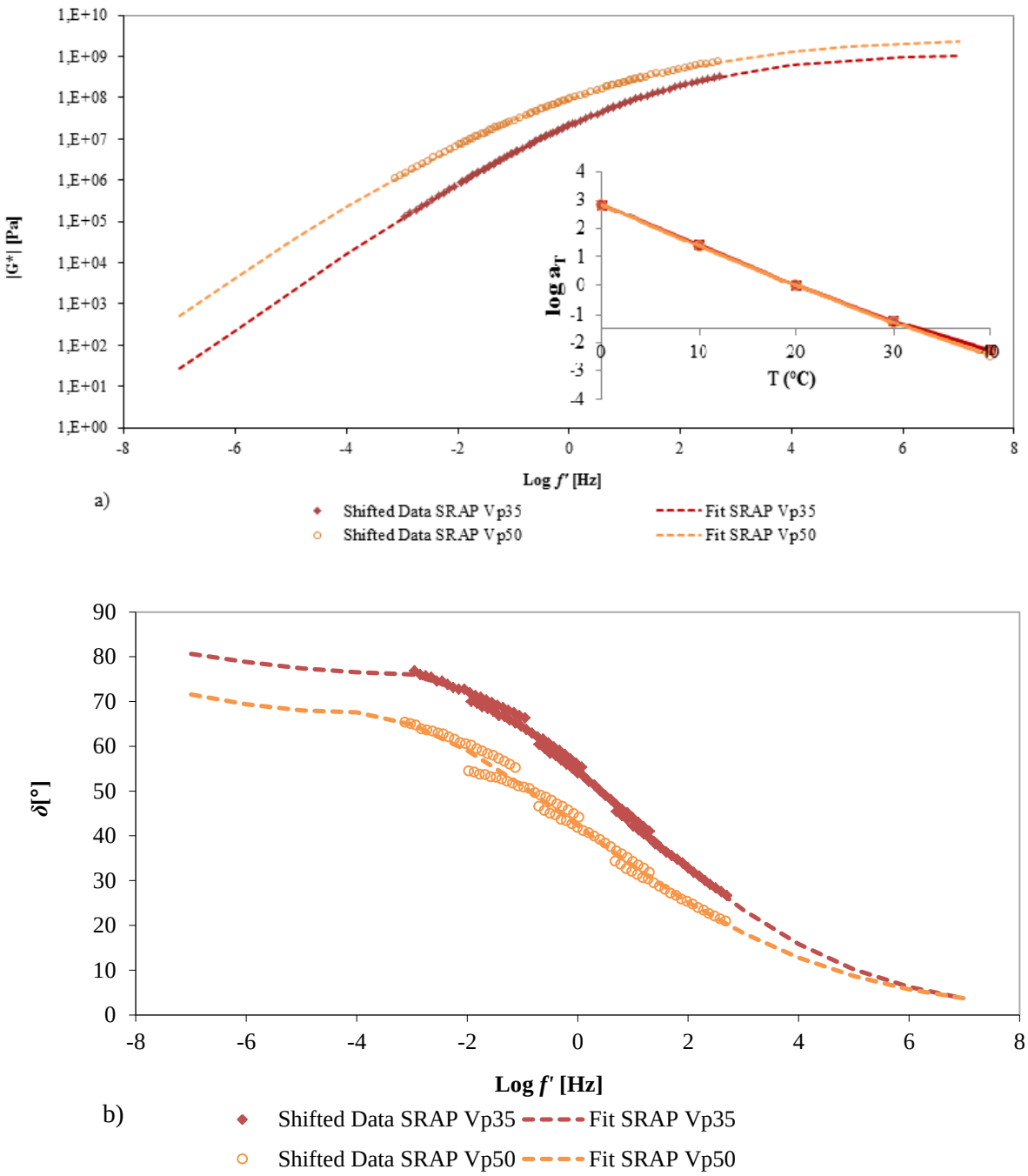

Fig. 17 *Master curves a) of the Complex modulus b) of the phase angle of the SRAP mortars.*

3.1.2.2 Italian RAP source

An Italian RAP source with two-component binders, obtained by mixing in different proportions a hard and a soft binder were used. In order to prepare the mortars to be tested with DSR, the RAP material was sieved with the #100 (0.149 mm) sieve. The asphalt content of this RAP fraction was

determined using the Soxhlet extractor and was found to be equal to 9.89% by weight of aggregate particles.

The virgin asphalt binder used to prepare the asphalt mortar specimens was obtained by mixing different percentages of a Hard (H) and a Soft (S) binder. The following three different bituminous blends were produced:

- 90%Hard+10%Soft, identified as 90H+10S;
- 80%Hard+20%Soft, identified as 80H+20S;
- 70%Hard+30%Soft, identified as 70H+30S.

The original H binder (100H) and the binder blends were characterized with traditional tests such as Penetration grade (EN 1426) and softening point (EN1427) according to the conventional European grading system (Table 2). The softer binder S could not be characterized due to its low consistence (Kinetic viscosity of 8000mm^2/s at 60°C). The Performance Grade (PG) (AASHTO M320 2010) of all blends was also determined (Table 2).

Table 2. *Asphalt binders*

Binder	**100H**	**90H+10S**	**80H+20S**	**70H+30S**
Pen 25°C (dmm)	41	44	58	75
Softening point R&B (°C)	52	51	47	44
Fraas Braking point (°C)	-6	-6	-9	-10
Viscosity at 135°C (mPa s)	370	330	295	230
PG	64-16	64-16	64-16	58-22

Using these three binders, SRAP and BSRAP mortars were produced. In total 18 mixes were prepared considering three different volume percentages, V_p, of SRAP and BSRAP (20%, 40%, 60%), and the three different percentage combinations of the H and S binders (90H+10S, 80H+20S, 70H+30S). The compositions of the different BSRAP and SRAP mortars are reported in Table 3 and 4 respectively. The percentage of BSRAP, SRAP, fresh and RAP binder in these tables are the weight percentage respect to the total mortars.

Table 3. *BSRAP mortars compositions*

V_p	**BSRAP**	**Fresh binder**
20	39.8%	60.2%
40	63.8%	36.21%
60	79.8%	20.2%

Table 4. *SRAP mortars compositions*

V_p	**SRAP**	**Fresh binder**	**RAP binder in the mortar**	**Total binder**
20	43.4%	56.6%	3.6%	60.2%
40	69.5%	30.5%	5.7%	36.2%
60	87.0%	13%	7.2%	20,2%

The specimens were obtained by mixing the preheated aggregate particles and the binder for two hours at 140°C; this was done to allow a complete diffusion process of the fresh binder in the RAP one, as recently demonstrated in a different study (Rad et al., 2014). In order to have the same binder aging, the BSRAP mortars were obtained following the same preparation method. The mortars were identified by a 7 digit code (00-00-00-B/S) which consists of four parts: two numbers each for the two H and S binder percentages, two numbers for the volume fraction of reclaimed material and a letter, B or S, indicating BSRAP or SRAP, respectively.

Both binders and mortars were tested using the DSR in the classical parallel plate configuration with diameter of 8 mm and gap of 2 mm, at test temperatures of 0°, 10°, 20°, 30°, 40°C. Frequency sweep tests were performed at constant strain amplitude of 0.05% for the binders and 0.005% for the mortars, in the frequency range of 0.2 to 20 Hz. The imposed strain was chosen in order to keep the material response in the (LVE) and was determined through amplitude sweep tests. The master curves are reported in Figure 18 for the binders.

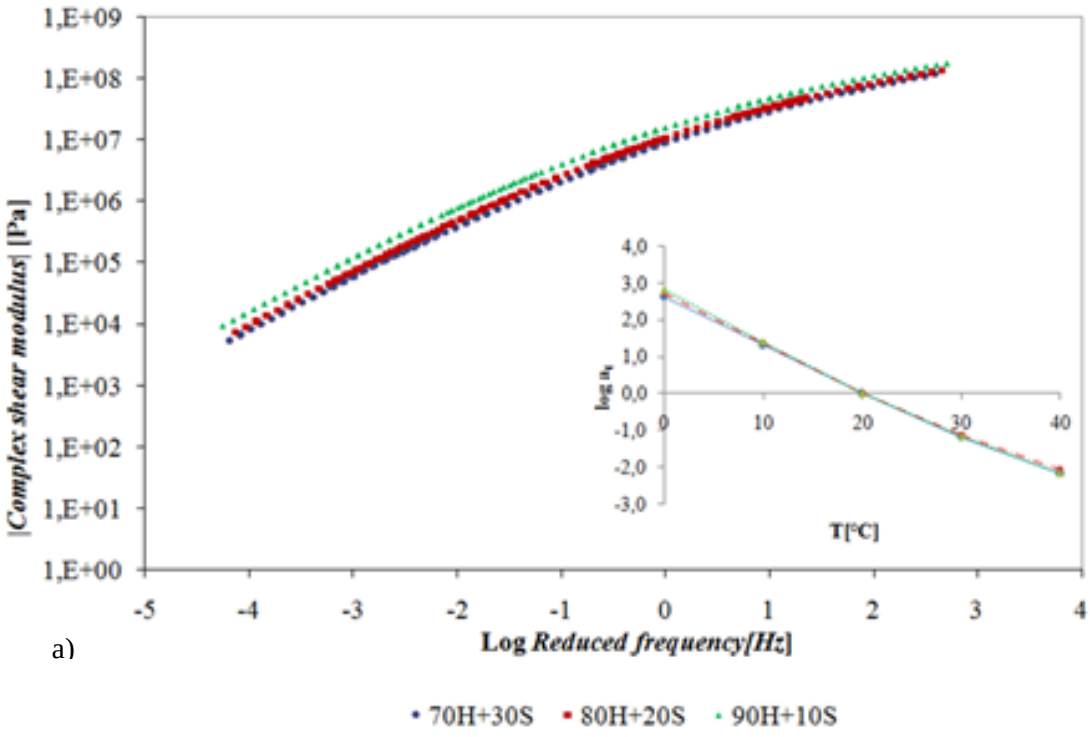

a)

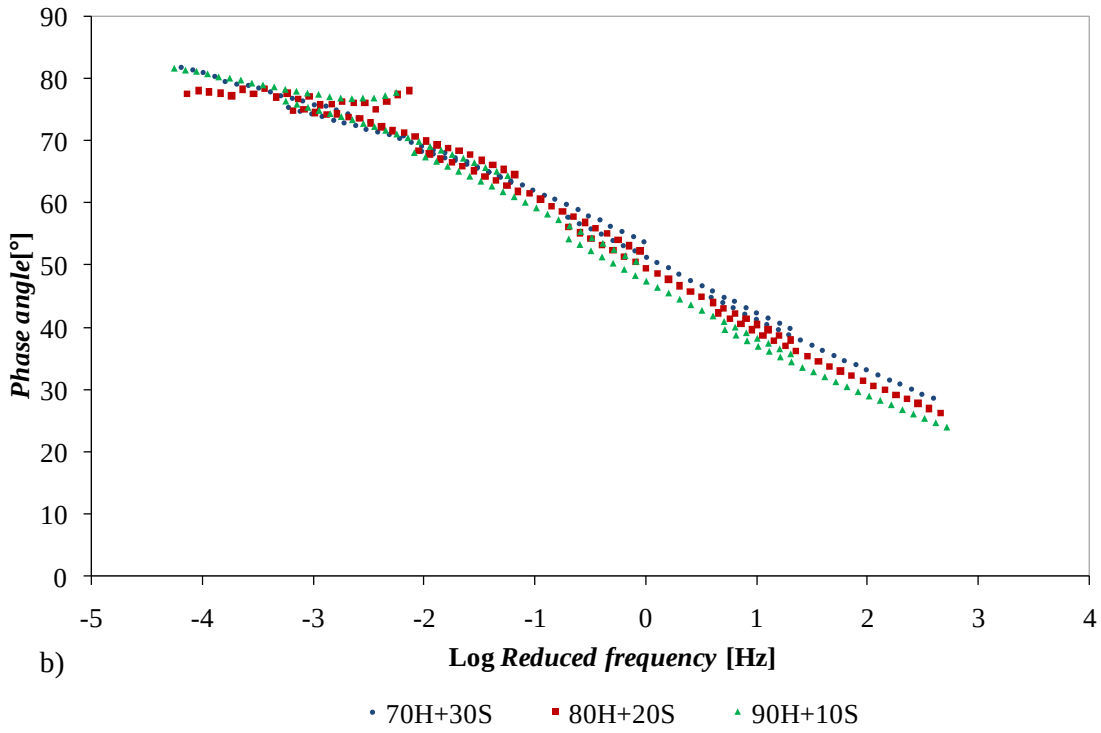

Fig. 18 *Master curves of a) the complex modulus and b) of the Phase angle of the different bituminous blends.*

Figures 19 and 20 show complex modulus and phase angle master curves of the different asphalt mortars containing the same percentage of SRAP and BSRAP (V_p=20%), respectively, at a reference temperature of 20°C. In these figures the fit of the master curves obtained with the procedure described in the NCHRP 459 (2001) are reported, while all the parameters of the master curves are summarized in Annex 1. In the case of SRAP mortar, a larger complex modulus and a smaller phase angle in comparison to the BSRAP mortar can be observed as shown in Figure 19c and 20c. This is due to the stiffening effect of the RAP binder present in the SRAP material. Moreover, the complex modulus of SRAP mortars significantly decreases as the percentage of the S binder increases due to the softening - rejuvenating effect of this softer binder. An opposite trend is observed for the phase angle.

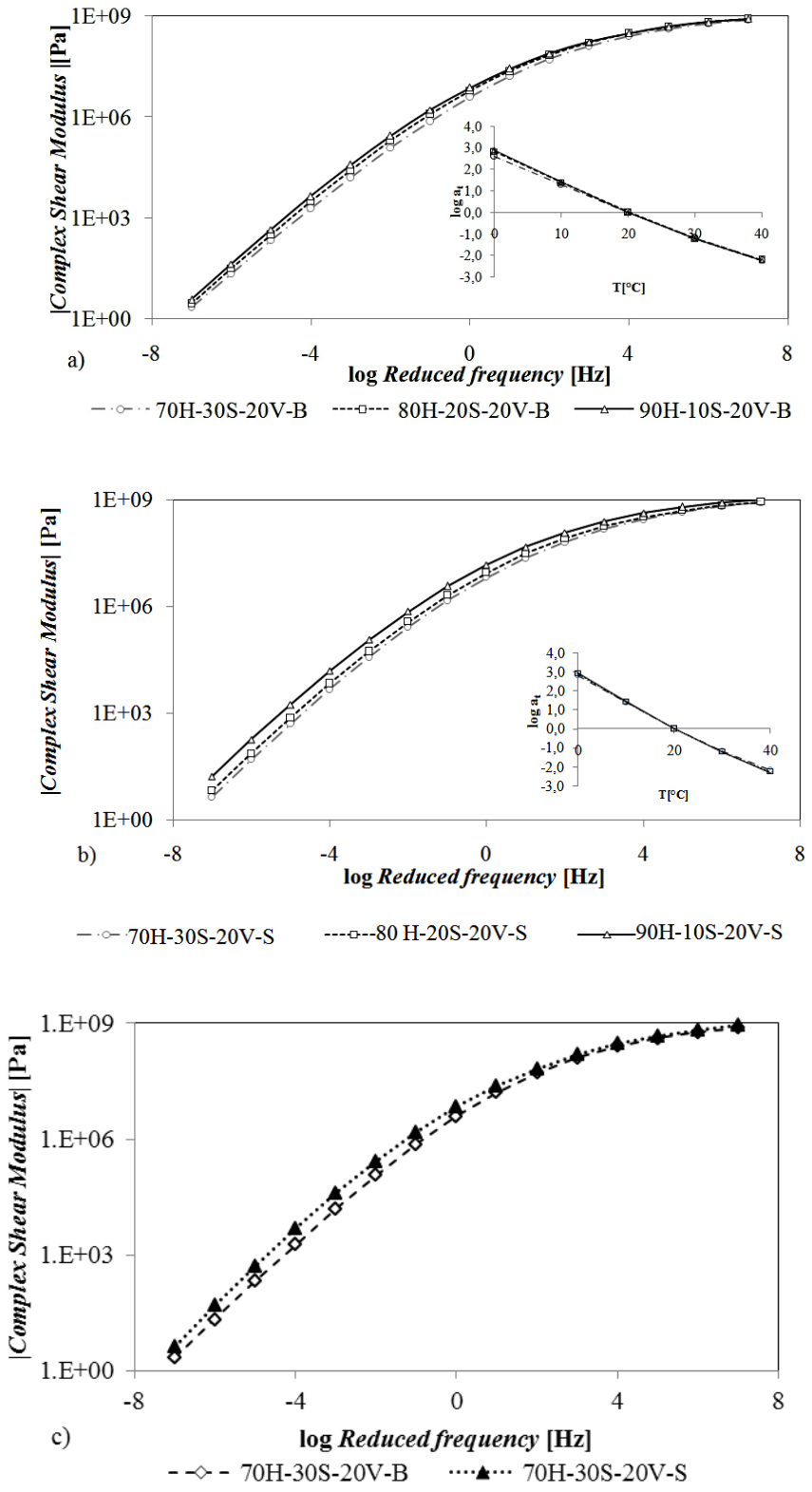

Fig. 19 *Complex modulus master curves of mortars at V_p=20% for different percentages of the H and S binders: a) BSRAP mortars; b) SRAP mortars; c) BSRAP and SRAP mortar for 70H+30S.*

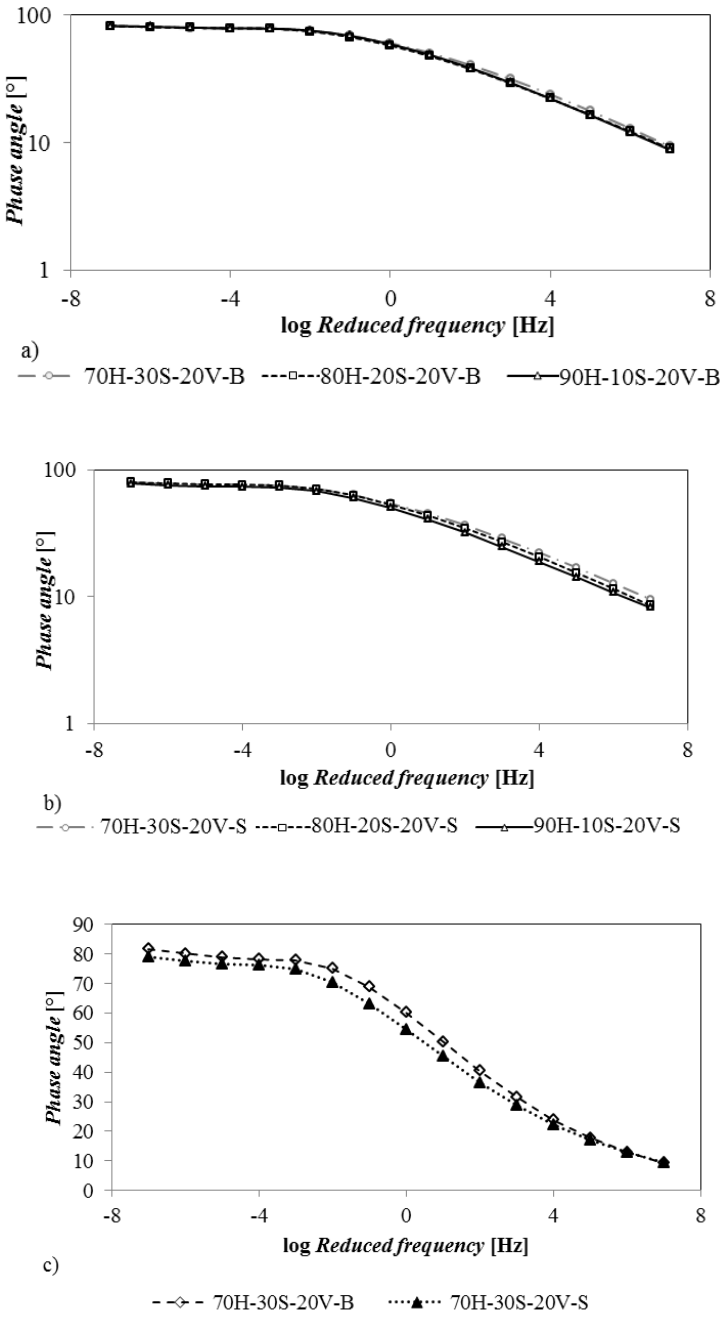

Fig. 20 *Phase angle master curves of mortars at V_p=20% for different percentages of the H and S binders: a) BSRAP mortars; b) SRAP mortars; c) BSRAP and SRAP mortar for 70H+30S.*

In Figures 21 and 22, the fit of the complex modulus and phase angle master curves of mortars prepared with binder blend 80H+20S and different percentages of BSRAP and SRAP are presented. The complex modulus increases while the phase angle decreases as the percentage of the aggregate particles increases; this is especially evident at lower frequency where the binder presents a softer response and the relative stiffening effect due to the aggregate particle is dominant.

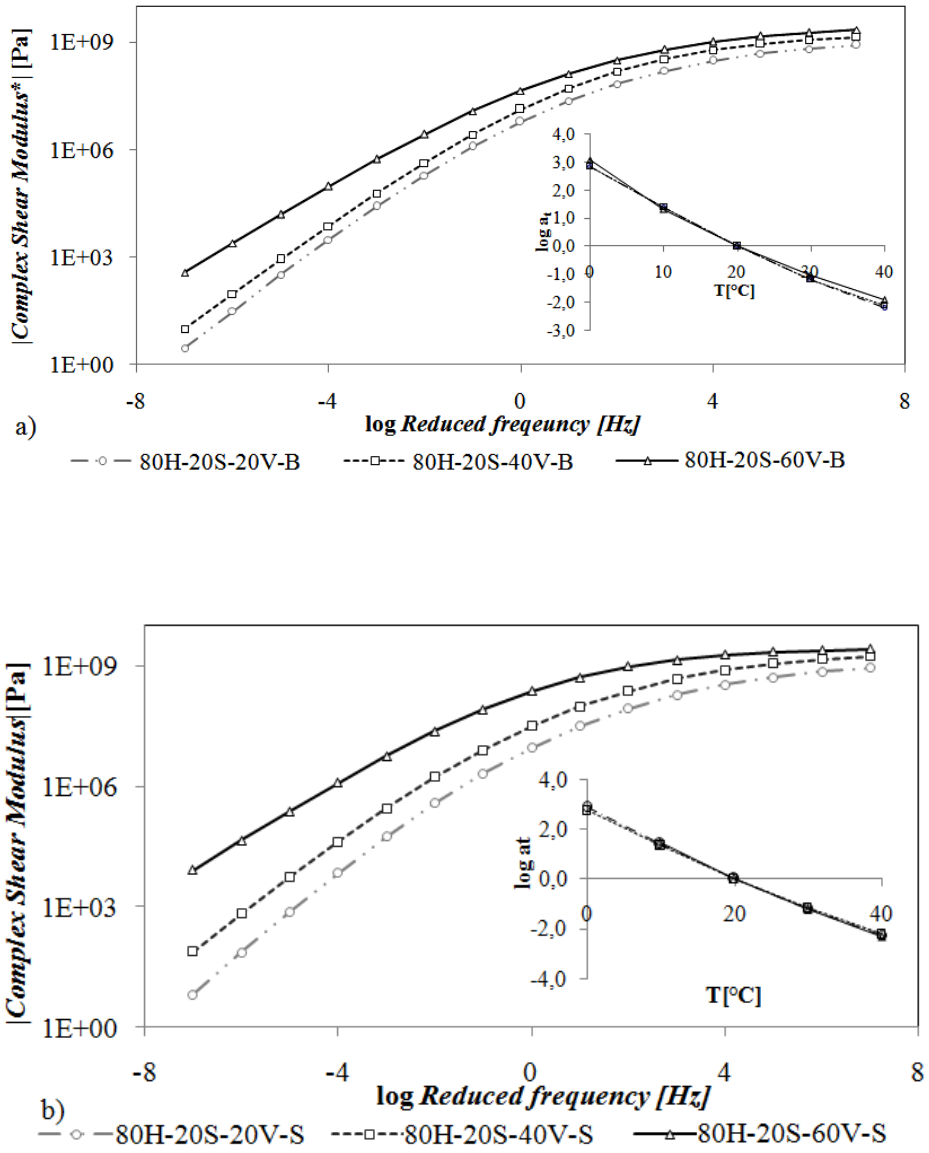

Fig. 21 *Complex modulus master curves of mortars at different V_p, for a constant percentage of Hard and Soft binder and T=20°C: a) BSRAP and b) SRAP mortars.*

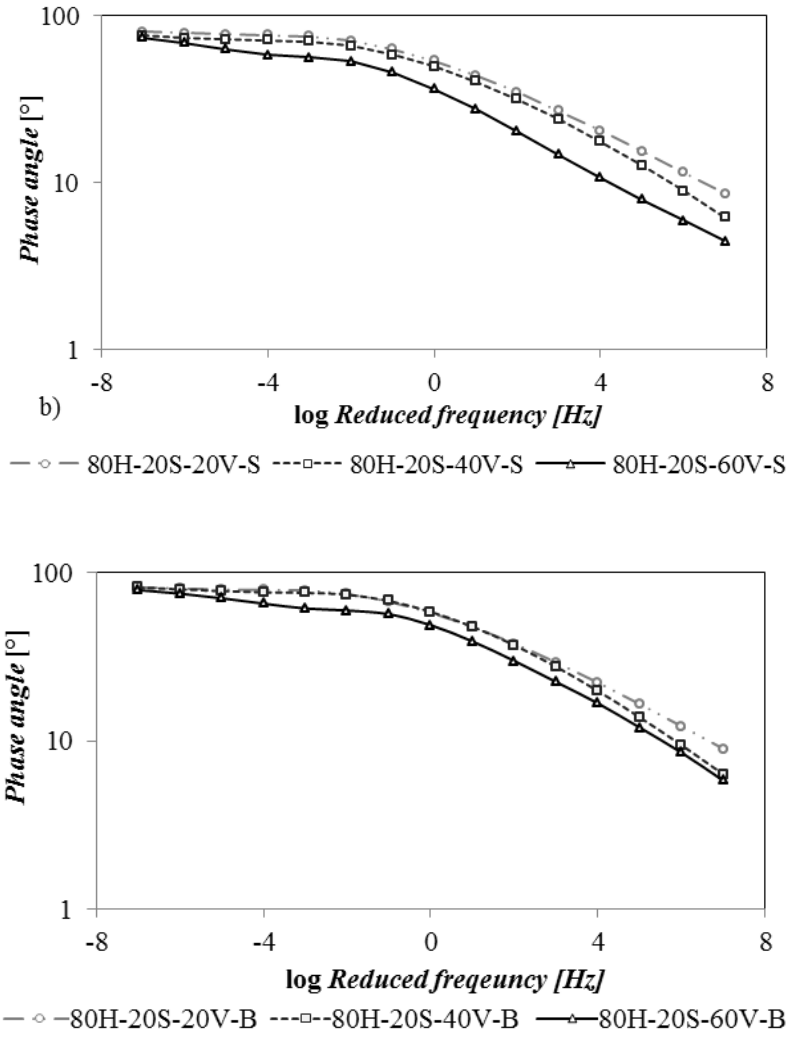

Fig. 22 *Phase angle master curves of mortars at different V_p, for a constant percentage of Hard and Soft binder and T=20°C: a) BSRAP and b) SRAP mortars.*

3.1.2.3 English RAP source

First, the aged binder contained in RAP was extracted and recovered using the fractionating column (Figure 23) with DCM (dichloromethane) as solvent (EN 12694-4:2005). Then, RAP material was sieved in order to collect the fine fraction passing #100 sieve (SRAP). Part of the SRAP was used to determine the percentage of RAP binder contained in SRAP, using the Soxhlet extractor, that results equal to 12.34% by weight respect to aggregates. The resulting aggregates were used as BSRAP and the density was determined in accordance to the EN 1097-7 and results 2.837 g/cm^3.

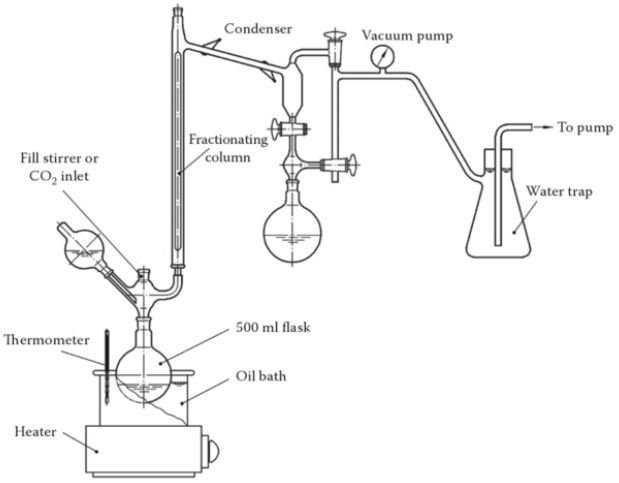

Fig. 23 *Extraction of the RAP binder using the fractionating column.*

The extracted and recovered binder contained in RAP and the virgin binder have the characteristics summarized in Table 5.

Table 5. *Characteristics of the extracted and virgin binder*

	Penetration at 25°C [1/10 mm]	Softening Point [°C]	Fraass breaking point [°C]	Viscosity at 135°C [mPa s]	Performance Grade
Extracted RAP binder	8.3	71.4	+9	1827	82-10
Virgin binder 50/70	68	47.6	-8	273	70-16

Three BSRAP mortars (V_p= 20, 35, 50) and two SRAP mortars (V_p= 35, 50) were produced with the compositions reported in Table 6 and 7 respectively.

Table 6. *BSRAP mortars compositions*

V_p	BSRAP	Fresh binder
20	40.9%	59.1%
35	59.8%	40.2%
50	73.5%	26.5%

Table 7. *SRAP mortars compositions*

V_p	SRAP	Fresh binder	RAP binder in the mortar	Total binder
20	45.9%	54.1%	5.1%	59.1%
35	67.2%	32.8%	7.4%	40.2%
50	82.5%	17.5%	9.1 %	26.5%

Frequency and temperature sweep tests with the DSR (EN 14770, 2012) were performed on BSRAP, SRAP mortars, on the fresh and extracted RAP binders and on the bituminous blends of fresh and the extracted RAP binder. For the mortars a strain amplitude of 0.05% for the lower V_p (20, 35%) and 0.005% for the V_p 50 were applied. For the binders a strain amplitude of 0.5% was applied. The master curves of the binders are reported in Figure 24, those of the BSRAP mortars are reported in Figure 25 and those of the SRAP mortars are reported in Figure 26. Frequency and temperature sweep tests were also performed on RTFO aged blends and mortars. The parameters of the master curves are reported in Annex 1.

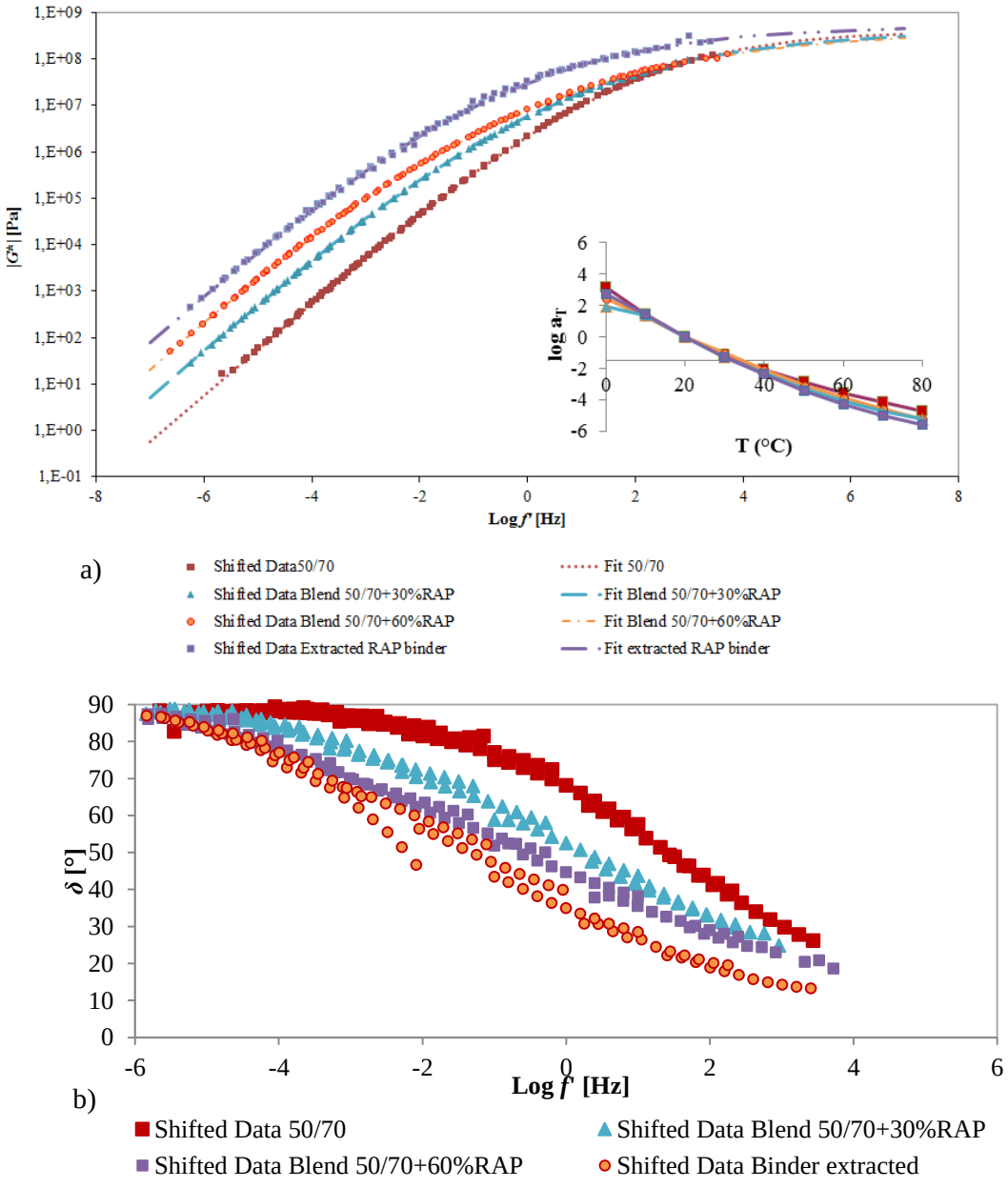

Fig. 24 *Master curves a) of the Complex modulus b) of the phase angle of the fresh binder, of the bituminous blends and of the extracted RAP binder.*

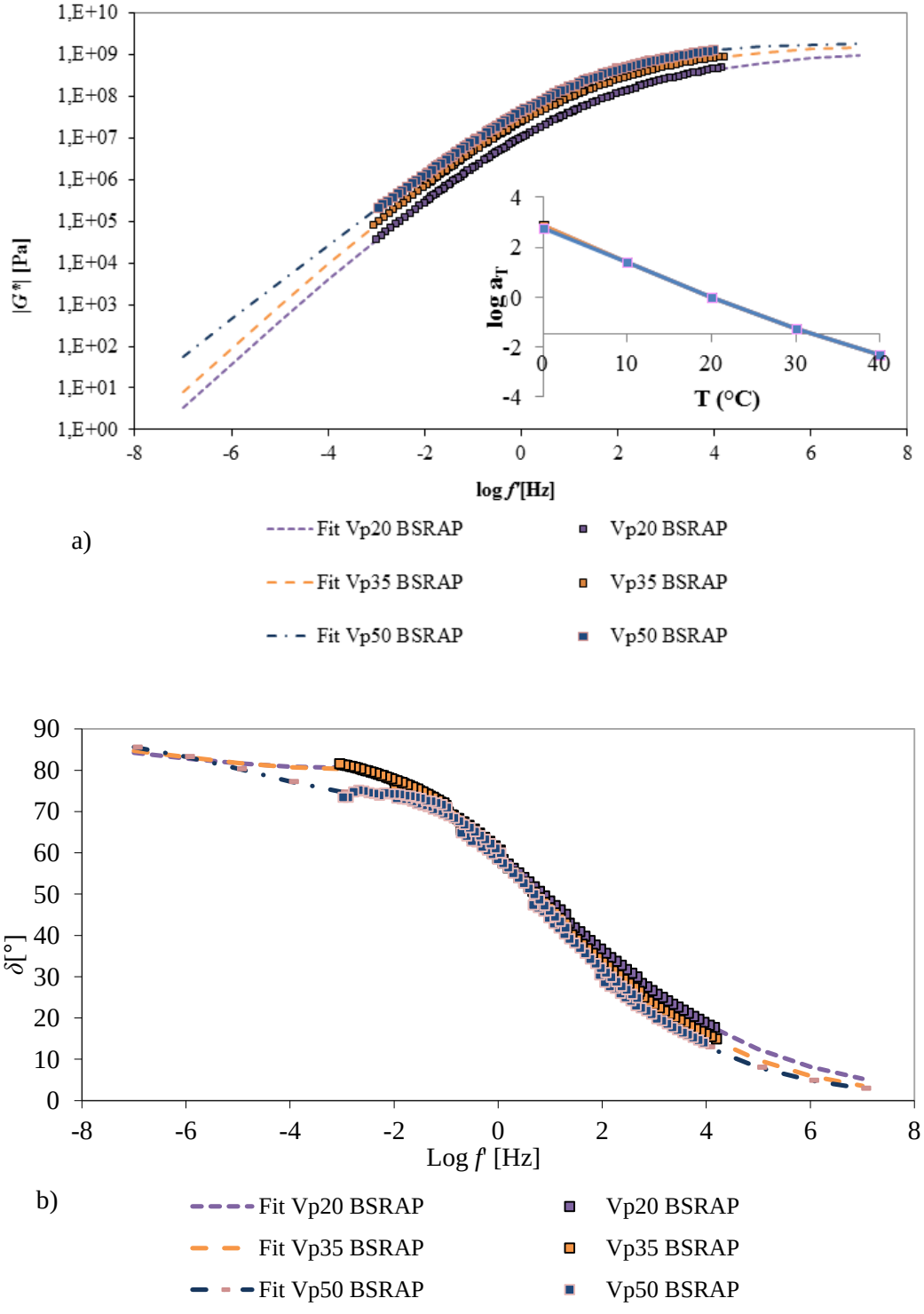

Fig. 25 *Master curves a) of the Complex modulus b) of the phase angle of the BSRAP mortars.*

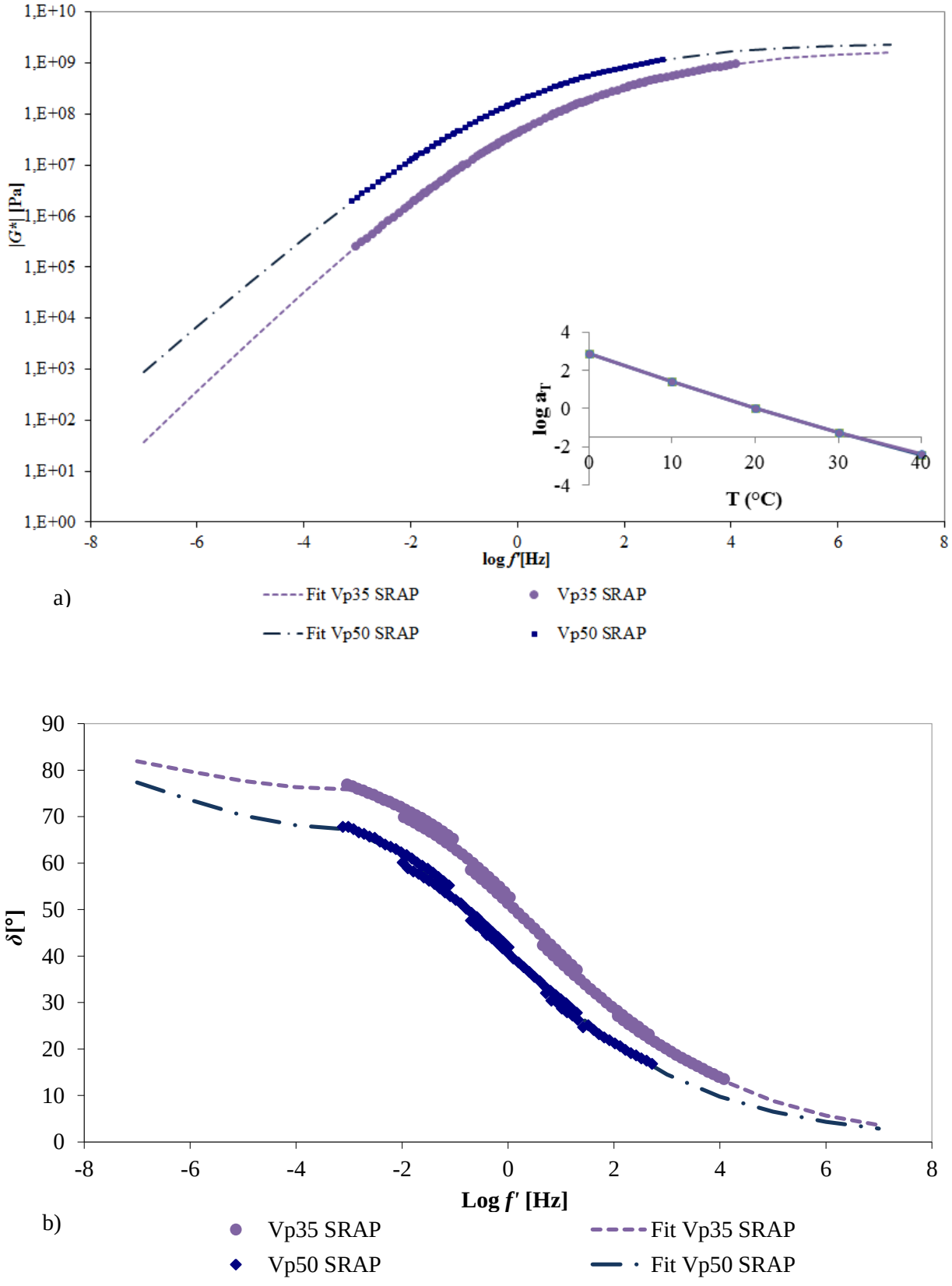

Fig. 26 *Master curves a) of the Complex modulus b) of the phase angle of the BSRAP mortars.*

3.1.2.4 German RAP source

In the case of the German RAP, the aged binder was extracted using the Rotatory Evaporator (Figure 27) in accordance to EN 12697-3, 2013 and then, it was characterized with traditional tests, according to the conventional European grading system EN 1426, 2015; EN 1427, 2015. Moreover, the Performance Grade was determined in accordance to AASHTO M320, 2010. As a fresh binder a traditional 50/70 Pen binder was used. The properties of the two binders are summarized in Table 8.

Table 8. *Characteristics of the extracted and virgin binder*

	Penetration at 25°C [1/10 mm]	Softening Point [°C]	Fraass Braking Point [°C]	Viscosity at 135°C [mPa s]	PG
Extracted RAP binder	18.6	65	-8	550	82-22
Virgin binder 50/70	55.3	49.8	-8	285	70-22

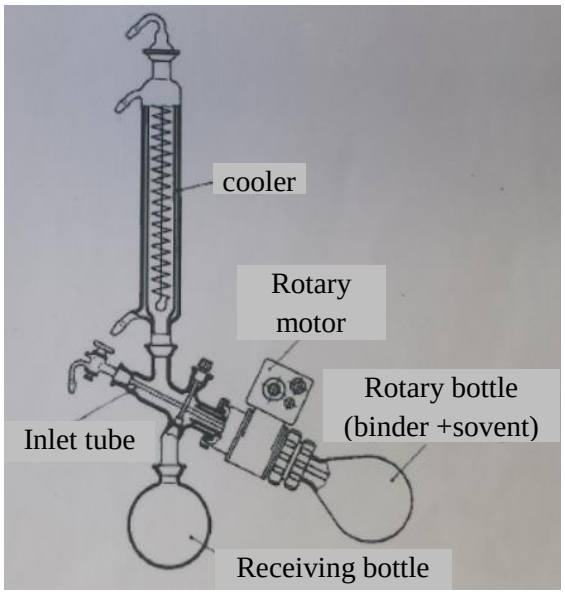

Fig. 27 *Extraction of the RAP binder using the Rotary evaporator.*

With the German RAP source, four different asphalt mixtures were produced, by mixing RAP materials with new aggregates and fresh binder in various volume proportions (0%, 20%, 35% and 50%). In this case, bituminous blends and SRAP mortars with the same proportion of fresh and RAP binder present in the mixtures were produced.

The compositions of the blends are reported in Table 9.

Table 9. *Composition of the bituminous blends.*

Bituminous Blends	Fresh binder	RAP binder
50/70+20%RAP	80.5%	19.5%
50/70+35%RAP	65.8%	34.2%
50/70+50%RAP	51.1%	48.9%

Considering that the fine fraction of the RAP passing sieve with an opening size of 0.149 mm, contains 14.95% of RAP binder respect to the aggregate and the BSRAP have a density of 2.751 g/cm^3, SRAP mortar with the composition reported in Table 10 were produced in order to recreate the same amount of fresh and RAP binder in the mixtures and in the bituminous blends.

Table 10. *Composition of the SRAP mortars.*

SRAP mortars	V_p	SRAP	Fresh binder	RAP binder in the mortar	Total binder
SRAP 20%RAP	29	61.8%	38.2%	9.24%	47.4%
SRAP 35%RAP	42	77.7%	22.3%	11.61%	33.9%
SRAP 50%RAP	51	86.5%	13.5%	12.93%	26.5%

Moreover, BSRAP mortars with the same volumetric composition of the SRAP mortars, as explained in chapter 3.2, were produced. The compositions of the BSRAP mortars are reported in Table 11.

Table 11. *BSRAP mortars compositions*

BSRAP mortars	V_p	BSRAP	Fresh binder
BSRAP 20%RAP	29	52.6%	47.4%
BSRAP 35%RAP	42	66.1%	33.9%
BSRAP 50%RAP	51	73.6%	26.4%

Frequency and temperature sweep tests were performed on binders, BSRAP and SRAP mortars. The plate-plate geometry was used, but in this case, three different dimensions of the plate were adoperated, in order to enlarge the spectrum of the reduced frequency and to verify the capability of the procedure at very low and high temperatures.

In particular, the 4 mm plate was used for temperatures between -30°C and +10°C; the 8 mm for temperatures between -10°C and +40°C and 25 mm for temperatures between +30°C and +80°C.

The tests were performed in stress controlled mode for low temperatures and in strain controlled mode for high temperatures. The different stress and strain levels adopted in order to remain in the LVE are summarized in Table 12.

Table 12. *Stress and Strain levels adopted for the different materials.*

Material	**4 mm**	**8 mm**	**25 mm**
50/70 fresh binder	σ=50 kPa	σ=1 kPa	γ= 1% from 30 to 50°C γ= 1.5% from 50 to 80°C
50/70+20%RAP			
50/70+35%RAP			
50/70+50%RAP	σ=100 kPa		γ= 0.5% from 30 to 50°C γ= 1.5% from 50 to 80°C
RAP binder	σ=100 kPa		
SRAP 20%RAP	σ=50 kPa	σ=10 kPa	γ= 0.5%
SRAP 35%RAP	σ=100 kPa	σ=1 kPa	γ= 0.05%
SRAP 50%RAP	σ=50 kPa		γ= 0.005%
BSRAP 20%RAP	σ=50 kPa	σ=10 kPa	γ= 0.5%
BSRAP 35%RAP	σ=100 kPa	σ=1 kPa	γ= 0.05%
BSRAP 50%RAP	σ=50 kPa		γ= 0.005%

The same DSR tests were also performed on RTFO aged binders and mortars. The master curves of the binders are reported in Figure 28, and those of the BSRAP and SRAP mortars are reported in Figure 29 and 30, respectively. All the parameters of the master curves are summarized in Annex 1.

As shown in the following figures, the stiffening effect due to the presence of the aged binder and due to particles addition is significant. In particular, the SRAP mortar with 50% RAP presents significant larger complex modulus and lower phase angle with respect to the corresponding BSRAP mortar; this is due to the stiffening effect of the aged binder contained in SRAP.

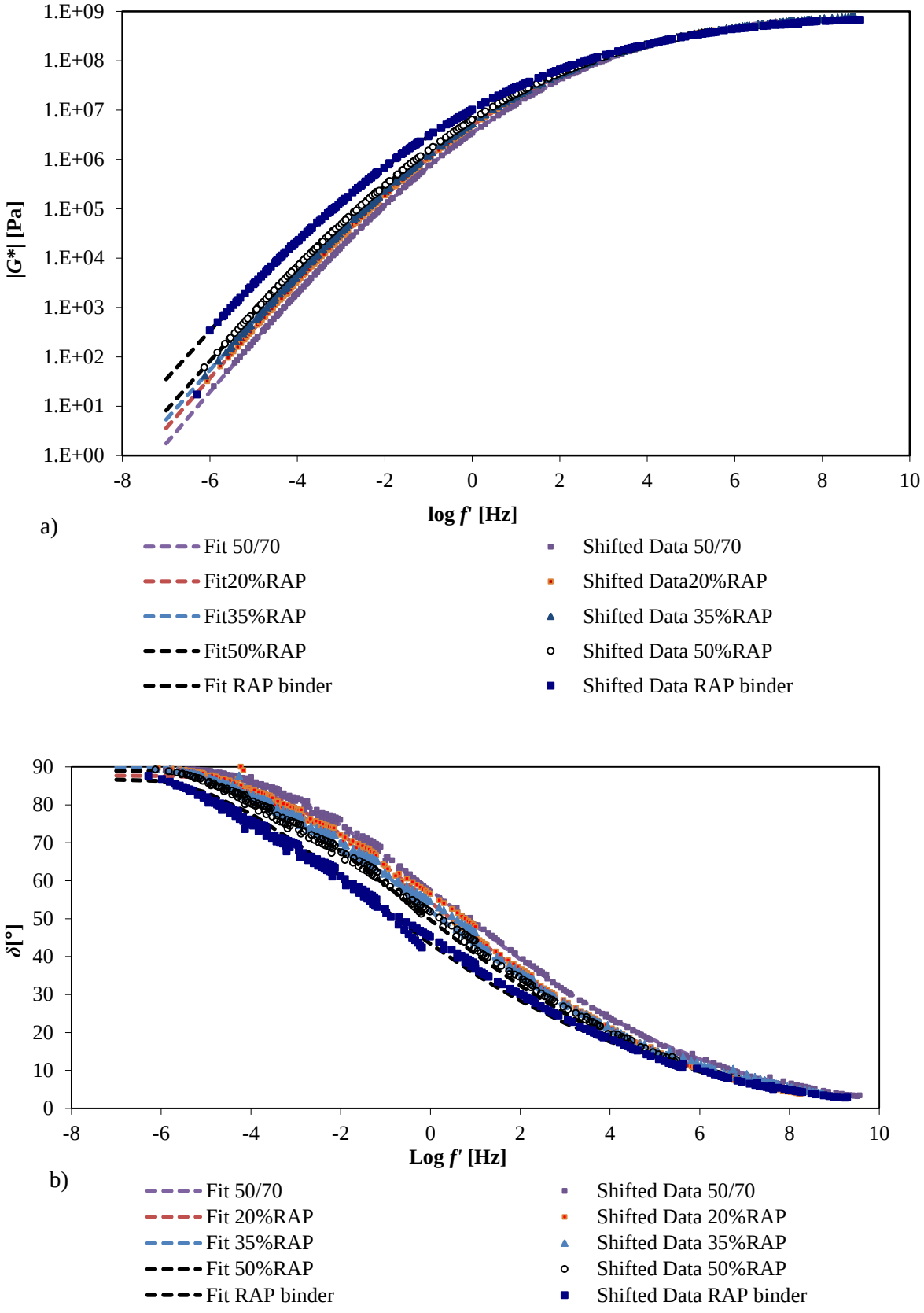

Fig. 28 *Master curves a) of the Complex modulus b) of the phase angle of the binders.*

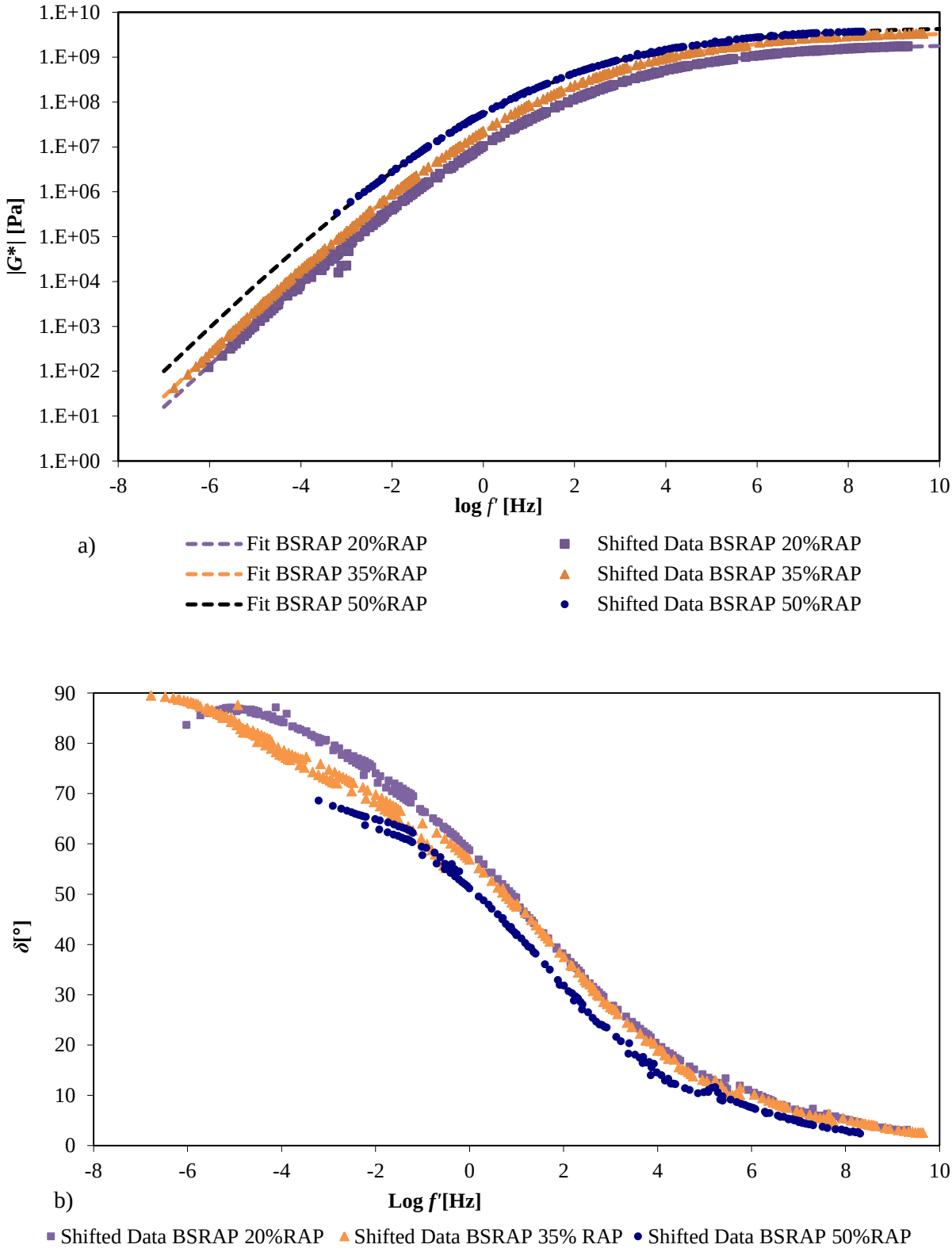

Fig. 29 *Master curves a) of the Complex modulus b) of the phase angle of the BSRAP mortars.*

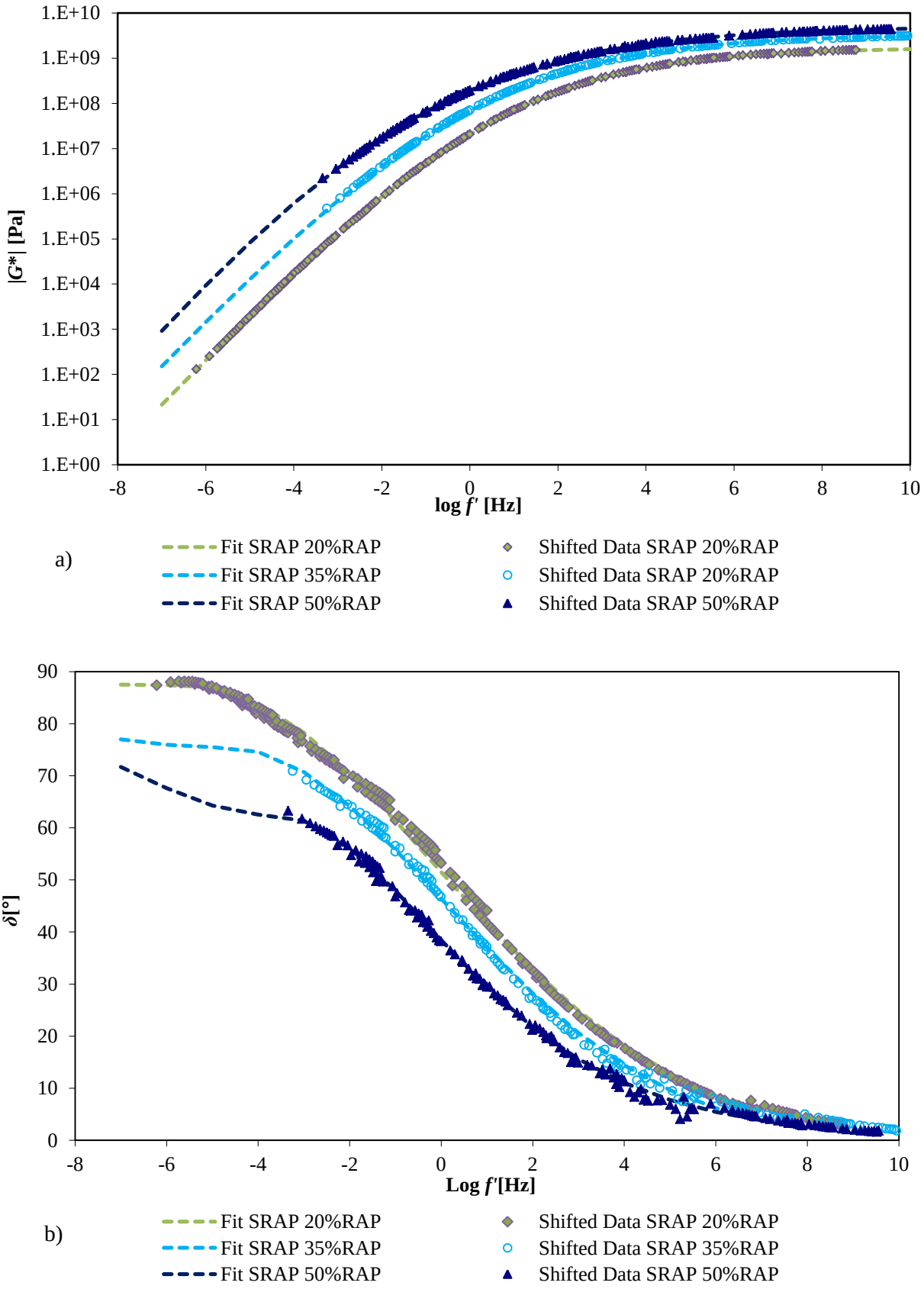

Fig. 30 *Master curves a) of the Complex modulus b) of the phase angle of the SRAP mortars.*

3.1.3 Practical application of the procedure

The modelling part is divided in three steps:

1. The calibration of the Nielsen model using the BSRAP data;
2. The application of the Nielsen model to SRAP data in order to back-calculate the complex modulus of the bituminous blends composed by fresh and RAP binder;
3. The application of the Voigt model to separate the contribution of the fresh and RAP binder in the blends and therefore back-calculate the rheological properties of the RAP binder;
4. The comparison between the back-calculated properties of the RAP binder and the measured one on the extracted RAP binder.

3.1.3.1 Calibration of the Enhanced Nielsen model parameters on BSRAP mortar

The model parameters of Equation 11 were calculated using the results of the DSR tests conducted on BSRAP mortars together with the properties of the component materials. The maximum volumetric packing fraction, φ, was first calculated as the ratio between the maximum volumes of aggregate particles obtained using the Rigden Voids apparatus and the apparent volume of aggregate particles determined in accordance to EN 1097-7 (2008). The average value of the particle maximum density, ρ_{cp}, was determined on three specimens of the compacted particles (Table 13). Therefore, knowing the apparent density of the particles, summarized in Table 13 for the different materials, the maximum volumetric packing fraction, φ, for the different materials was estimated and it results in very close agreement with literature values (Nielsen, Landel, 1994).

Table 13. *Parameters for the calculation of the maximum volumetric packing fraction.*

Materials	ρ_{cp} [g/cm^3]	ρ_{rd} [g/cm^3]	φ
Artificially aged mortars	1.727	2.735	0.631
Italian RAP sources	1.719	2.708	0.634
English RAP sources	1.757	2.837	0.620
German RAP sources	1.785	2.751	0.650

The parameters φ and A were determined by non linear curve fitting the Master Curve data of the different percentage of BSRAP mortars to Equation 11, let the parameter A to vary with the reduced frequency and fixing a single value for φ.

The parameter φ resulting from the fitting are summarized in Table 14 for the different materials, it can be observed that the value of φ from the fitting is lower than the value obtained using the Rigden

Voids apparatus, indicating that filler does not behave in asphalt like it does in air as previous researchers have demonstrated (Shashidhar et al., 1999).

Table 14. *Maximum volumetric packing fraction from the fitting of Equation 11.*

Materials	φ
Artificially aged mortars	0.59
Italian RAP sources with:	
70H+30S	0.65
80H+20S	0.64
90H+10S	0.64
English RAP sources	0.69
German RAP sources	0.56

The parameter *A* was found to vary linearly with the reduced frequency (f') as reported in Figure 31 for the artificially aged mortars as an example. A decreasing trend of *A* versus f' was found, which is in accordance with the pattern of the complex Poisson's ratio, ν^*, versus reduced frequency confirming that *A* depends on ν^*. Similar linear trends were found also for the other RAP sources. The parameters *A* for all the other RAP sources are reported in Table 15 versus the reduced frequency.

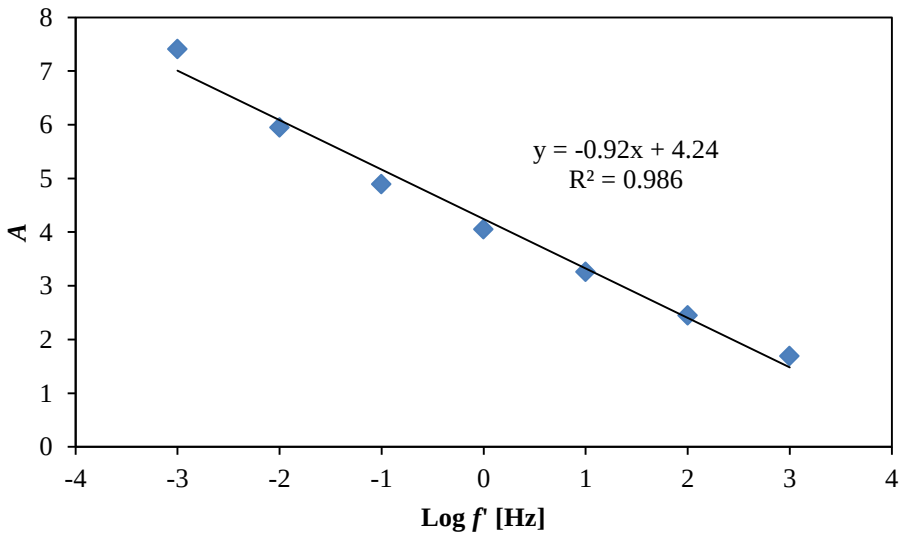

Fig. 31 *Parameter A of Equation 11 versus log reduced frequency.*

Table 15. *Parameters A and B of the Nielsen model (Equation 11) for the different RAP sources.*

RAP source		*Log f'*	*A*	*B*
Italian	70H+30S+BSRAP	-3	9.31	1,00
		-2	8.51	1.00
		-1	7.72	1.00
		0	6.91	1.00
		1	6.03	1.00
		2	5.13	0.99
		3	4.24	0.99
	80H+20S+BSRAP	-3	16.93	1.00
		-2	15.15	1.00
		-1	13.14	1.00
		0	10.99	1.00
		1	8.90	1.00
		2	7.07	0.99
		3	5.61	0.98
	90H+10S+BSRAP	-3	15.69	1.00
		-2	13.06	1.00
		-1	10.49	1.00
		0	8.12	1.00
		1	6.10	1.00
		2	4.51	0.99
		3	3.35	0.98
English		-3	15.26	1.00
		-2	12.93	1.00
		-1	10.94	1.00
		0	9.06	1.00
		1	7.18	1.00
		2	5.42	0.99
		3	3.97	0.98
German		-3	5.09	1.00
		-2	3.64	1.00
		-1	2.78	1.00
		0	2.18	1.00
		1	1.65	1.00
		2	1.09	0.99
		3	0.53	0.98

3.1.3.2 Extension of the calibrated Enhanced Nielsen model to SRAP mortars

The Nielsen model was then applied on SRAP mortars. In fact, BSRAP and SRAP mortars share the same aggregate particles and, hence, both have the same aggregate skeleton. Based on this consideration, the stiffening effect of aggregate particles is the same and, therefore, the parameters of the Nielsen model obtained on BSRAP mortars can be used also for SRAP mortars.

This consideration was verified on artificially aged mortars, on the English RAP mortars and on the German RAP mortars comparing the stiffening ratio $|G_m^*/G_b^*|$ of the measured complex modulus of BSRAP and fresh binder and of the measured complex modulus of SRAP and the corresponding blend. For the artificially aged mortars and for the English one, the higher differences between the stiffening ratio of BSRAP and SRAP mortars are around 20% at 40°C, while for the German RAP source the differences are around 50% at high temperature (from 60°C to 80°C) and high V_p, but in the range of intermediate and low temperatures (from -30°C to +40°C) the maximum error observed is around 20%. These big differences at high temperature may be due to the RAP source itself, since the German RAP binder was a modified asphalt binder.

Consequently, the complex modulus of the bituminous blend $(G^*_b)_{SRAP}$ composed by the fresh and the artificially RAP binder can be calculated using the results of the DSR tests on SRAP mortars and the Nielsen model. In Figure 32, the master curves of the bituminous blends obtained using this procedure were compared to the master curves measured directly with the DSR. In Figure 32a are reported the complex modulus of the bituminous blends predicted using the Nielsen model, considering the equation of the master curves of the SRAP data, versus the measured values. As shown in Figure 32a, the errors for the artificially aged mortars are in the range of 15 and 18%; while, the errors for the English RAP source are in the range of 9 and 24% (Figure 32b); and for the German RAP sources are in the range of 2% for the lower of RAP and 27% for the highest percentage of RAP (Figure 32c).

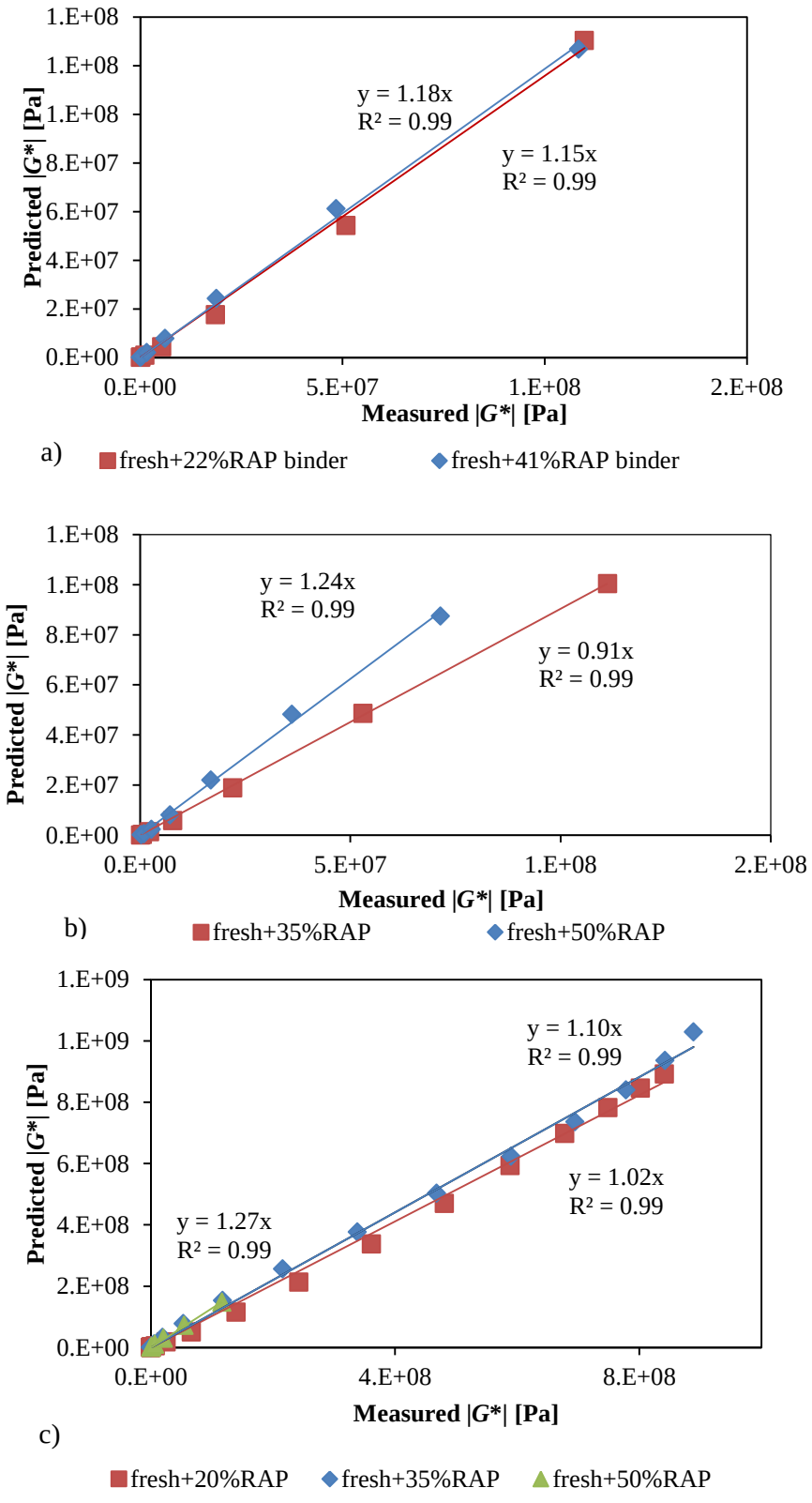

Fig. 32 *Predicted versus measured complex modulus of the bituminous blends composed by fresh and RAP binder a) artificially aged mortars; b) English RAP mortars; c) German RAP mortars.*

3.1.3.3 Application of the Voigt model to estimate the rheological properties of RAP binder

Furthermore using the simple Voigt model, described previously in Chapter 2, and assuming that the phases 1 and 2 correspond to the fresh and RAP binder, respectively, the rheological properties of the RAP binder can be easily calculated as:

$$G^*_{RAPbinder} = \frac{(G^*_b)_{SRAP} - G^*_F V_F}{V_{RAPbinder}} \quad [23]$$

Where G_F^*, $G^*_{RAP\ binder}$ and $(G^*_b)_{SRAP}$ are the complex moduli of the fresh binder, of the RAP binder, and of the blend of fresh and RAP binder, respectively; and V_F and $V_{RAPbinder}$ are the percentages of the fresh and of RAP binder. In Figure 33 are reported the predicted data of the artificially aged binder, of the English and German RAP binder, applying the Voigt model to the Master curves data, versus the Master curve data obtained from directly measured data.

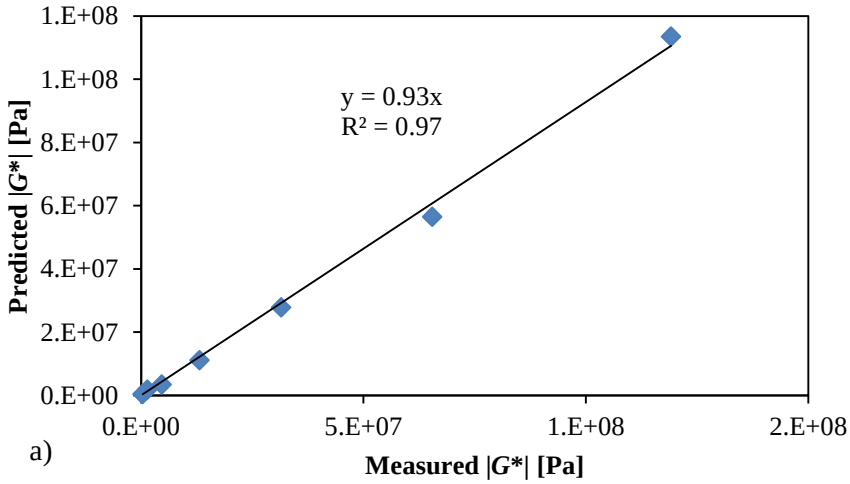

a)

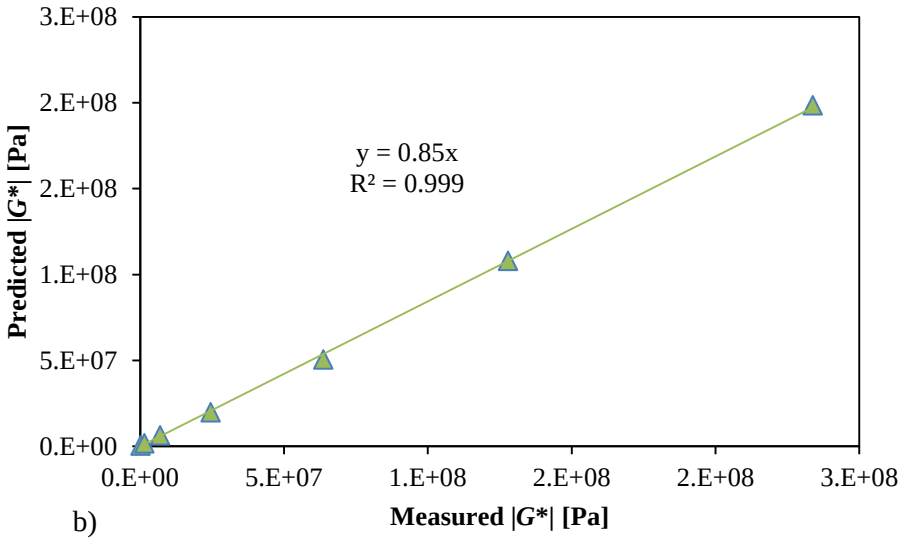

b)

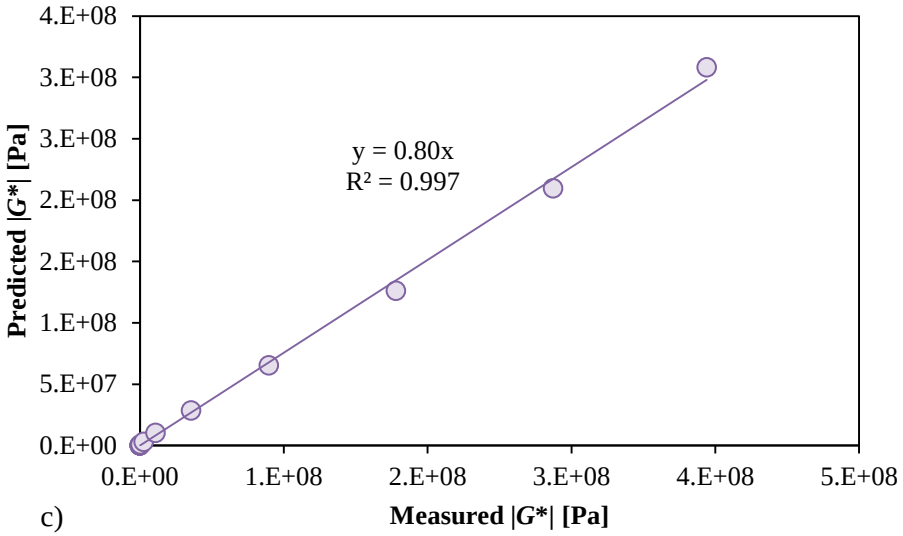

c)

Fig. 33 *Predicted versus measured complex modulus a) of the artificially RAP binder; b) of the English RAP source; c) of the German RAP source.*

According to studies by Christensen (1969) and Hashin (1970), the phase angle of a composite material is theoretically equal to that of the material matrix. Based on this consideration, the phase angle master curve of the SRAP mortar can be used also for estimating the phase angle of a blend of fresh and RAP binder. The phase angle of the artificially RAP binder can then be obtained through Equation 24:

$$(tan\delta_b)_{SRAP} = \frac{V_F tan\delta_F + V_{RAPbinder}\frac{G'_{RAPbinder}}{G'_F} tan\delta_{RAPbinder}}{V_F + \frac{G'_{RAPbinder}}{G'_F} V_{RAPbinder}} \quad [24]$$

Where $(tan\delta_b)_{SRAP}$, $tan\delta_F$ and $tan\delta_{RAPbinder}$ are the loss tangent of the bituminous blends (fresh and RAP binder), of the fresh binder and of the RAP binder, respectively; $G'_{RAPbinder}$ is the real part of the complex modulus of the RAP binder equal to ($G^*_{RAPbinder} \times \cos\delta_{RAPbinder}$); and G'_F is the real part of the complex modulus of the fresh binder. Therefore, the only unknown in Equation 24 is the phase angle of the RAP binder that can be calculated using the Levenberg-Marquardt's algorithm (Levenberg, 1944; Marquardt, 1963). In Figure 34 the predicted phase angle using Equation 24 is reported versus the measured values.

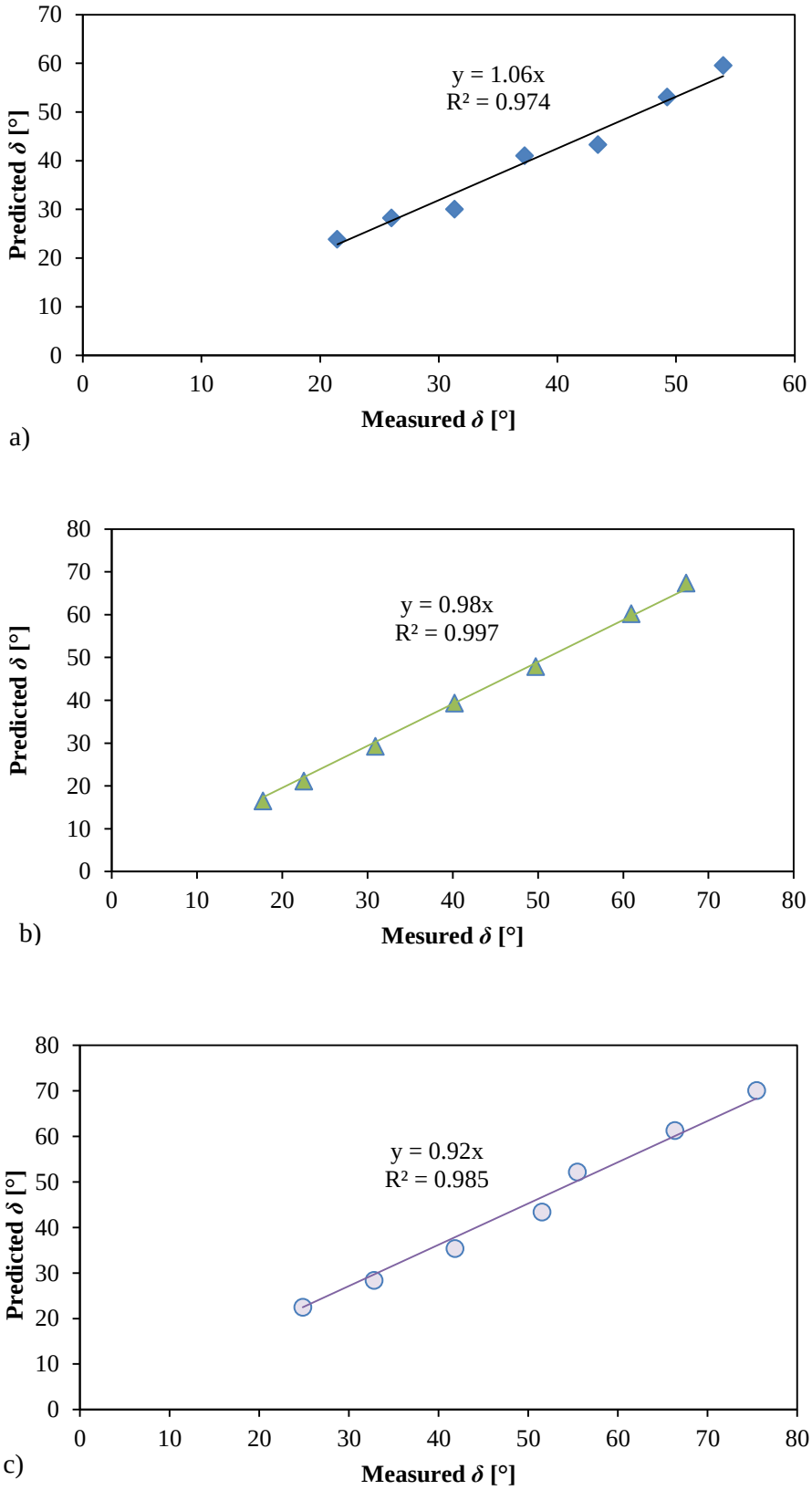

Fig. 34 *Measured versus back-calculated phase angle of a) the artificially RAP binder; b) the English RAP source; c) the German RAP source*

3.1.3.4 Global validation of the procedure

First, the strong hypothesis that the stiffening ratio remains approximately the same, passing from BSRAP to SRAP mortars is verified. In Table 16, the stiffening ratios of BSRAP and SRAP for the artificially aged mortars are summarized with the error percentage between them. As shown, the errors are smaller in the range of lower volume fraction of aggregate particles.

Table 16. *Stiffening ratio of artificially aged BSRAP and SRAP mortars.*

	V_{p35}			V_{p50}		
Reduced frequency	$\lvert G_m^*/G_b^* \rvert_{BSRAP}$	$\lvert G_m^*/G_b^* \rvert_{SRAP}$	Error %	$\lvert G_m^*/G_b^* \rvert_{BSRAP}$	$\lvert G_m^*/G_b^* \rvert_{SRAP}$	Error %
-3	6.00	6.79	11.88	22.91	18.50	-23.6
-2	5.70	6.16	7.51	19.17	16.12	-18.8
-1	5.38	5.52	2.61	16.49	13.93	-19.1
0	5.00	4.89	-2.49	14.38	11.68	-23.1
1	4.56	4.24	-7.72	12.35	97.42	-26.9
2	4.09	3.59	-14.1	10.22	8.07	-26.7
3	3.66	2.94	-24.4	8.24	6.74	-22.4

Furthermore, in order to verify the use of the Nielsen model on SRAP data, the master curves of the complex modulus of the bituminous blends composed by fresh and RAP binder back-calculated were compared with those directly measured on the bituminous blends as shown in Figure 32.

Moreover, the hypothesis that the phase angles of the bituminous blends are the same of the corresponding material (Christensen, 1969 and Hashin, 1970) was verified. In Figure 35, as an example, the phase angle master curves of the bituminous blend composed with 70/100+22% artificially aged binder is compared to the master curve of the corresponding mortar.

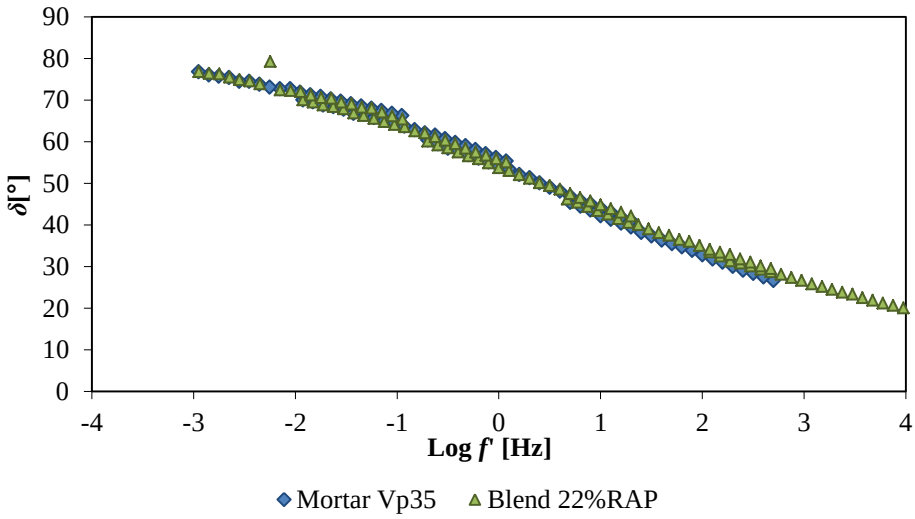

Fig. 35 *Phase angle master curves of the bituminous blend and of the corresponding mortar*

Finally, the use of the Voigt model to estimate the rheological properties of RAP binder was verified.

In particular, the Voigt model was applied on the bituminous blends in order to back-calculate the complex modulus and the phase angle of the artificially aged binder. The back-calculated master curves of the artificially RAP source were then compared to the master curves measured and the good agreement between measured and back-calculated values can be observed in Figure 36 and 37 for the complex modulus and for the phase angle respectively.

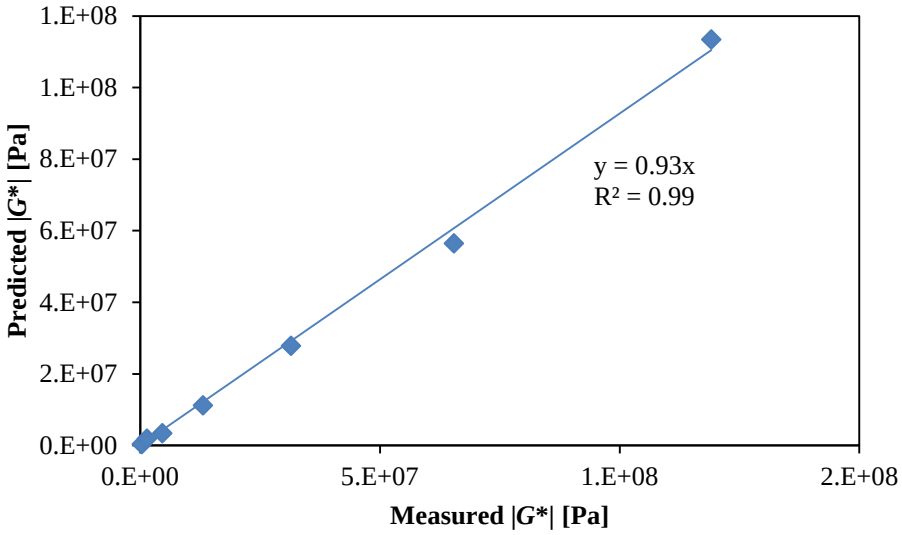

Fig. 36 *Predicted versus measured complex modulus of artificially aged binder.*

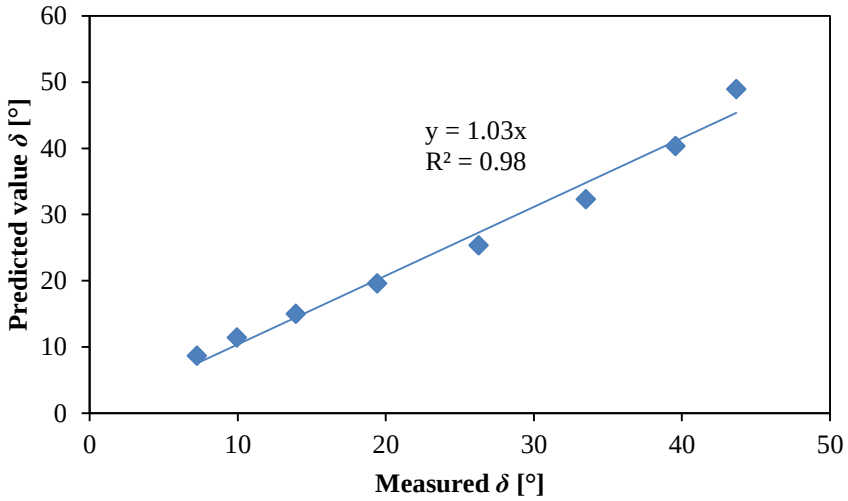

Fig. 37 *Predicted versus measured phase angle of artificially aged binder*

Moreover, in order to further validate the use of the Voigt model, it was also applied to the German RAP source. Starting from the rheological properties of the fresh and of the extracted RAP binder, the complex modulus and the phase angle of the bituminous blends were back-calculated and compared to those measured as shown in Figure 38 and 39 respectively.

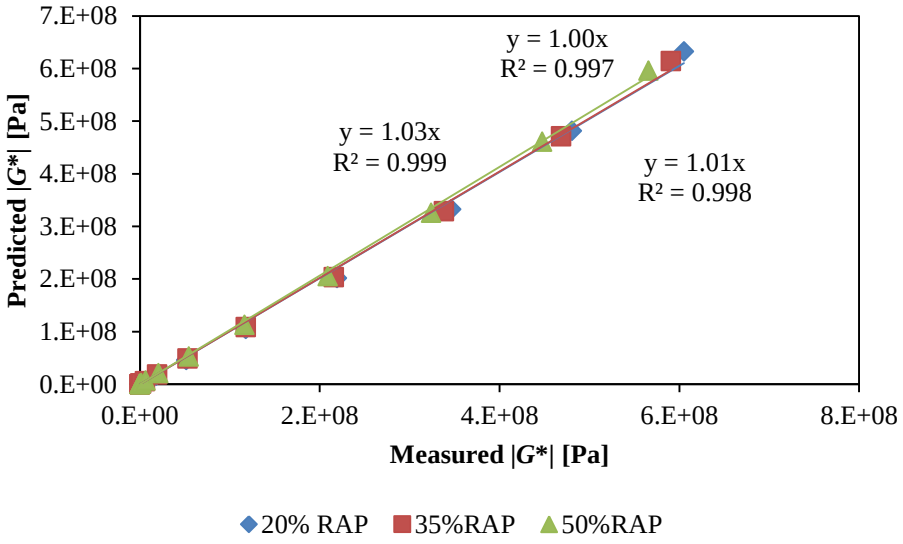

Fig. 38 *Predicted with the Voigt model versus measured complex modulus of the bituminous blends of the German RAP source.*

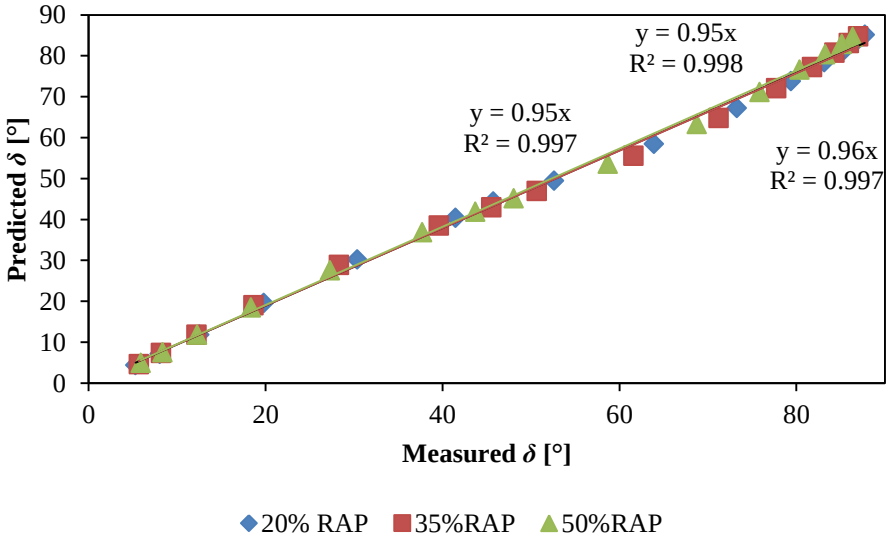

Fig. 39 *Predicted with the Voigt model versus measured phase angle of the bituminous blends of the German RAP source.*

The highest differences of the complex modulus between the measured and predicted value with the Voigt model for the bituminous blends of the German RAP source are in the range of high temperatures (above 40°C corresponding to a log reduced frequency of -2). Therefore, the Arrhenius model reported in Equation 19 was used to predict the complex modulus of the bituminous blends and a very good agreement between measured and back-calculated values are observed as shown in Figure 40. Similar results were obtained using the RTFO aged blends.

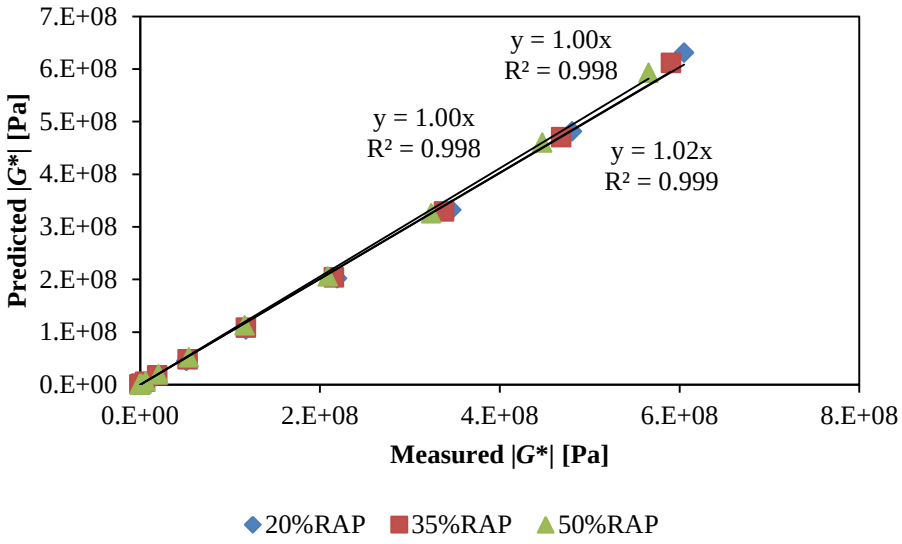

Fig. 40 *Predicted with Arrhenius equation versus measured complex modulus of the bituminous blends of the German RAP source.*

Therefore, the Voigt model can be used until 40°C and for higher temperature it is more suitable to use the Arrhenius equation.

3.1.3.5 Application of the procedure to Italian RAP source

As explained before, BSRAP and SRAP have the same aggregate skeleton. Based on this consideration, the stiffening effect of aggregate particles is the same and, therefore, the parameters of the Nielsen model obtained on BSRAP mortars can be used also for SRAP mortars.

Consequently, the complex modulus of the bituminous blend $(G^*_b)_{SRAP}$ composed by the H, the S and the RAP binder can be calculated using the results of the DSR tests on SRAP mortars and the Enhanced Nielsen model. The complex modulus master curves of the fresh binder (80H+20S) and of the blends of the same fresh binder and three different contents of SRAP binder (6%, 16%, 36%) are reported in Figure 41. The SRAP binder content of 6%, 16% and 36% by weight of total binder (virgin and SRAP binder) corresponds to volume fraction of aggregate particles in mortars of 20%, 40% and 60% respectively.

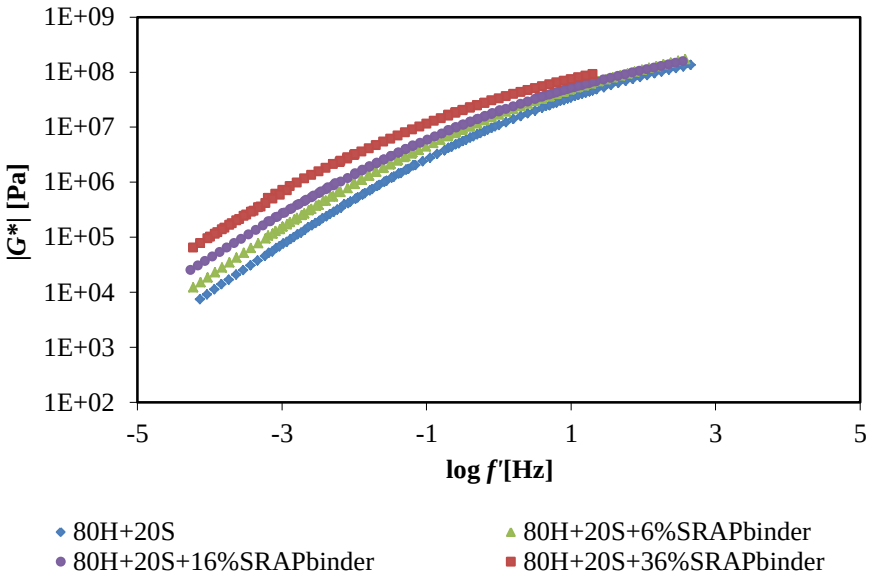

Fig. 41 *Complex modulus master curve of bituminous blends composed by fresh and RAP binder.*

Once the master curves of the bituminous blends are obtained using the Nielsen model, the Voigt model can be used, as explained previously, in order to back-calculate the complex modulus and the phase angle of the RAP binder. As shown in Figure 42, the values of the complex modulus calculated for both the percentages of RAP binder are approximately the same, the mean-squared error between the two series of data is equal to 0.12. Since the complex modulus of RAP binder has to be the same regardless of the percentage in the mortar, these results demonstrate the accuracy of the proposed procedure.

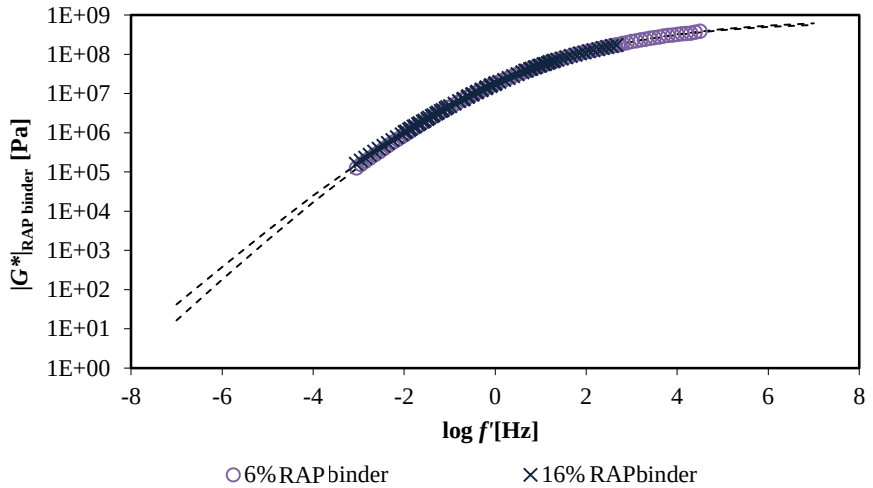

Fig. 42 *Calculated Complex modulus master curves of the RAP binder obtained from two different bituminous blends.*

The phase angle master curve of the RAP binder calculated with Equation 24 for two blends composed with two different percentages of RAP binder (6% and 16%) are reported in Figure 43. Also in the case of phase angle, approximately the same master curve is obtained from the two blends confirming the accuracy and precision of tests and analysis procedure.

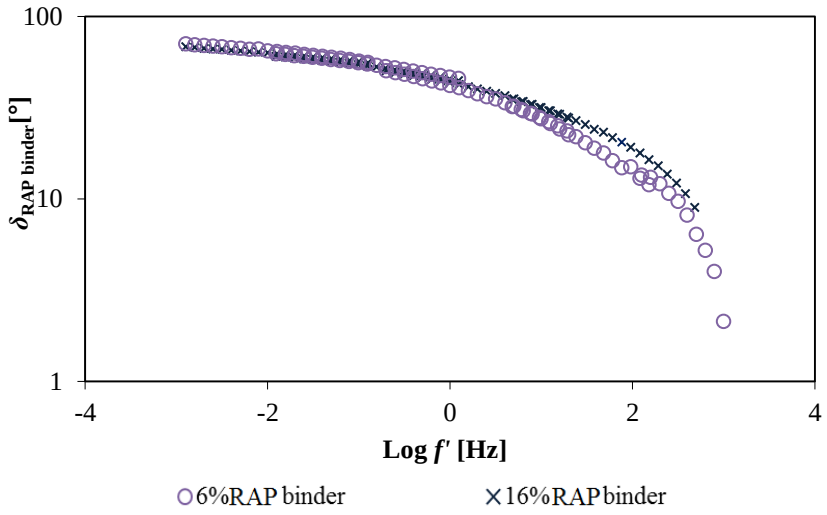

Fig. 43 *Calculated Complex modulus master curves of the phase angle of the RAP binder obtained from two different bituminous blends.*

3.2. Implementation of a new procedure to back-calculate the Performance Grade (PG) of binders from Master Curves

Once, the master curves of the bituminous blends and of the RAP binder are back-calculated, the critical temperatures of these binders can be evaluated. The US specification (AASHTO PP6) defines three critical temperatures:

- High critical temperature, that is the lower between the temperature at which $G^*/\sin\delta$ at 10Hz is equal to 1 kPa on the unaged binder and the temperature at which $G^*/\sin\delta$ is equal to 2.2 kPa on RTFO residue;
- Intermediate critical temperature, that is the temperature at which the parameter $G^*\sin\delta$ at 10 Hz on PAV residue is maximum 5000 kPa;
- Low critical temperature that is the higher temperature between the temperature at which the stiffness *S* at 60 second, measured with the BBR is 300 MPa and the temperature at which the *m-value* is -0.30 measured on PAV residue for the fresh binder and of RTFO residue for the RAP binder.

Regarding the last point, there is a study of the Western Research Institute (Farrar et al., 2016) that allows to determine the Low critical temperature of asphalt binder using the DSR, finding a relationship between the stiffness *(S)* measured with the BBR and the shear relaxation modulus *G(t)* measured with the DSR.

This method follows the guidelines of a previous work by Sui et al., 2011, in which the slope and the magnitude of the shear stress relaxation modulus *G(t)* master curve at 2 hours and at true low PG grading temperature are correlated with the corresponding *S(t)* and *m-value* at 60 seconds and 10°C above the true low PG grade temperature from BBR tests.

In order to reduce the test time and increase the test temperature, the procedure proposed by Sui and co-workers (Sui et al., 2011) was modified measuring the *G(t)* slope and the magnitude at 60 seconds at different low temperatures. In Figure 44 the stiffness *S(t)* at 60 seconds measured at three different temperatures (-12, -18 and -24°C) for five different binders are plotted versus the relaxation modulus *G(t)* in the same conditions.

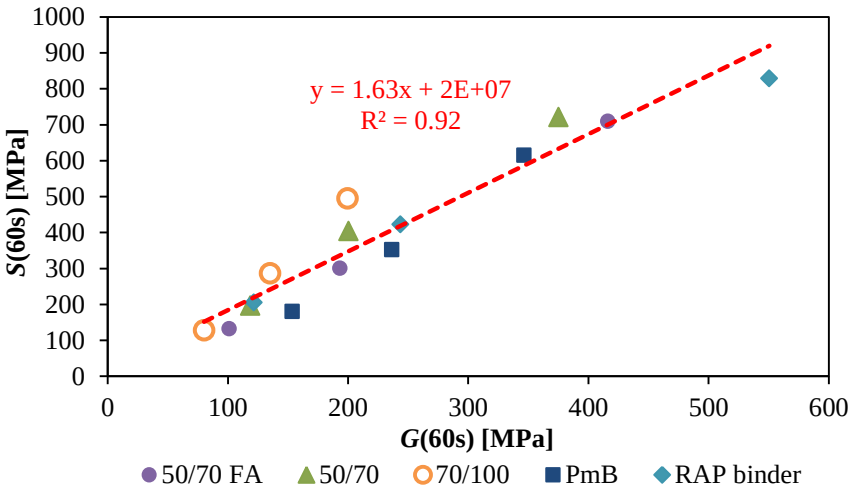

Fig. 44 *Correlation between creep stiffness, S(60s) measured with BBR in ethanol and relaxation modulus G(60s) measured with DSR.*

From the plot shown in Figure 44, the value of *G*(60s) corresponding to *S*(60s)=300 MPa is determined to be equal to 172 MPa. This value can be potentially used as limit to find the low PG when ethanol is used as cooling medium. In Figure 45 the *m-value* of the BBR in ethanol is plotted against the slope of *G*(*t*), called m_r, at 60 second for the DSR, in absolute value.

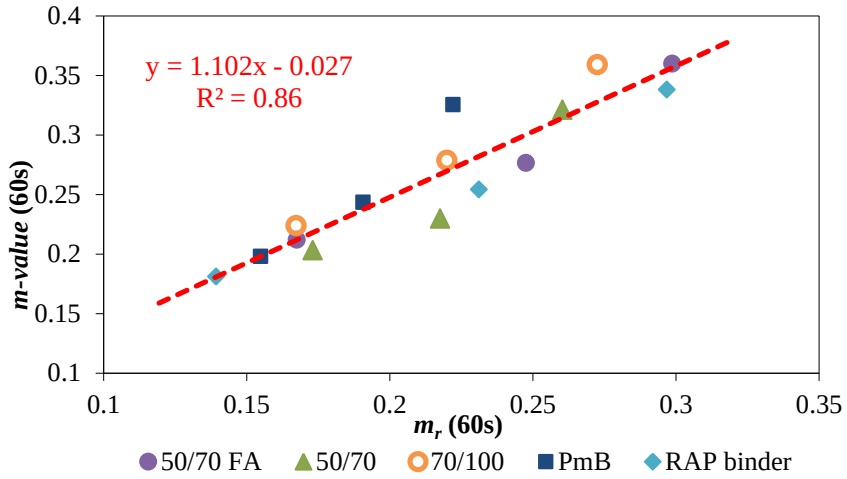

Fig. 45 *Correlation between m-value measured with the BBR in ethanol and m_r-value measured with DSR.*

From this latter plot, the m_r-*value* corresponding to *m-value* of 0.300 is equal to 0.250. As shown a simple linear relationship between BBR and DSR data was obtained. Therefore, using this simple relationship it is easy to estimate stiffness, *S*(*t*) and *m*-value from DSR measurements carried out using the 4 mm plate. In addition, using these correlations at 60 s, it is possible to find the low PG of the binder, based on DSR test results. In fact, the temperature at which *G*(60s) is 172 MPa or m_r-*value* is 0.250 corresponds to the low critical temperature. Therefore, based on Figures 44 and 45, the following simple, linear experimental relationships were obtained for *S*(*t*) and *m*-value, respectively:

$$S(t) = 1.63 \cdot G(t) + 2\mathrm{E} + 07 \quad [25]$$

$$m(t) = 1.102 \cdot m_r(t) - 0.027 \quad [26]$$

3.2.1 High Temperature PG

In order to determine the higher temperature of the PG, the parameters $G^*/\sin\delta$ at 10 rad/s can be calculated using the following procedure (Riccardi et al., 2016b).

The master curves of the fresh binders, of the artificially aged binder and of the extracted English and German RAP binder are considered. The parameters of the master curves, expressed by Equations 20 and 21, are reported in Table 17 for the complex modulus and in Table 18 for the phase angle.

Table 17. *Parameters of the complex modulus Master Curve*

Materials	G^*_e *(Pa)*	G^*_g *(Pa)*	f_c *(Hz)*	k *(-)*	m_e *(-)*
Artificially aged binder	0	$1 \cdot 10^9$	0.175	0.126	0.932
50/70 English	0	$6 \cdot 10^8$	32.381	0.232	1.035
50/70 German	0	$1 \cdot 10^9$	7.719	0.166	1.102
English RAP binder	0	$6 \cdot 10^8$	0.259	0.199	1.056
German RAP binder	0	$1 \cdot 10^9$	0.194	0.145	1.117

Table 18. *Parameters of the phase angle Master Curve*

Materials	δ_m *(°)*	f_d *(Hz)*	R_d *(-)*	m_d *(-)*
Artificially aged binder	57.27	$2.43 \cdot 10^{-5}$	8.513	3.341
50/70 English	81.83	$1.15 \cdot 10^{-3}$	134.33	1035.840
50/70 German	88.95	$3.53 \cdot 10^{-6}$	376.85	4177.820
English RAP binder	85.17	$2.54 \cdot 10^{-6}$	6.165	3.002
German RAP binder	86.60	$3.42 \cdot 10^{-7}$	14.268	7.409

The Williams–Landel–Ferry (WLF) formulation expressed in Equation 3 is used in the model to express the temperature-shift factor a_T. The parameters C_1 and C_2 for the master curves at a reference temperature of 20°C are summarized in Table 19.

Table 19. *Parameters of the WLF equation*.

Materials	C_1	C_2
Artificially aged binder	25.56	190.7
50/70 English	18.80	146.6
50/70 German	17.76	149.4
English RAP binder	27.15	235.8
German RAP binder	20.76	171.2

First of all, the temperature shift factor is determined for three or more different temperatures, as an example 68°C, 76°C, 80°C are considered (Table 20).

Then, the reduced frequency that corresponds to 10 rad/s (1.59 Hz) is calculated and, by using the equations (20) and (21), the complex modulus and the phase angle at 1.59 Hz and at the three different temperatures are calculated; therefore the values of the parameter $G^*/\sin\delta$ are calculated. As an example, Table 20 shows the value for 50/70 German unaged binder.

Table 20. *Parameters to determine $G^*/\sin\delta$*

T [°C]	log a_t	f' [Hz]	G^* [Pa]	δ [°]	$G^*/\sin\delta$ [Pa]
68	-4.80	4.78×10^{-5}	1448	90	1448
76	-5.37	1.43×10^{-5}	448	90	448
80	-5.64	8.11×10^{-6}	255	90	225

A relationship of the parameters $G^*/\sin\delta$ versus temperature can be determined, as reported in Figure 46, and the temperature corresponding to the limit value G*/sinδ > 1000 Pa is determined. Thus, the High temperature PG of the unaged German 50/70 binder is 70.6.

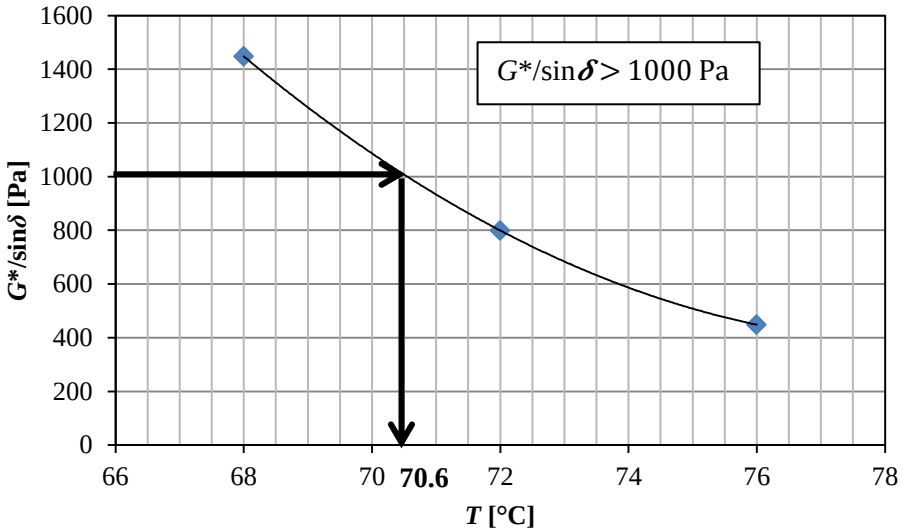

Fig. 46 *G*/sinδ versus temperature for the German 50/70 unaged binder*

The same procedure was also applied on the RTFO residue of the binders and for the 50/70 German binder the temperature at which $G^*/\sin\delta$= 2200 Pa results 69.8 °C. Therefore, the actual high temperature of the PG grade is 69.8°C and the PG is 68.

3.2.2 Low Temperature PG

In order to determine the Low temperature PG, the data from the RTFO and PAV binders and the data of RTFO RAP binder, as reported in NCHRP 452, 2001 are used.

Since the master curves are obtained from DSR frequency sweep tests, an inter-conversion method is applied for converting temperature shear properties to low temperature creep properties. Two different methods are used: the first is the one proposed by Anderson et al., 1994, reported in SHRP 369-A, in which the DSR test conditions that correspond to a user defined BBR loading time and temperature are defined based on the relationship provided in Equation 27:

$$T_d = \left[\frac{1}{273+T_s} - \frac{2.303\,R\log(t_s\omega)}{250000}\right] - 273 \qquad [27]$$

where T_d is the test temperature (°C) for cyclic testing at frequency ω. In the case in exam T_d =10°C can be fixed; T_s is the specified temperature (°C) for creep testing (three different temperatures: -6,

-12, -18°C can be chosen); R is the ideal gas constant, 8.31 J/°K-mol; t_s is the specified creep loading time (60 s), ω is the testing frequency (rad/s).

Therefore, solving Equation 27, the corresponding DSR test conditions were found: the DSR testing temperature is 10°C and the corresponding frequencies ω for the German RAP binder are reported in Table 20.

Using the equations of the master curves of the complex modulus and of the phase angle on RTFO + PAV aged residue, G^* and δ can be calculated at the corresponding reduced frequency, as reported in Table 20.

Therefore, the BBR parameters $S(60)$ and $m(60)$ can be estimated by using the shear properties of the complex modulus and phase angle through application of Equation 28 for the stiffness and 29 for *m-value*.

$$S(t) \approx \frac{3G^*(\omega)}{(1+0.2\sin(2\delta))} \quad [28]$$

where $S(t)$ is the creep stiffness at time t (Pa); $G^*(\omega)$ is the complex modulus at frequency ω (Pa); δ is the phase angle at frequency ω

$$m = \frac{d(\log G^*)}{d(\log \omega)} \quad [29]$$

where m is the slope of G^* vs frequency plot at a given frequency; δ is the phase angle; G^* is the complex modulus; ω is the frequency (rad/s).

All the parameters are summarized in Table 21.

Table 21. *Parameters of the inter-conversion DSR-BBR*

	Temperature °C		
	-6	-12	-18
ω (rad/s)	9.72	129.62	1951.25
log a_t	1.49	1.49	1.49
f' (Hz)	48.27	643.80	9691.52
*G**(Pa)	5.27E+07	1.13E+08	2.09E+08
δ	34.07	27.95	20.26
S(60) (Pa)	1.89E+08	3.84E+08	5.89E+08
m(60)	1.74	0.97	0.70

Interpolating *S(60)* found for the three different temperatures, the low temperature performance grade corresponding to the limit of 300 MPa can be determined. As shown in Figure 47, BBR test

temperature results -9.5°C that corresponds to -19.5°C, therefore the low temperature PG is equals to -16.

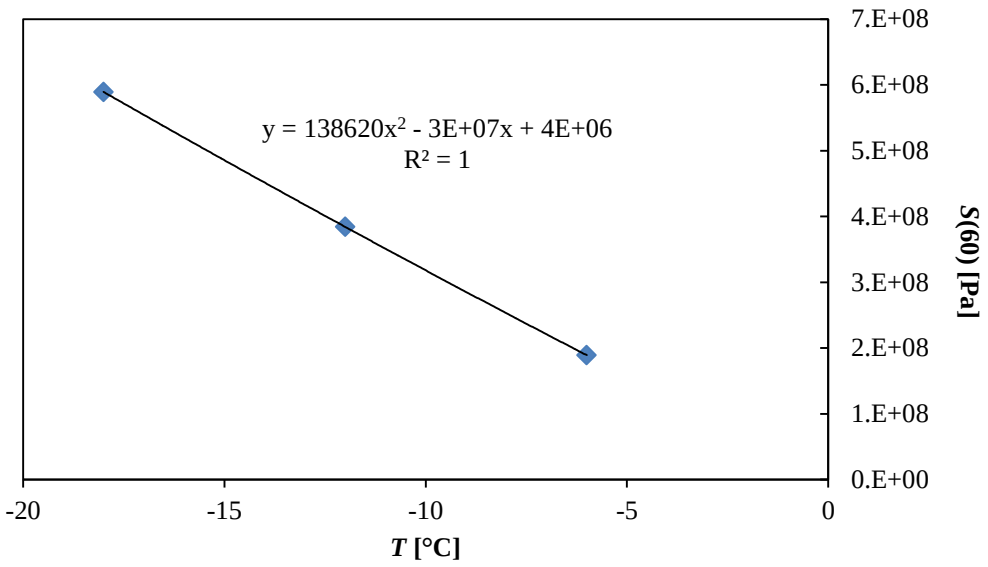

Fig. 47 *S(60) versus temperature for the German 50/70 RTFO+PAV binder*

The actual PG considering the back-calculation procedure proposed is 69.8-19.5 and therefore the PG grade is 68-16. The actual PG grade measured, performing DSR and BBR tests, results 70 – 23.75 and therefore the PG grade is 68-22.

The other method of interconversion between DSR data and BBR results is based on the relationship, explained at the beginning of Chapter 3, between the stiffness *(S)* measured with the BBR and the shear relaxation modulus *G(t)* measured with the DSR.

First of all, the master curves of the storage modulus are plotted at different reference temperatures (-20°C;-10°C; 0°C), then the relaxation modulus *G(t)* is determined by the approximate expression developed by Christensen (1982):

$$G(t) = G'(\omega)|_{\omega=2/\pi t} \qquad [30]$$

In Figure 48 the log of the relaxation modulus versus time for the RTFO+PAV 50/70 German binder at -20°C, is reported. Then, the log of the relaxation modulus versus time is fitted with a 2nd order polynomial function and solving the equation, considering *t*=60 s, the value of *G(60)* can be calculated. The parameter m_r is the slope of the relaxation modulus at 60 s and it is determined taking the first derivative of the 2nd order polynomial function.

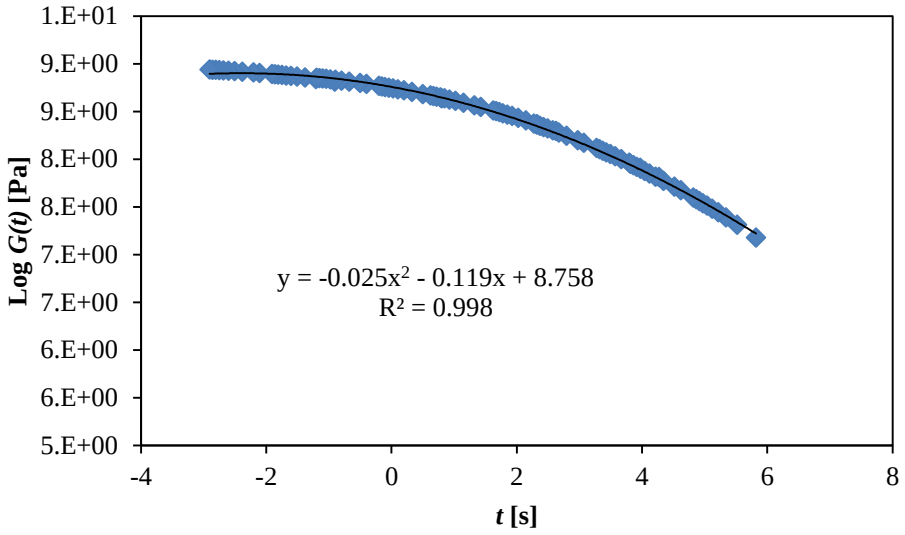

Fig. 48 *Log G(t) versus time for the German 50/70 RTFO+PAV binder*

Once the parameter *G(60)* and m_r at -20°C; -10°C; 0°C are found, fitting the trend of *G(60)* and m_r versus temperature, the critical temperature corresponding to *G(60)*=172 MPa and m_r =-0.25 is found. The low critical temperature of the PG corresponds to the lower one. In the case of the 50/70 German binder RTFO+PAV aged, the critical temperature results -11.6 °C that corresponds to -22.6°C and therefore the low PG results -22.

Summarizing the results, the actual low critical temperature back-calculated with the SHRP 369-A for the German binder results -19.5 and therefore the Low PG results -16, while the actual low critical temperature, back-calculated using the second procedure based on the relaxation modulus, results -22.6°C and therefore the Low PG is -22.

Therefore, the second procedure of back-calculation of the low critical temperature seems to give results in better accordance to the measured value.

Regarding the high temperature PG, the value measured with the DSR results 70°C for the RTFO residue, in accordance to the value obtained from the back-calculation using the master curve that results 69.8°C.

In Table 22 are reported the actual PG measured directly with DSR and BBR on the fresh binder used with the English and German RAP source and on the extracted RAP binders with the actual PG back-calculated using the last procedure based on the relaxation modulus, that is in better accordance to the measured value.

Table 22. *Critical temperature measured and back-calculated.*

Materials	Critical Temperature measured		PG measured	Critical Temperature back- calculated		PG back - calculated
	High	Low		High	Low	
50/70 English	66	-26.00	64-22	64.2	-22.48	64-22
50/70 German	70	-23.75	68-22	69.8	-22.65	68-22
English RAP binder	87	-16.00	82-16	84	-16.48	82-16
German RAP binder	83.85	-22.74	82-22	82.96	-22.15	82-22

As shown in Table 22, a very good prediction of the critical temperatures can be done using the described procedure. There are small differences between the actual critical temperatures but at the end the PG back calculated is the same as the one measured. Therefore, this procedure can be used on the different bituminous blends determined using the Nielsen model and on the RAP binder back-calculated using the Nielsen and Voigt model in order to find the PG of these binders.

3.3 Determination of the maximum amount of RAP that can be added in a mixture without compromising its performance

In this Section, two methods for determining the maximum amount of RAP that can be added to a mixture without compromising its performance are proposed. The first one is based on the use of the blending charts reported in NCHRP 452 (Riccardi et al., 2015); and a second one is a procedure proposed by the author (Riccardi et al, 2016c, d).

3.3.1 Blending charts to determine the maximum amount of RAP

In Figure 49 the flow chart of the procedure adopted to determine the maximum amount of RAP that can be added to a mixture without compromising its performance, based on blending charts, and on tests on mortars is presented (Riccardi et al., 2015).

First, using the procedure described in Chapter 3, the complex modulus and the phase angle of the RAP binder, using the Nielsen and the Voigt model, is back-calculated from tests on mortars, then, the critical temperatures of the RAP binder, using the procedure described previously, are determined and finally using the blending chart the maximum amount of RAP that can be added to the mixture without compromising its rutting, fatigue or thermal cracking performance can be found.

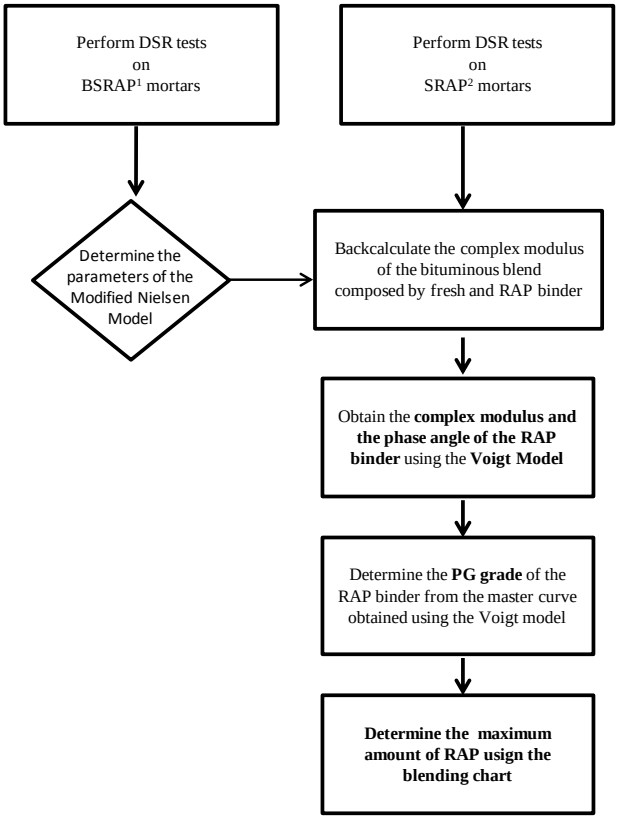

Fig.49 *Flow chart of the procedure to determine the maximum amount of RAP that can be added in a mixture using the blending chart*

In the NCHRP 452, two different approaches can be used:

- *Method A: Blending at a known RAP percentage:*

If the final blended binder grade, percentage of RAP, and RAP binder properties are known, then the properties of an appropriate virgin asphalt binder grade can be determined using the following equation:

$$T_{virgin} = \frac{T_{Blend} - (\%RAP \times T_{RAP})}{(1 - \%RAP)} \quad [31]$$

where T_{Virgin} is the critical temperature of the virgin asphalt binder, T_{Blend} is the critical temperature of the blended asphalt binder (final desired), %RAP is the percentage of RAP expressed as a decimal (i.e., 0.30 for 30 percent); and T_{RAP} is the critical temperature of RAP binder.

- *Method B: Blending at a known Virgin Binder Grade:*

There may be cases in which a particular virgin binder in a RAP mixture should be used. The binder grade may be fixed based on economics and availability or on the specifications for a given project. In these cases, the percentage of RAP that can be used with a specific virgin binder grade and that still meets the final blended binder properties have to be found. Therefore, if the final blended binder

grade, virgin asphalt binder grade, and RAP binder properties are known, then the appropriate amount of RAP can be determined using the following equation:

$$\%RAP = \frac{T_{Blend} - T_{Virgin}}{T_{RAP} - T_{Virgin}} \quad [32]$$

Where T_{Virgin} is the critical temperature of the virgin asphalt binder, T_{Blend} is the critical temperature of the blended asphalt binder (final desired), %RAP is the percentage of RAP expressed as a decimal (i.e., 0.30 for 30 percent); and T_{RAP} is the critical temperature of RAP binder.

3.3.2 Analytical procedure to determine the maximum amount of RAP

The second procedure, summarized in Figure 50, (Riccardi et al., 2015c and 2016 c, d) is based on the fatigue parameter $G^*\sin\delta$ of the bituminous blend of fresh and RAP binder back-calculated from the Nielsen model. A 50/70 Pen grade binder with good fatigue performance was used as a reference material and the value of $G^*\sin\delta$ = 2201 kPa, measured at 25°C and at 10 rad/s was kept as benchmark. Therefore, plotting the parameter $G^*\sin\delta$ versus the percentage of RAP binder is possible to determine the maximum percentage of RAP that can be added in a mixture, that results for the specific study equal to 23.3% (Figure 51).

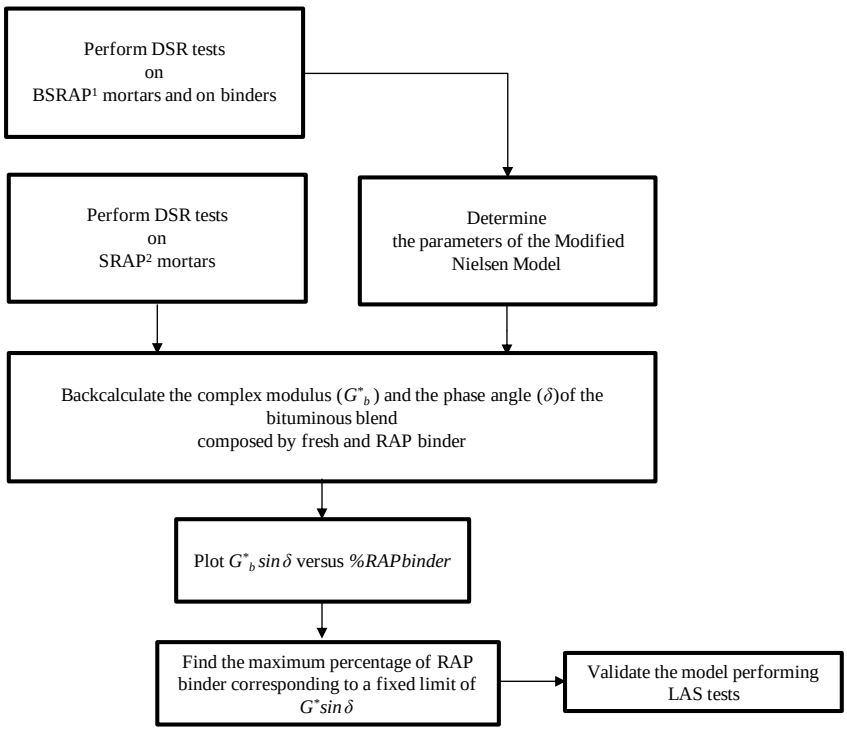

[1] BSRAP: Burned SRAP consists of the aggregate particles contained in the recycled material and obtained through ignition
[2] SRAP : Selected RAP consists of the aggregate fraction passing the # 100 sieve (0.15 mm)
G^*_b: Complex modulus of binder

Fig.50 *Flow chart of the procedure to determine the maximum amount of RAP binder that can be added in a mixture without compromising the fatigue resistance based on binder properties.*

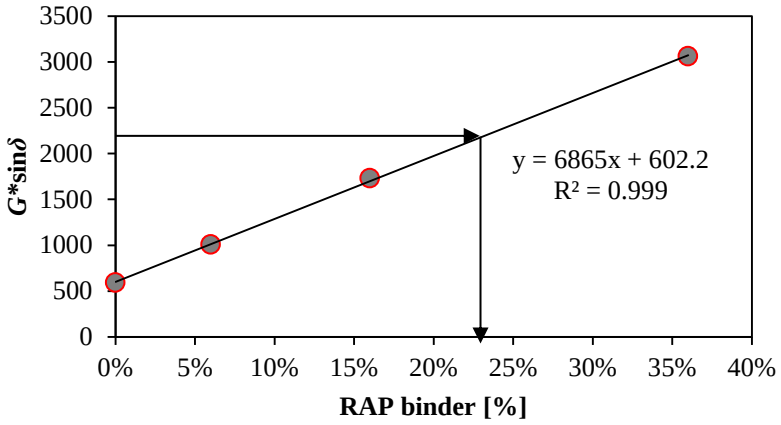

Fig. 51 *G*sinδ* versus RAP binder percentage.

In order to ensure that the imposed limit of *G*sinδ* = 2201 kPa and the maximum percentage of RAP binder found are reasonable, Linear Amplitude Sweep (LAS) tests (AASHTO TP101, 2012) and time sweep tests were performed on RTFO and PAV aged mortar composed by 70H + 30S with 48.7% volume fraction of SRAP materials which corresponds to a mortar with a RAP binder percentage of 23.3%. LAS tests were also performed on RTFO and PAV aged mortars composed of 50/70 pen grade binder and 48.7% volume fraction of BSRAP materials. LAS tests consist in a frequency sweep followed by an amplitude sweep. The frequency sweep test data is used to determine the undamaged material properties, while the amplitude sweep is used to cause accelerated fatigue damage and it allows evaluating the ability of the material to resist to damage (Hintz et al., 2011, Johnson et al., 2010). The continuum damage approach is used to calculate the fatigue resistance from rheological properties and amplitude sweep results. Therefore, from LAS tests results, the fatigue laws (Hintz et al., 2011, Johnson et al., 2010) corresponding to the two mortars were determined; the one of the BSRAP mortar composed of 50/70 binder represents the fatigue law benchmark. It was verified that the fatigue durability of the mortar composed of 70H+30S binder and SRAP materials is reasonably close to the benchmark one, as shown in Figure 52.

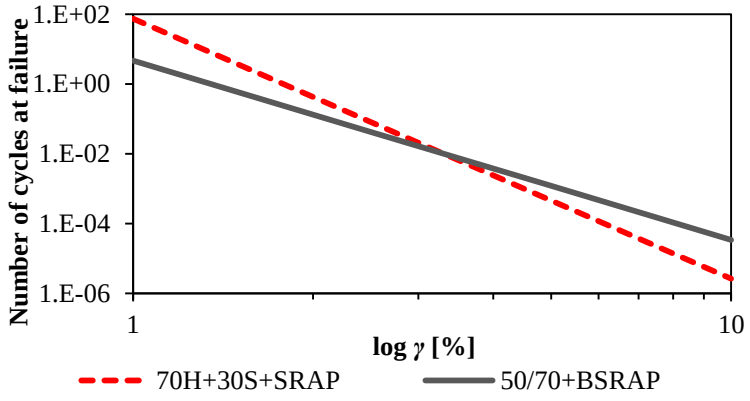

Fig.52 *Fatigue laws of the mortars composed by 70H+30S+SRAP materials and the mortar composed by 50/70+BSRAP*

Another verification was done performing time sweep tests at five different strain levels on RTFO and PAV aged mortars. In Figure 53 are reported the fatigue laws of both mortars determined considering as a failure criteria the 20% deviation from the initial linear trend of Dissipated Energy Ratio (DER) (Martono et al., 2007). As shown, the fatigue law of the 70H+30S+SRAP is above the benchmark fatigue law of the 50/70+BSRAP.

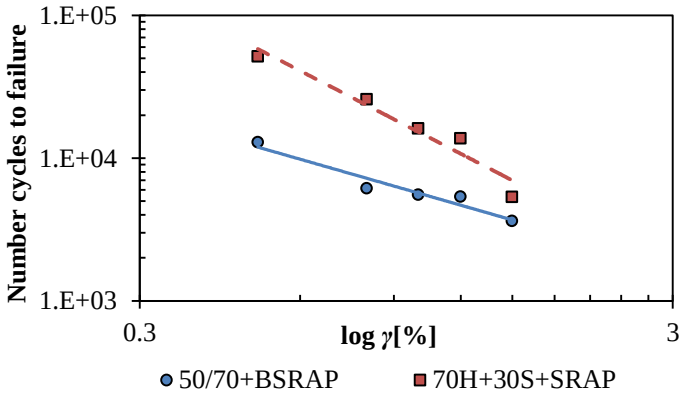

Fig. 53 *Fatigue laws based on time sweep results*

Chapter 4

4. Implementation of the 2S2P1D Model for multiscale modeling of asphalt mixtures

In the present chapter, the 2S2P1D model is used to link the binder, mortar and mixture phases.

As shown in Chapter 1, the SHStS transformation depends upon the parameter α, that links the characteristic time of the binder with that of the mixture. In the present work, relationships between the characteristic time of the binder and of the mortar, and between the characteristic time of the mortar and of the mixture, containing different percentages of RAP materials, were found. Therefore, using the found relationships, from tests on asphalt binder, the complex modulus of the mortar and of the mixture can be back-calculated for any percentages of RAP materials, or starting from tests on asphalt mortars, the complex modulus of the binder and of the mixture can be back-calculated.

4.1 Extension of the 2S2P1D model to binder/mortar (N.2)

In the present study a relationship between the characteristic time of binders and that of mortars is established (Riccardi et al., 2016e). The research approach, summarized in Figure 54, consists in a combination of experiments and modeling. First, a set of asphalt mortars were prepared by mixing five asphalt binders and different types of fillers. Then, asphalt binders and mortars were tested with the Dynamic Shear Rheometer (DSR) to obtain complex modulus and phase angle. The experimental results were then fitted by the analogical 2S2P1D model. A new relationship linking the characteristic time of binder and corresponding mortar depending on the filler content is proposed and used as transformation parameter in the SHStS transformation to evaluate its effectiveness, as well as to verify the SHStS transformation. With this expression, the complex modulus of the mortar can be back-calculated from the complex modulus of the binder.

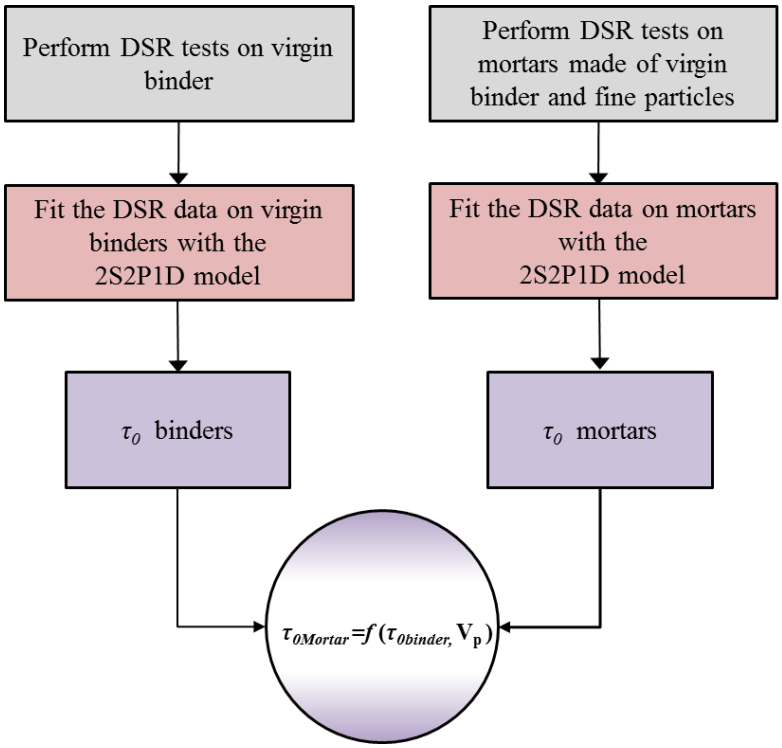

Fig.54 *Research approach*

4.1.1. Materials and Tests

In the present research, five different asphalt binders were selected to prepare asphalt mortar samples. The first and the second binders consisted of virgin unmodified binders having penetration grade 70/100 and 50/70, respectively. The other three asphalt binders were the same used for the Italian RAP source, obtained by mixing hard (H) and soft (S) plain binders with the following proportions: 90%H+10%S; 80%H+20%S; 70%H+30%S.

All asphalt binders were characterized using traditional tests, such as penetration and softening point tests, in agreement with the conventional European grading system (Table 23). Performance Grade (PG) was also determined according to AASHTO standards (Table 23).

Table 23. *Asphalt binders grading*

Binder ID	70/100	50/70	90H+10S	80H+20S	70H+30S
Pen 25°C (dmm)	82	56	44	58	75
Softening point R&B (°C)	45	48	51	47	44
PG	64-28	64-22	64-16	64-16	58-22

A total of twenty different mortars were obtained, mixing the selected five asphalt binders with the following three types of filler at four different percentages (20, 40, 50%, 60% by volume): white

limestone, rose limestone and Burned Selected Recycled Asphalt Pavement (BSRAP) filler. BSRAP consists of finer aggregate (smaller than 150 μm) obtained from recycled asphalt material (RAP) after incineration in the ignition oven, for which all the asphalt binder was completely removed. The white limestone filler and the rose limestone filler were mixed only with the 70/100 and 50/70 pen grade binders, respectively. The BSRAP filler was used together with the different blends of Hard and Soft binders (90H+10S; 80H+20S; 70H+30S.). All the different mortars produced are summarized in Table 24.

Table 24. *Asphalt mortars prepared for the present study*

Binder type	**Filler nature**	**Filler content**
70/100	White limestone	20%, 40%, 50%, 60%
50/70	Rose limestone	20%, 40%, 50%, 60%
90H+10S	BSRAP	20%, 40%, 50%, 60%
80H+20S	BSRAP	20%, 40%, 50%, 60%
70H+30S	BSRAP	20%, 40%, 50%, 60%

Mortars were produced by adding a specific amount of filler, pre-heated at 105°C, to the designed amount of asphalt binder pre-heated at 160°C. Filler was added gradually with a continuous stirring action in order to prevent any formation of lump and cluster, and to achieve a homogenous distribution of the filler particles in the binder.

All these binders and mortars were tested using the DSR performing temperature and frequency sweep, in order to plot the Master curves of the complex modulus and of the phase angle. Amplitude sweep tests were performed in order to find the limits of the LVE, the strains and stresses adopted for the binders are summarized in Table 25 and those used for the mortars are summarized in Tables 26.

Table 25. *Stress and strain levels for the binders for the different DSR testing geometries and temperatures*

Diameter	Temperature range	Stress/Strain
4 mm	-40°C to +10°C	$\sigma=5\cdot10^4$ Pa
8 mm	0°C to +40°C	$\sigma=10^3$ Pa
25 mm	+34°C to +52°C	$\gamma=0.5$ %
	+52°C to +80°C	$\gamma=6$ %

Table 26. *Stress level for mortars at different volume fraction of filler and for different testing temperatures*

V_p	Temperature range	Stress
20	-12°C to +40°C	σ=500 Pa
40	-12°C to +24°C	σ=1000 Pa
	+24°C to +40°C	σ=100 Pa
60	-12°C to +24°C	σ=500 Pa
	+24°C to +40°C	σ=10 Pa

4.1.2 Calibration of the 2S2P1D model

The seven constants of the 2S2P1D model were computed by minimizing the sum of the square of the distance between the experimental complex modulus and the predictions obtained from the model at N points of the pulsation ω.

In order to calibrate all parameters, the same values of k, h and δ were assumed for binders and corresponding mortars, since these parameters depend only on binder source (Olard & Di Benedetto 2003; Di Benedetto et al., 2004; Delaporte, Di Benedetto, Chaverot, & Gauthier, 2007).

Figure 55 provides a comparison between the experimental measurements and the shear modulus, G^*, predicted with the 2S2P1D model in the Cole-Cole diagram for binder 50/70 and the corresponding mortars. As shown in the plot, the model predictions fit reasonably well the experimental data. Similar trends were observed for the remaining asphalt binders and mortars. The entire set of 2S2P1D model parameters are summarized in Table 27 for all binders and corresponding mortars.

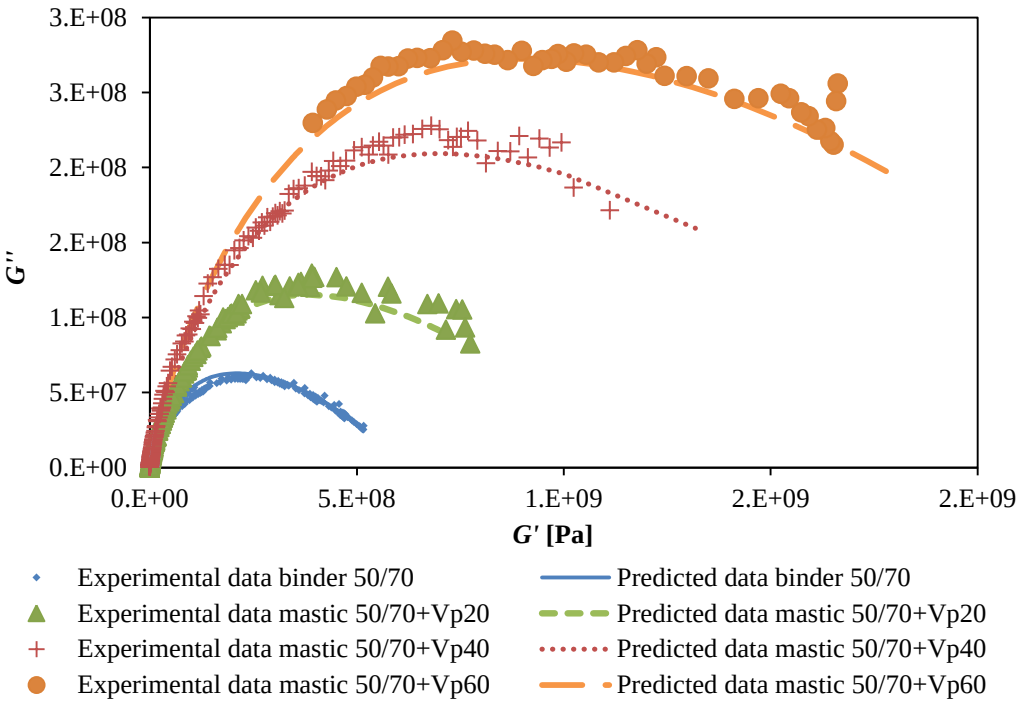

Fig. 55 *Comparison between experimental shear modulus and 2S2P1D model predictions for binder 50/70 and corresponding mortars*

Table 27. *Parameters of the 2S2P1D model for all binders and corresponding mortars*

Material	δ	k	h	G_0(Pa)	G_∞(MPa)	β	$log(\tau_0)$	R^2
50/70 binder	2.05	0.21	0.58	0	600	61	-3.00	0.999
50/70 mastic V_p20	2.05	0.21	0.58	193	1100	60	-2.83	0.998
50/70 mastic V_p35	2.05	0.21	0.58	2000	2000	89	-2.40	0.993
50/70 mastic V_p50	2.05	0.21	0.58	2052	2600	90	-2.03	0.998
70/100 binder	2.60	0.19	0.60	0	600	106	-3.44	0.997
70/100 mastic V_p20	2.60	0.19	0.60	100	1400	150	-3.26	0.998
70/100 mastic V_p40	2.60	0.19	0.60	400	2000	170	-2.19	0.995
70/100 mastic V_p60	2.60	0.19	0.60	3000	3000	200	-2.12	0.998
70H+30S binder	2.61	0.19	0.56	0	600	143	-3.85	0.999
70H+30S mastic V_p20	2.61	0.19	0.56	50	1400	150	-3.74	0.997
70H+30S mastic V_p 40	2.61	0.19	0.56	100	2500	229	-3.38	0.995
70H+30S mastic V_p 60	2.61	0.19	0.56	200	2600	367	-2.95	0.997
80H+20S binder	3.13	0.22	0.56	0	1300	140	-4.32	0.999
80H+20S mastic Vp20	3.13	0.22	0.56	100	1300	200	-4.26	0.999
80H+20S mastic Vp40	3.13	0.22	0.56	200	2500	250	-3.69	0.996
80H+20S mastic Vp60	3.13	0.22	0.56	500	3000	345	-2.82	0.995
90H+10S binder	4.90	0.28	0.65	0	800	43	-2.99	0.999
90H+10S mastic Vp20	4.90	0.28	0.65	200	1300	70	-2.56	0.998
90H+10S mastic Vp40	4.90	0.28	0.65	350	1500	90	-2.22	0.998
90H+10S mastic Vp60	4.90	0.28	0.65	600	2700	100	-1.64	0.996

4.1.3 Relationship between the characteristic times of binder and of mortar

Plotting the characteristic time of the five mortars versus the characteristic time of the corresponding binders for different $V_{p,}$ at T_0= 10°C, the logarithmic linear trends reported in Figure 56 and described by Equation 33 are obtained:

$$log\tau_{0mortar} = log\tau_{0binder} + f \quad [33]$$

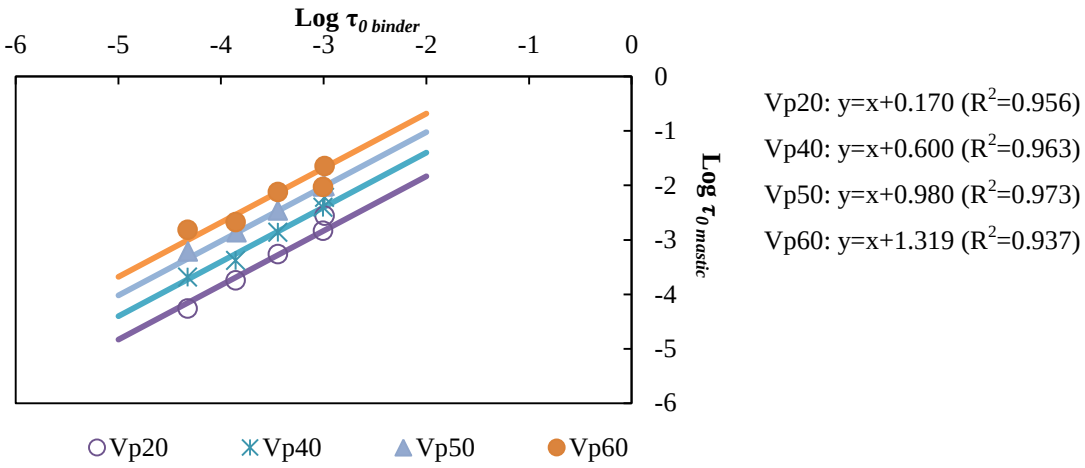

Fig. 56 *Relationship between Log $\tau_{0\ binder}$ and Log $\tau_{0\ mortar}$*

As shown in the plot in Figure 56 the intercept f depends on the volume fraction of filler. A power trend can be observed when plotting f versus V_p as shown in Figure 57 and mathematically expressed by Equation 34.

$$f = \mu V_p^{\sigma} \quad [34]$$

Therefore, by combining Equations 33 and 34 the following expression can be formulated:

$$log\tau_{0mortar} = log\tau_{0binder} + \mu V_p^{\sigma} \quad [35]$$

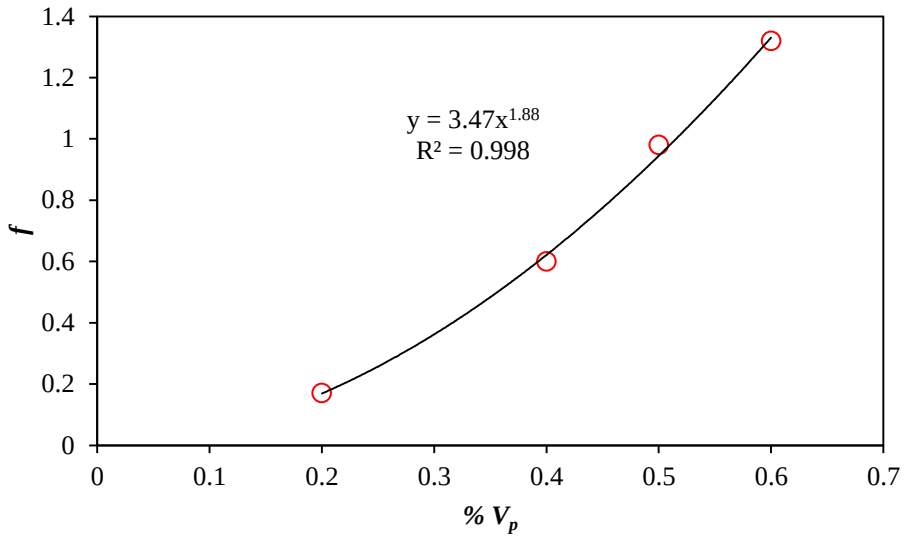

Fig. 57 *Relationship between constant f and the volume percentage of filler*

Equation 35 can be rewritten in exponential form as:

$$\tau_{0\,mortar} = \tau_{0\,binder} \cdot 10^{(\mu V_p{}^{\sigma})} \qquad [36]$$

It is worth noting that parameter f actually corresponds to the SHStS transformation parameter, α, (Olard & Di Benedetto, 2003; Di Benedetto et al., 2004; Delaporte et al., 2007) and, therefore, Equation (36) can be written in the well-known compact form of Equation (37):

$$\tau_{0\,mortar} = \tau_{0\,binder} \cdot 10^{\alpha} \text{ and } \alpha = f = \mu V_p{}^{\sigma} \qquad [37]$$

where μ and σ are two constants which most likely depend on the statistical spatial distribution of the aggregate particles in the mortar and, hence on the associated autocorrelation function (Berryman, 1985; Torquato, 2002; Cannone Falchetto, Montepara, Tebaldi & Marasteanu, 2012 and 2013; Moon, Cannone Falchetto, & Hu, 2014). This assumption seems to be confirmed by a recent research work (Cannone Falchetto & Moon, 2015) in which an explicit expression of parameter α is proposed for asphalt mixture, where the autocorrelation length of all the three material phases (aggregate, mastic and air voids) was taken into account and used to estimate the SHStS transformation parameter.

The identification of the physical meaning of μ and σ will be done in a follow up study.

4.1.3.1 Influence of RAP percentage

In this section the DSR test results on binders, BSRAP and SRAP mortars, composed with the Italian RAP source, were used to find how the percentage of RAP can influence the characteristic time of the 2S2P1D model (Riccardi et. al., 2015b). The effect of SRAP on the properties of asphalt binders and

mortars was evaluated through rheological and analogical models. Specifically, the response of the combined virgin and RAP binders in the mortar was investigated and back-calculated with the new approach based on the enhanced version of the Nielsen model avoiding binder extraction and recovery, explained in detailed in Chapter 3 and published in Leandri et al., 2015, Riccardi et al., 2016. At the same time, the parameters of the 2S2P1D model were estimated both for asphalt mortar and for the back-calculated binder rheological properties. Finally, a new expression linking characteristic time and RAP content was proposed. Figure 58 provides the flow chart of the research approach used in this study.

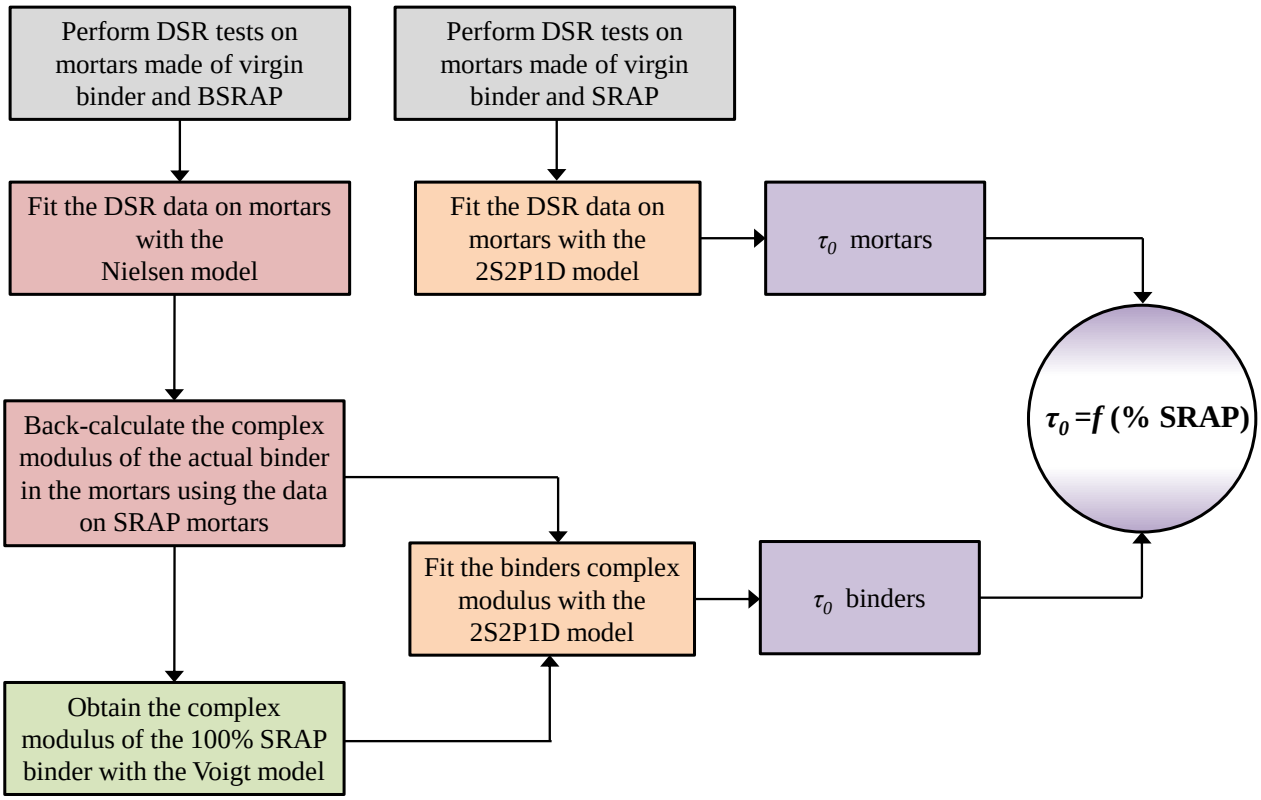

Fig. 58 *Flow chart of the Research approach.*

All the parameters of the 2S2P1D model are summarized in Table 28 for the binders and the corresponding mortars.

Table 28. *Parameters of the 2S2P1D model*

Material	δ	k	h	G_0 (Pa)	G_∞ (MPa)	β	log(τ_0)	R^2
70H+30S binder	2.61	0.19	0.56	0	600	143	-3.85	0.999
70H+30S+6% $SRAP_{binder}$	9.68	0.32	0.65	0	700	99.5	-3.47	0.998
70H+30S +16% $SRAP_{binder}$	5.59	0.25	0.64	0	800	174	-3.36	0.996
70H-30S-20V-S	9.68	0.32	0.65	400	1300	99.5	-3.35	0.997
70H-30S-40V-S	5.59	0.25	0.64	500	2300	174	-2.70	0.995
70H-30S-60V-S	2.61	0.28	0.58	700	2600	250	-2.21	0.997
80H+20S binder	3.13	0.22	0.56	0	1300	140	-4.32	0.999
80H+20S +6% $SRAP_{binder}$	5.55	0.25	0.65	0	1300	250	-3.73	0.998
80H+20S +16% $SRAP_{binder}$	13.6	0.32	0.73	0	1500	265	-3.59	0.999
80H-20S-20V-S	11.9	0.34	0.80	500	1500	250	-3.61	0.999
80H-20S-40V-S	13.6	0.32	0.73	650	2400	270	-2.98	0.996
80H-20S-60V-S	4.14	0.35	0.70	800	2700	300	-2.02	0.995
90H+10S binder	4.90	0.28	0.65	0	800	43	-3.98	0.999
90H+10S +6% $SRAP_{binder}$	9.68	0.31	0.77	0	1400	250	-3.67	0.999
90H+10S+16% $SRAP_{binder}$	9.52	0.28	0.70	0	1600	270	-3.31	0.996
90H-10S-20V-S	9.68	0.31	0.77	550	1700	250	-3.54	0.998
90H-10S-40V-S	9.52	0.28	0.70	700	2500	270	-2.62	0.998
90H-10S-60V-S	3.67	0.29	0.66	1000	2800	300	-1.83	0.996
100%$SRAP_{binder}$	8.21	0.37	0.83	0	3000	250	-2.24	0.999

Plotting the logarithmic of the characteristic time in function of RAP binder content for back-calculated complex modulus of asphalt binders the trend reported in Figure 59 is obtained.

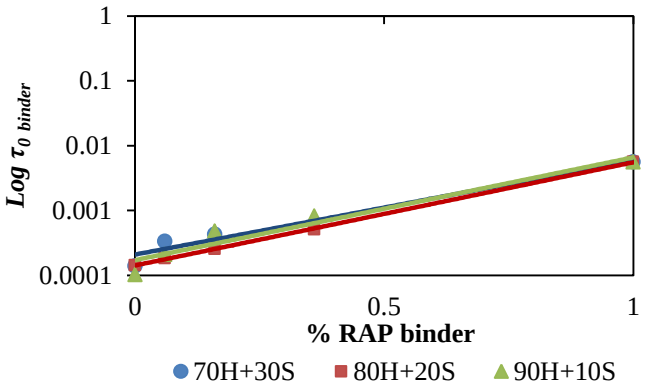

Fig.59 *Relationship between Log $\tau_{0binder}$ and RAP binder percentage*

The characteristic time presents a minimal increase for small RAP binder percentage, while above 50% it reaches significantly higher values. Figure 60 shows the trend of the characteristic time of mortars versus the different volume fraction, V_p, of SRAP (20, 40 and 60%).

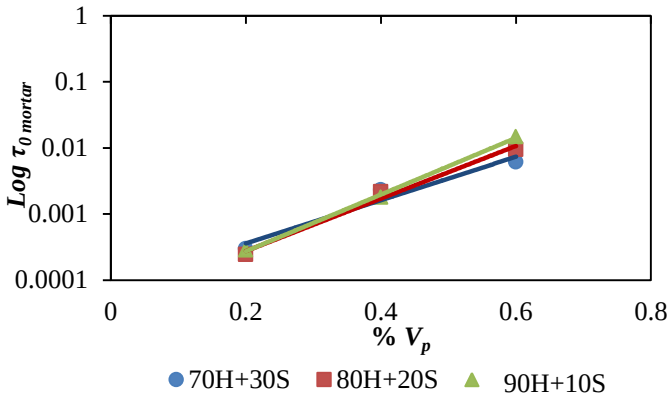

Fig.60 *Relationship between $\tau_{0mortar}$ and percentages of SRAP*

The characteristic time presents small changes for small SRAP content, while beyond a 40% SRAP threshold it starts increasing significantly, with higher values for mortars prepared with larger amount of stiffer binders.

Based on Figure 59, it can also be observed that the relationship between the characteristic time of asphalt binders and of mortars and SRAP percentage is exponential; in the case of asphalt binder, it can be expressed by Equation [38]:

$$\log \tau_0 = a \cdot e^{k \cdot \%SRAP_{binder}} \quad [38]$$

Where *a* and *k* are fitting constants and $\%SRAP_{binder}$ is the percentage of SRAP binder. This equation is equivalent to the one found by other authors (e.g. Mangiafico et al., 2013). Equation [39] is also valid for mortars when $\%SRAP_{binder}$ is replaced by the volume percentage of SRAP, $\%V_{p,SRAP}$:

$$\log \tau_0 = c \cdot e^{w \cdot \%V_{p,SRAP}} \quad [39]$$

Where *c* and *w* are fitting constants.

4.1.4 Validation

Using the relationship described in the previous sections, the complex modulus of mortar was predicted from complex modulus data of the corresponding binder and then compared with the experimental measurements on mortars.

Since the shift factors obtained from the WLF equation are the same for binders and corresponding mortars, as well as for parameters *δ*, *k* and *h* of the 2S2P1D, writing Equation 1 for binder and mortar and taking into account Equation 36, the relationship between mortar and binder complex modulus can be formulated as in Equation 40:

$$G^*_{mortar}(\omega,T) = G_{0\,mortar} + \left[G^*_{bind}\left(10^{(\mu Vp^{\sigma})}\omega,T\right) - G_{0\,bind}\right]\frac{G_{\infty mortar}-G_{0mortar}}{G_{\infty\,bind}-G_{0\,bind}} \quad [40]$$

Therefore, if the binder complex modulus (G^*_{bind}) is known at a given temperature *T*, Equation 40 gives the complex modulus of the mortar at the same temperature *T*, when the constants: $G_{0\ mortar}$, $G_{\infty mortar}$, μ and σ are known. Equation 40 provides the mathematical expression of the SHStS transformation (Olard & Di Benedetto, 2003; Di Benedetto et al., 2004; Delaporte et al., 2007) in the frequency domain. Moreover, if the TTSP is verified, the following relationship can be included in Equation 40:

$$G^*_{bind}\left(10^{(\mu V_p{}^{\sigma})}\omega,T\right) = G^*_{bind}\left(10^{(\mu Vp^{\sigma})}\omega a_T(T),T_s\right) \quad [41]$$

Since the parameters of the 2S2P1D model do not appear in Equation 40, the SHStS transformation and, therefore, the relation between mortar and binder complex modulus do not depend on the specific selected model used to derive it. This further confirms the findings of several studies (Olard & Di Benedetto, 2003; Di Benedetto et al., 2004; Delaporte et al., 2007; Cannone Falchetto, Marasteanu, & Di Benedetto, 2011; Cannone Falchetto, Montepara, Tebaldi, & Marasteanu, 2012; Moon et al., 2014; Cannone Falchetto & Moon, 2015).

As an example, Figure 61 provides a comparison between the complex modulus of mortar 70/100 + V_p40 predicted using Equation 40 and the experimental data. The Mean Squared Error of prediction in Percentage (MSEP) equals to 0.4%; this suggests that the model predictions are satisfactory.

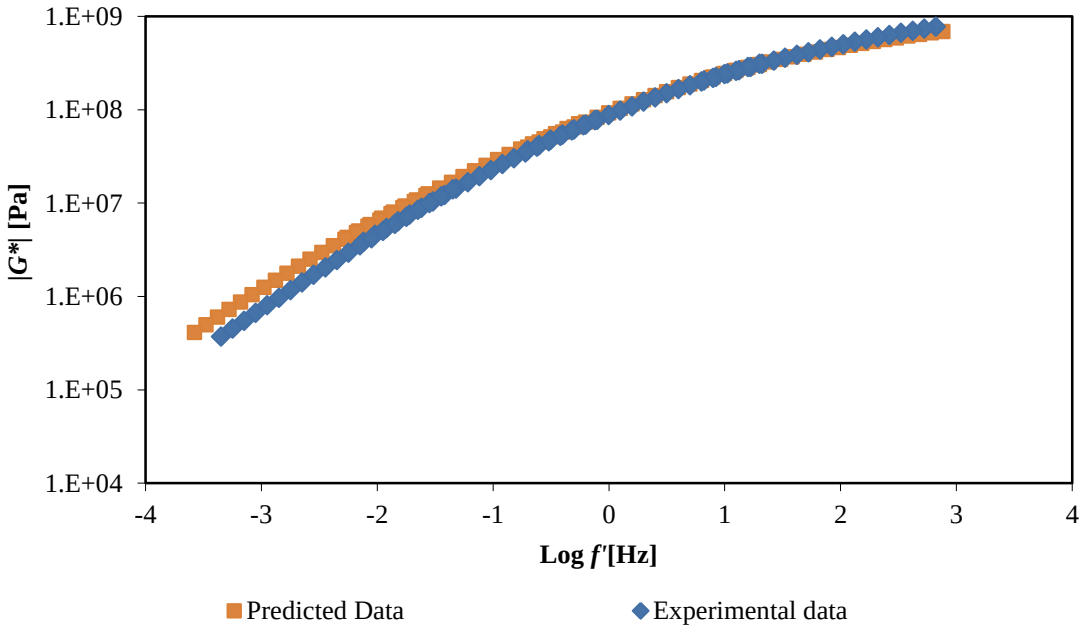

Fig. 61 *Comparison between the experimental data on mortar 70/100 Vp40 filler and the complex modulus predicted using Equation 40.*

In addition, in order to further validate the use of the equations from 33 to 37, they were used to calculate the characteristic time of the BSRAP and SRAP mortars, composed with the German RAP source, from the characteristic time of the binder. First, the parameter *f* corresponding to the different V_p was found, using the relationship reported in Figure 57 and then using Equation 35 the characteristic time of the mortars were found. All the parameters for the BSRAP mortars unaged and RTFO aged are reported in Table 29 and those of the SRAP mortars are reported in Table 30.

Table 29. *Experimental and back-calculated characteristic time for the German BSRAP mortars*

	V_p	Log $\tau_{0\ \text{experimental}}$	f	Log $\tau_{0\ \text{back-calculated}}$
Unaged	29	-3.03	0.36	-3.06
	42	-2.52	0.68	-2.74
	51	-2.34	0.98	-2.43
RTFO aged	29	-2.56	0.36	-2.45
	42	-2.22	0.68	-2.13
	51	-1.84	0.98	-1.83

Table 30. *Experimental and back-calculated characteristic time for the German SRAP mortars*

	V_p	Log $\tau_{0\ \text{experimental}}$	f	Log $\tau_{0\ \text{back-calculated}}$
Unaged	29	-2.74	0.36	-2.93
	42	-1.93	0.68	-2.36
	51	-1.18	0.98	-1.96
RTFO aged	29	-2.84	0.36	-2.76
	42	-2.05	0.68	-2.26
	51	-0.98	0.98	-1.76

Moreover, in order to further validate the exponential trend reported in Equation 38 and 39 between the characteristic time of the binder or mortar and the percentage of the RAP, the 2S2P1D model was fitted with the rheological data obtained on the bituminous blends of the German RAP source and on the corresponding BSRAP and SRAP mortars.

The parameters of the model are summarized in Table 31.

Table 31. *Parameters of the 2S2P1D model in the unaged condition.*

Material	δ	k	h	G_0 **(Pa)**	G_∞ **(MPa)**	β	**log(τ_0)**
50/70 binder	3.00	0.22	0.60	0	900	170	-3.42
50/70+20%RAP	3.14	0.22	0.58	0	900	873	-3.26
50/70+35%RAP	3.50	0.23	0.60	0	950	192	-3.04
50/70+50%RAP	3.72	0.22	0.60	0	1000	357	-2.94
50/70+BSRAP 20%	3.00	0.22	0.60	6082	1700	170	-3.03
50/70+BSRAP 35%	3.00	0.22	0.60	6724	3300	99	-2.52
50/70+BSRAP 50%	3.00	0.22	0.60	10700	4200	82	-2.34
50/70+SRAP 20%RAP	3.14	0.22	0.58	6582	1800	117	-2.74
50/70+SRAP 35%RAP	3.50	0.23	0.60	27600	3800	118	-1.93
50/70+SRAP 50%RAP	3.72	0.22	0.60	32500	5000	260	-0.98
RAP_{binder}	4.97	0.25	0.61	0	1350	376	-2.54

In Figure 62, the characteristic time of the bituminous blends versus the RAP binder percentage is reported. In addition, in Figure 63, the characteristic times of the SRAP mortars are reported versus the volume fraction of the SRAP particles. As shown, the exponential trend is verified.

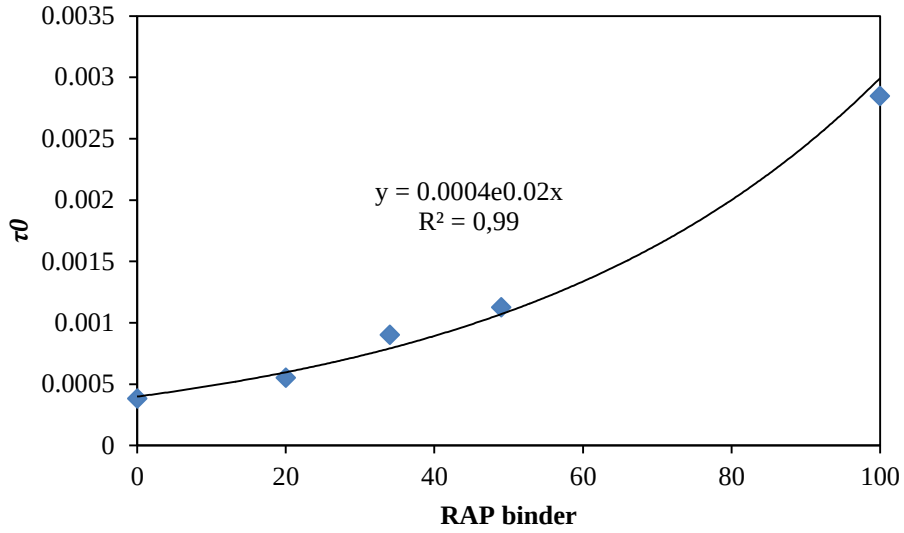

Fig. 62 *Characteristic time versus the RAP binder percentage*

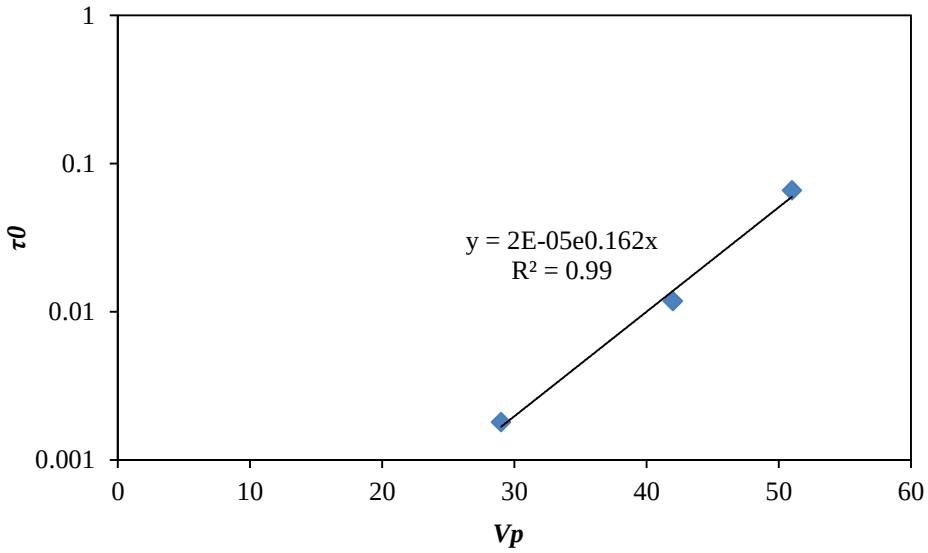

Fig. 63 *Characteristic time versus the volume percentage of SRAP.*

In addition, the data on RTFO aged materials were analyzed and similar results were obtained.

Analyzing the parameters of the 2S2P1D reported in Table 31, a linear increase of the parameter δ with the percentage of RAP binder can be observed, while the parameters k and h do not vary significantly with the RAP binder content. Similar results were found in other studies (Mangiafico et al., 2013; Mangiafico et al., 2014).

4.2 Extension of the 2S2P1D model to mortar/mixture (N.3)

In this chapter a relationship between the characteristic time of the mortar and of the mixture, containing different percentage of RAP materials, is derived. This relationship can be used to back-calculate the complex modulus of the mixture at any RAP binder percentage.

The research approach is summarized in Figure 64. First, four asphalt mixtures were produced by mixing the German RAP source with virgin aggregates and fresh binder in different portions (0%, 20%, 35% and 50%) and they were tested in tension-compression in order to measure the complex modulus and the phase angle. Then, bituminous blends and mortars, corresponding to the same amount of fresh and RAP binder present in the mixtures, were produced and tested with the Dynamic Shear Rheometer (DSR) to obtain the complex modulus and the phase angle. The experimental results were then fitted by the analogical 2S2P1D model and a relationship linking the characteristic time of mortars and corresponding mixtures was proposed. With this expression, the complex modulus of the mixture can be calculated using the 2S2P1D model, knowing from the complex modulus of the mortars.

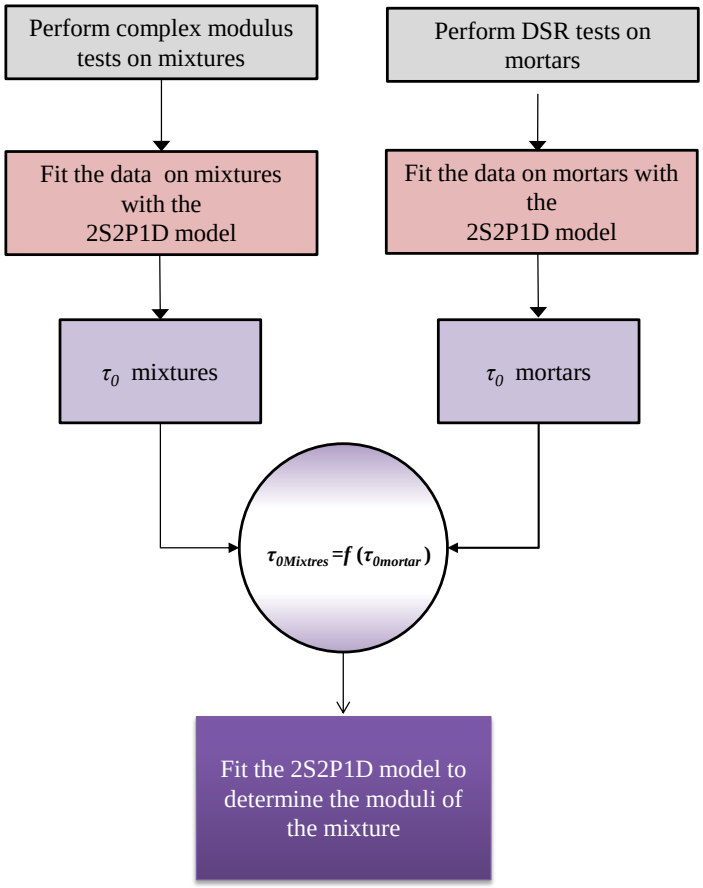

Fig.64 *Research approach*

4.2.1. Materials and Tests

4.2.1.1 Asphalt mixtures

Four different asphalt mixtures were produced by mixing the German RAP source with new aggregates and a conventional 50/70 binder, as a fresh binder, in various proportions (0%, 20%, 35% and 50%). All mixes have the following common characteristics:

- The same gradation curve reported in Figure 65, typical of a binder course commonly used in Italy;
- Gabbro virgin aggregates (the following aggregate sizes were used: 11/16, 8/11, 5/8, 2/5, 0/2) and RAP material obtained from a single lot;
- 5% total binder content by weight of the dry mix;
- Void content target at 4%±1.5%.

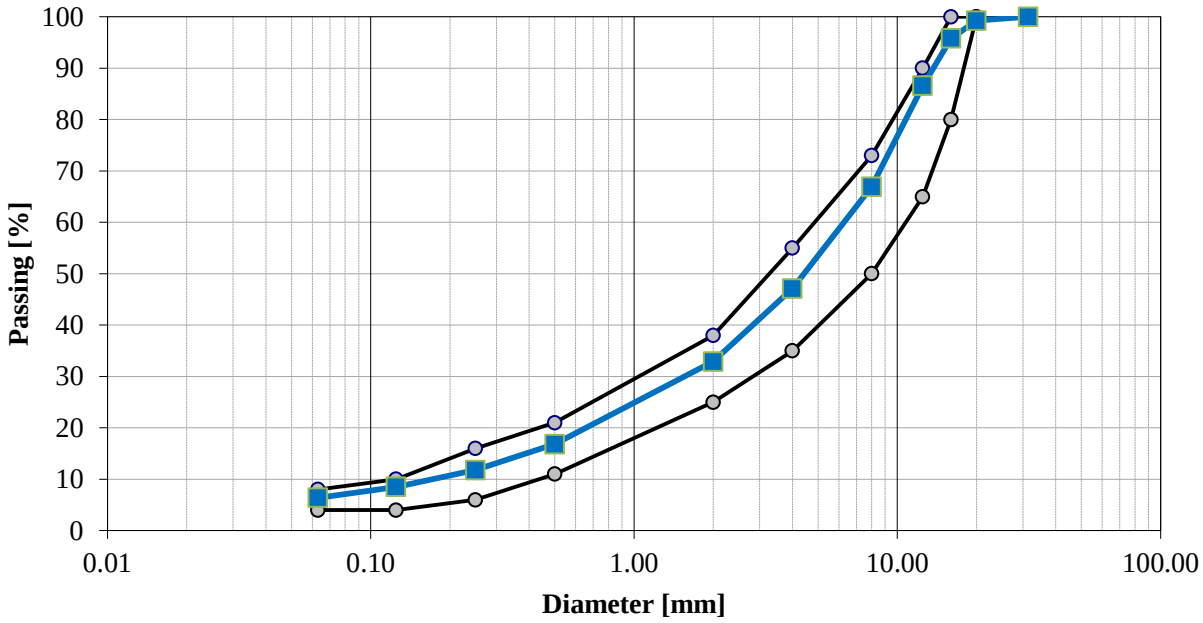

Fig.65 *Gradation curve used for mixtures.*

The RAP content percentages (0%, 20%, 35% and 50%) in the mixtures were calculated by volume of the dry mixture, therefore they correspond to 0%, 19.6%, 34.2% and 48.5% by weight of the total mixture. All the mixtures were mixed at 160°C and compacted at 150°C using a segment roller compactor (Wistuba, M.,2016), producing slab with dimensions of 320x200 mm. From each slab, three cylindrical samples were cored with a dimeter of 60 mm and a height of 180 mm.

The gradation curves of the different size of the Gabbro aggregates are reported in Figure 66. In Table 32 are summarized the particle density (the apparent specific gravity ρ_a, the bulk specific gravity

determined on particles pre-dry in the oven ρ_{rd}, the bulk saturated surface dry ρ_{ssd}), the water absorption W_{A24} and the porosity determined in accordance to EN 1097-6.

Table 32. *Density and water absorption of the different aggregate sizes*

Material	ρ_{rd} [g/cm^3]	ρ_a [g/cm^3]	ρ_{ssd} [g/cm^3]	W_{A24} [%]	Porosity [%]
Aggregates 2/5	2.832	2.879	2.857	0.6	1.65
Aggregates 2/5	2.831	2.886	2.859	0.7	1.95
Aggregates 5/8	2.848	2.889	2.871	0.5	1.42
Aggregates 5/8	2.848	2.885	2.870	0.5	1.30
Aggregates 8/11	2.833	2.870	2.854	0.5	1.30
Aggregates 8/11	2.843	2.884	2.866	0.5	1.47
Aggregates 11/16	2.882	2.917	2.903	0.4	1.23
Aggregates 11/16	2.861	2.891	2.880	0.4	1.03
RAP post 10-31	2.836	2.905	2.868	0.8	2.41
RAP post 0.063-10	2.842	2.901	2.865	0.8	2.08

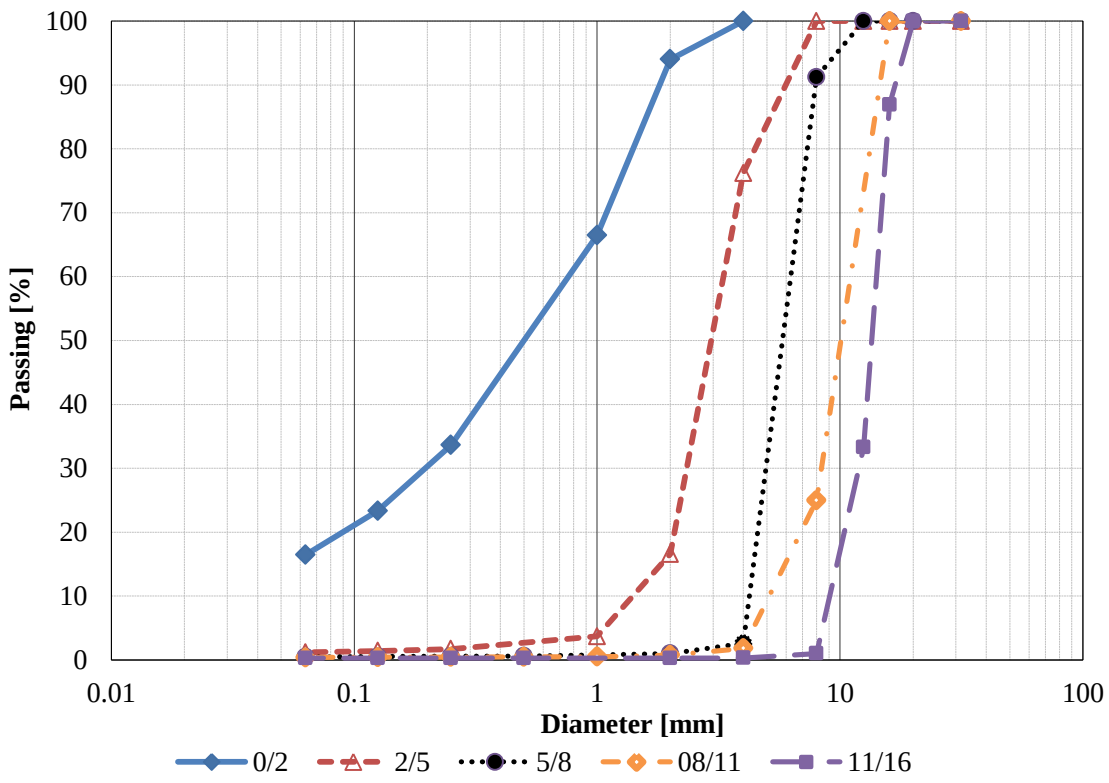

Fig.66 *Gradation curves of the Gabbro virgin aggregates.*

Regarding the RAP source, physical, geometrical and mechanical properties were evaluated. In particular, five different samples of 2500 g were sieved in accordance to EN 12697-2 and EN 13108-8

in order to obtain the black curves of the RAP source. Then, on the same materials, the binder content was evaluated using the Rotatory Evaporator in accordance to EN 12697-3, 2013 and the binder was recovered. The average value of the binder content determined on 5 samples results 4.93%. The maximum specific gravity was also determined in accordance to EN 12697-5 and results 2.925 g/cm^3. After the extraction, the resulting aggregates were used to evaluate the white curve in accordance to EN 12697-2 and the specific gravity reported in Table 32. Both the black and white curves are reported in Figure 67.

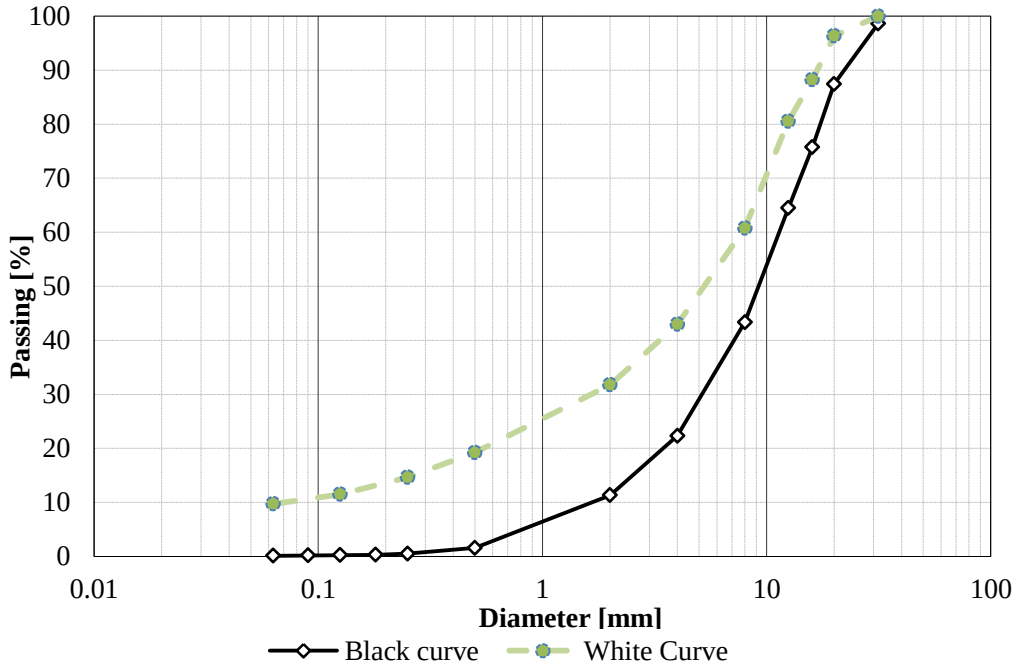

Fig.67 *Black and White curves RAP source.*

As mentioned before, all the mixtures were manufactured using the same gradation curve reported in Figure 65, using the grading band limits, shown in the same figure, according to ANAS (Azienda Nazionale Autonoma delle Strade - Italian road authority) specification for a common binder layer used in Italy.

In order to find the optimum binder content of the mixture, the Marshall method was adopted. Three mixtures with three different binder contents (4.5%, 5% and 5.5%) and composed with only virgin aggregates were produced. After the production, the grading curve and the effective content of the binder were controlled; moreover, the maximum specific gravity (G_{mm}) and the bulk specific gravity (G_{mb}) were determined in accordance to EN 12697-5 and to EN 12697-6 respectively, in order to obtain the air voids in the mixtures. For each binder content, five samples were produced and tested in order to determine Marshall stability, flow and stiffness. All the samples were compacted with 50

blows each side and the optimum binder content was determined following the Asphalt Institute (MS-2, 2015) specification. The optimum binder content results equal to 5% that is the average value corresponding to the maximum stability, to the maximum density and to the air voids of 4%. Finally, the stability, the flow and the air voids corresponding to 5% binder content were calculated in order to compare them with the specifications of the Asphalt Institute and of ANAS reported in Table 33. As shown in Table 33 all the limits are respected.

Table 33. *Marshall Parameters and Specification limits.*

	Stability (daN)	Flow (mm)	Stiffness (daN/mm)	Air Voids (%)
Mixture 5%	1130	3	376	5
ANAS Specification	≥900	3	≥300	4-6
Asphalt Institute Specification	≥533	2-4	≥266	3-5

In order to produce mixtures with 5 % binder respect to the dry mix, the binder content in RAP materials need to be taken into account. Therefore, considering that the RAP materials contained an average value of binder equal to 4.93%, the fresh binder percentages reported in Table 34 need to be added to the different mixture composed by RAP materials.

Table 34. *Percentage of Fresh and RAP binder with respect to the dry mix in the different mixtures*

Mixture	%RAP binder	%Fresh binder to add
20%RAP	1	4
35%RAP	1.7	3.3
50%RAP	2.4	2.6

The virgin aggregates composition and the percentage of RAP materials, expressed in weight with respect to the dry mix, in the different mixtures are summarized in Table 35. The reported percentages of RAP take into account the presence of the aged binder on them.

Table 35. *Virgin Aggregate composition and percentage of RAP materials to add in the different mixtures.*

	20% RAP	35%RAP	50%RAP
Aggregates 0/2	32%	27%	30%
Aggregates 2/5	21%	26%	28%
Aggregates 5/8	12%	15%	22%
Aggregates 8/11	17%	23%	20%
Aggregates 11/16	18%	9%	0%
RAP material	20.6%	35.9%	50.9%

Four different slab plates (320x220 mm) for each material were produced and three cylindrical samples with a diameter of 60 mm and a height of 180 mm were cored from each slab. The produced mixtures were also subjected to control tests such as the binder content, the grading curves, the evaluation of G_{mm} and G_{mb} in order to evaluate the air voids. Moreover, the binders extracted from the different mixtures were recovered in order to see the differences with the bituminous blends composed in laboratory and subjected to RTFO aging.

The characteristics of the samples tested are summarized in Table 36.

Table 36. *Geometrical and volumetric composition of the tested samples.*

Samples	G_{mb} g/cm^3	Air Voids %	Diameter mm	Height mm
0%RAP 3-2	2.562	1.84	59.8	181.72
0%RAP 2-2	2.557	2.03	59.7	180.07
0%RAP 2-1	2.565	1.72	59.8	180.61
20%RAP 2-3	2.590	2.37	59.9	181.13
20%RAP 4-2	2.598	2.07	60.11	181.37
20%RAP 3-1	2.583	2.63	59.99	180.85
35%RAP 3-3	2.591	2.41	60.23	180.84
35%RAP 2-3	2.596	2.22	60.19	180.70
35%RAP 2-2	2.595	2.64	60.06	180.36
50%RAP 1-3	2.580	2.95	60.42	180.08
50%RAP 2-3	2.582	2.88	60.36	180.60
50%RAP 1-1	2.564	3.56	60.34	180.15

All these samples were tested in tension-compression mode (DTC-CY) according to EN 12697-26 (Annex D) applying a sinusoidal strain with an amplitude of 50 micro strain in order to remain in the LVE and to avoid damage in the samples. The tested temperatures were -20, -10, 0, 10, 20, 30, 40°C and the frequencies were 0.1, 0.3, 1.59, 3, 5, 10 Hz. For each test temperature, the specimen was kept for 5 hours at lower temperatures (-20, -10, 0°C) and for 4 hour at the other temperatures (10, 20, 30, 40°C). Complex modulus and phase angle were calculated from test results and the master curves of the different mixtures were plotted considering the Christensen Andersen Maresteanu (CAM) model, reported in Equation 20 and 21, used also for binders and mortars, and the sigmoidal model reported in Equation 22. In order to plot the master curves, the average value of the complex moduli and of the phase angles of the three samples tested for each type of mixtures, was used. The master curves obtained are reported in Figures 68 and 69 respectively.

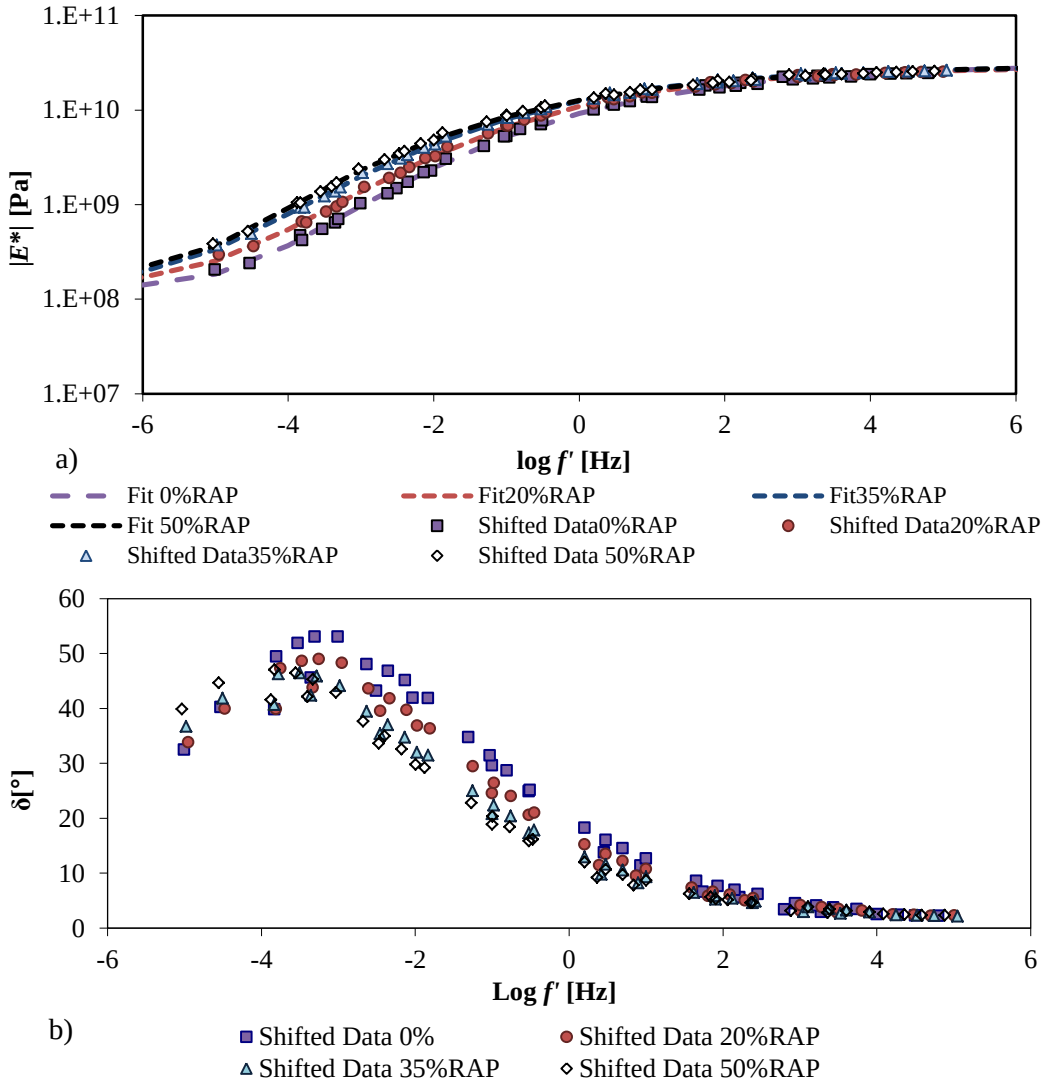

Fig.68 *Master curves of the different mixtures using the CAM model: a) Complex modulus, b) Phase Angle.*

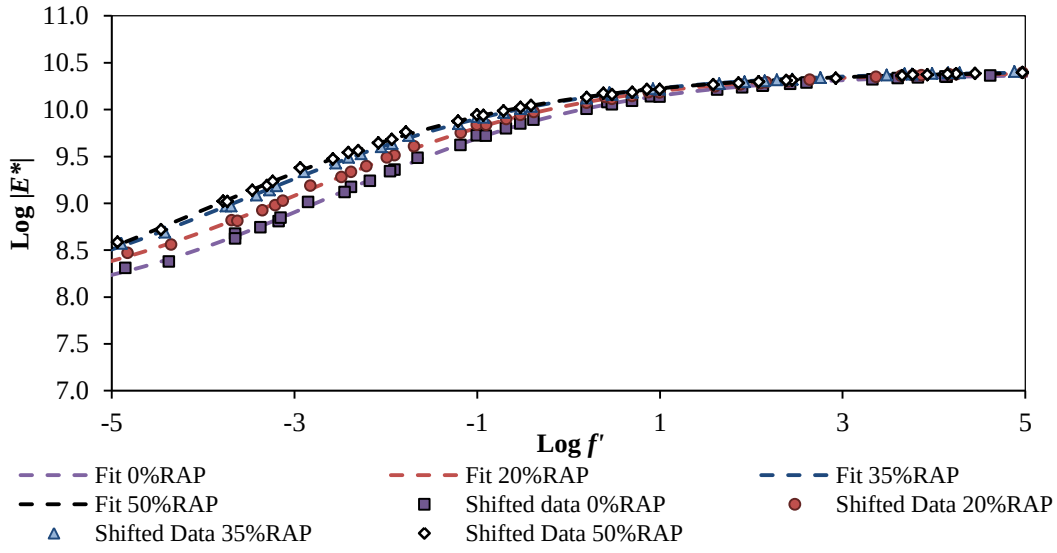

Fig.69 *Master curves of the different mixtures using the sigmoidal model.*

As shown, increasing the RAP content the complex modulus increases, while the phase angle decreases, since the mixture becomes stiffer due to the presence of RAP binder. For both the models used to plot the Master curves, the Root Mean Squared Error (RMSE) in percentage was calculated to evaluate the capability of the models to approximate the experimental data. It results equal to 2.82% for the sigmoidal function and 1.32% for the CAM model. Therefore, both models are satisfactory in predicting the measured value.

4.2.1.2 Asphalt mortars and asphalt blends

As mentioned in Chapter 3, bituminous blends and mortars composed with RAP material passing sieve with an opening size of 0.15 mm (SRAP) in different proportions, in order to recreate the same amount of fresh and RAP binder in the mixtures, were produced. The compositions of the different mortars are reported in section 3.1.2.4 together with the master curves.

4.2.2 Calibration of the 2S2P1D model

The 2S2P1D model was fitted imposing the same values of k, h and δ for mixtures and the corresponding binders and mortars in RTFO aged condition, since these parameters depend only on binder source. The RTFO aged condition was used to simulate the aging that the binder and mortars suffer during the manufacture process of the asphalt mixtures. Complex moduli E^* for binders and mortars were calculated from measured shear complex modulus G^* by applying a Poisson's ratio of 0.5 ($E^*=3G^*$). The seven parameters of the different materials phases are reported in Table 37.

Table 37. *2S2P1D model parameters in RTFO aged condition.*

Material	δ	k	h	E_0 (Pa)	E_∞ (GPa)	β	log(τ_0)
RTFO 50/70 binder	3.89	0.24	0.65	0	2.8	146	-3.42
RTFO mortar: 50/70+BSRAP 20%RAP	3.89	0.24	0.65	8259	6	178	-2.56
RTFO mortar: 50/70+BSRAP 35%RAP	3.89	0.24	0.65	22230	9	73	-2.22
RTFO mortar: 50/70+BSRAP 50%RAP	3.89	0.24	0.65	$0.454 \cdot 10^6$	13.5	160	1.84
Mixture 0%RAP	3.89	0.24	0.65	$130 \cdot 10^6$	27	10	0.42
RTFO blend: 50/70+20%RAP	3.42	0.23	0.57	0	2.8	790	-3.12
RTFO mortar:50/70+SRAP 20%RAP	3.42	0.23	0.57	19750	7	113	-2.84
Mixture 20%RAP	3.42	0.23	0.57	$143 \cdot 10^6$	28	4.33	0.57
RTFO blend: 50/70+35%RAP	2.97	0.21	0.58	0	3	274	-3.24
RTFO mortar: 50/70+SRAP 35%RAP	2.97	0.21	0.58	76500	9.9	176	-2.05
Mixture 35%RAP	2.97	0.21	0.58	$150 \cdot 10^6$	30	33	0.70
RTFO blend: 50/70+50%RAP	3.62	0.22	0.61	0	3.4	216	-3.00
RTFO mortar: 50/70+SRAP 50%RAP	3.62	0.22	0.61	82800	11	115	-0.97
Mixture 50%RAP	3.62	0.22	0.61	$189 \cdot 10^6$	30	769	0.93

As shown in Table 37, the characteristic time increases, if RAP content is increased, this can be seen for all the different material's phases. Plotting the characteristic time of the blend versus the RAP binder percentage and the characteristic time of the mortar versus the SRAP percentage, exponential trend similar to the one reported in section 4.1.3.1 was obtained. In addition, as shown in section 4.1.4, the relationship between the characteristic time of the binder and the corresponding mortar was validated.

In order to confirm that the time and temperature dependency of the different material phases originates from the binder behavior, regardless of the aggregate skeleton and that it is possible to predict the LVE behavior of a mixture from the LVE properties of the corresponding binder or mortar and vice versa, the normalized moduli, expressed by Equation 42 is introduced:

$$E^*_{norm} = \frac{E^* - E_0}{E_\infty - E_0} \qquad [42]$$

Plotting in the Cole Cole plot the normalized moduli of the different material's phases, curves that reasonably superimpose with each other are generated, as shown in Figure 70 for the blend, mortar and mixture corresponding to 50% RAP. Similar results were obtained for all the other mixtures.

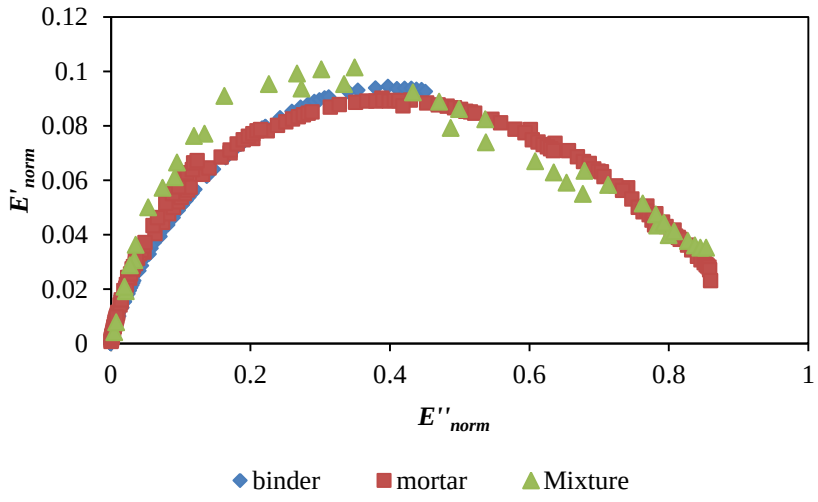

Fig.70 *Normalized Cole-Cole plot of 50/70+50%RAP binder, SRAP mortar, Mixture.*

Therefore, using Equation 42, starting from the normalized (storage and loss) moduli of the binder or of the mortar and knowing the glassy modulus $|E_\infty|$ and $|E_o|$ of the mixture is possible to back-calculate the storage and loss moduli of the mixture.

4.2.3 Relationship between the characteristic time of mortar and of mixture

Plotting the characteristic time of the mixtures versus the characteristic time of the corresponding mortars, the linear trend reported in Figure 71 was found. The slope and the intercept of the linear

relationship may depend on the mix design and on the microstructure. Further investigations using different mixture are needed to better understand these parameters.

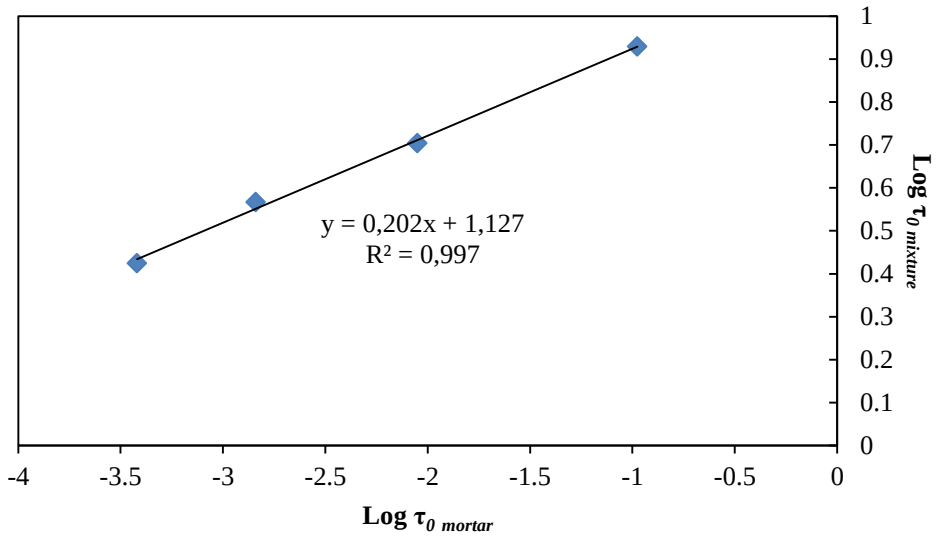

Fig.71 *Relationship between Log* $\tau_{0\ mortar}$ *and Log* $\tau_{0\ mixture}$

At this point, knowing the characteristic time of the mortar, using the simple linear relationship reported in Figure 71, the characteristic time of the mixture can be determined. Finally, using Equation 6, knowing $|E_0|$ and $|E_\infty|$ of the mixtures, the complex modulus $|E^*|$ of the different mixtures can be back-calculated.

4.2.4 Validation

In order to validate the use of the linear relationship found in the previous section, a mortar and a mixture composed with 40% RAP was produced. In Figure 72, the predicted values, using Equation 6 with $\tau_{0mixture}$ determined using the linear relationship reported in Figure 71, versus the measured values are reported.

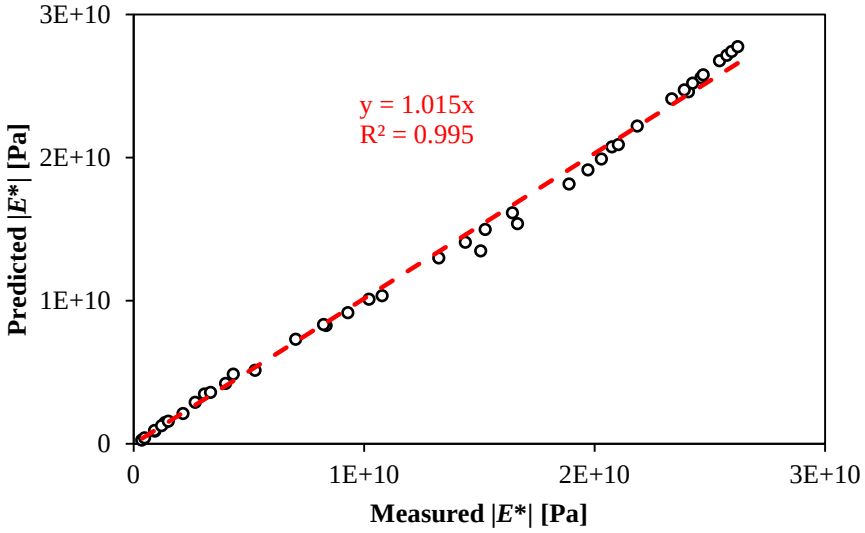

Fig.72 *Predicted versus measured value.*

4.3 2S2P1D Model linking binder/mixture phases

As explained in Chapter 2, in order to use the SHStS transformation to back-calculate the complex modulus of the mixture, starting from those of binder, the parameter α, which links the rheological properties of asphalt binder to those of the corresponding mixture, need to be derived. The procedure proposed first by Di Benedetto et al., 2004, consists in finding the transformation parameter α, fitting binder and mixture experimental data. According to Di Benedetto et al. (2004) the SHStS transformation parameter depends on the mix design and, therefore, it may be potentially related to the contribution of the different material phases or constituents: air voids, mastic, aggregates. Cannone Falchetto and Moon (2015) recently proposed a theoretical approach in order to obtain a mathematical expression for the SHStS transformation parameter. This approach is based on mixture microstructure, and it needs the determination of six parameters that can be determined using Digital Image Processing and 2-point correlation function of the microstructure components (Berryman, 1985; Moon, Cannone Falchetto & Jeong, 2014). This approach is promising, but it requires the use of complex theoretical concepts, which may not be easily implemented for practical purposes. For this reason, in this work, a simple approach to link the SHStS transformation parameter to the volumetric properties of the asphalt mixtures is determined. For this purpose, two parameters were identified: the binder content and the aggregates fractal dimension, which provides information on the volumetric configuration of the aggregate grading.

In order to achieve this aim, the research approach summarized in Figure 73 was used. First, Dynamic Shear Rheomether (DSR) tests were performed on different binders in order to determine the complex modulus (G^*) and the phase angle (δ). Then, the rheological properties of binders and the volumetric composition of corresponding mixtures, determined on gyratory compacted samples, were used to

predict the complex modulus (E^*) and the phase angle (δ) of asphalt mixture samples with the semi empirical Hirsch model. The test results on binders and the predicted values of the asphalt mixture complex modulus were then fitted using the 2S2P1D model in order to determine the characteristic time of the binder and that of the corresponding mixture. Finally, the transformation parameter α was determined and a simple equation linking α to the aggregate fractal dimension and to the binder percentage was derived.

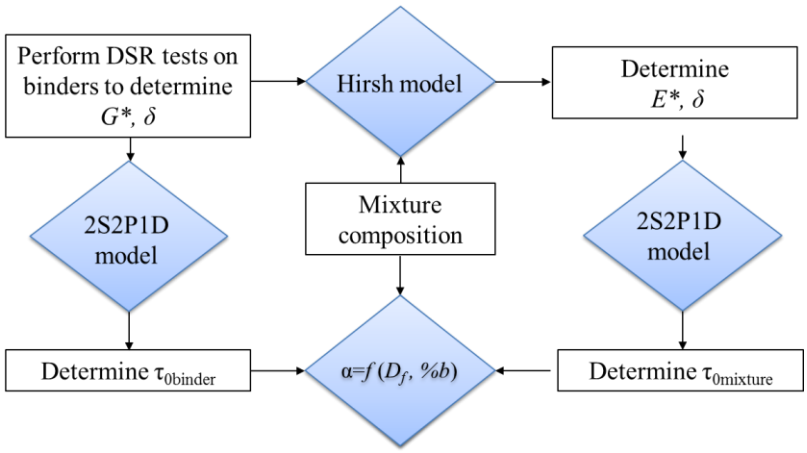

Fig. 73 *Flow chart of the research approach*

4.3.1. Materials and Tests

Three different asphalt binders with the characteristics reported in Table 38, were used.

Table 38. *Asphalt Binders Properties*

Binder	35/50	50/70	70/100
Pen 25°C (dmm)	41	58	75
Softening point R&B (°C)	52	47	44

In order to determine the complex modulus (G^*) and the phase angle (δ) of binders, frequency and temperature sweep tests were performed on the different asphalt binders using the DSR, in the classical parallel plates configuration (8 mm diameter and 2 mm gap). The temperature ranged between 0 and 40°C and the frequency between 0.2 and 20 Hz. The complex modulus E^* was calculated from measured shear complex modulus G^* by applying a Poisson ratio of 0.5 ($E^* = 3\,G^*$).

The resulting master curves of the complex modulus and of the phase angle for the different binders are reported in Figure 74 and 75 respectively.

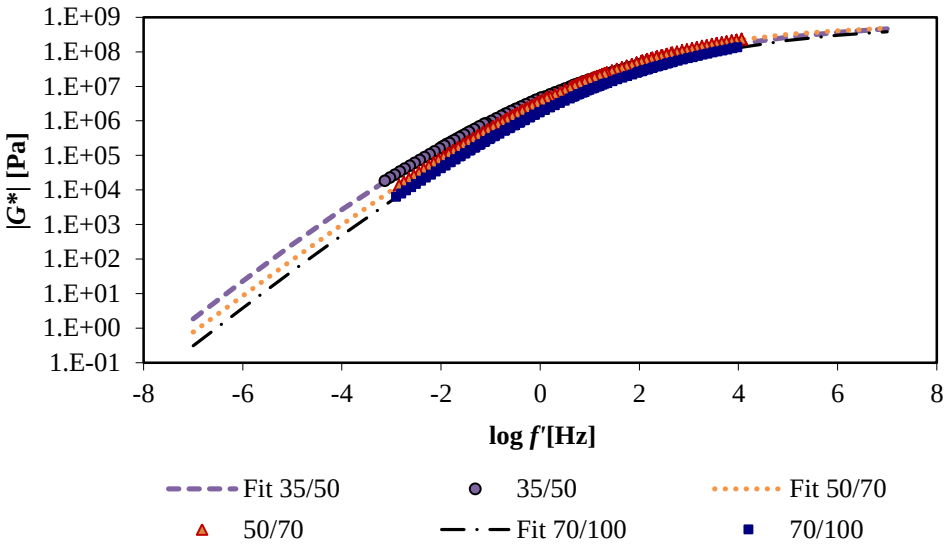

Fig. 74 *Complex modulus master curves of the different binders.*

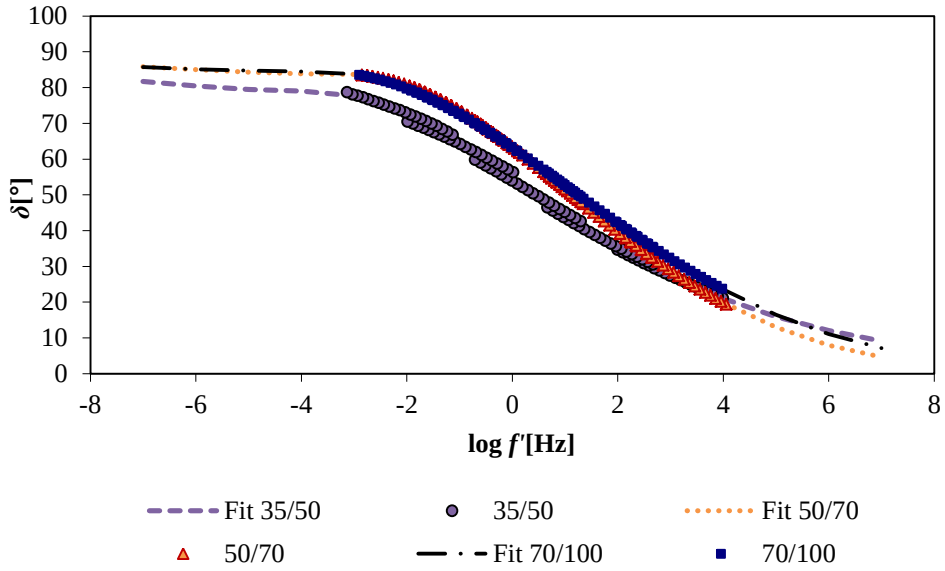

Fig. 75 *Phase angle master curves of the different binders.*

These data on binders were used to generate complex modulus and phase angle of asphalt mixture. In particular, eighteen different mixes were analyzed; they were obtained by considering four different grading curves for surface layers and different percentages of asphalt binder. Specifically, the same grading curve was considered for the three different binders at three different binder contents (5.5%; 6%; 6.5%). In addition, three different grading curves with the same percentage of the different binders (6%) were considered. The characteristics of the different mixtures: binder content, the voids in mineral aggregate (VMA), the voids in aggregates filled with mastic (VFA), the nominal maximum aggregate size (NMAS) and the aggregate fractal dimension (D_f) are reported in Table 39.

Table 39. *Characteristics of the Mixes*

ID no	Binder type	%Binder	VMA	VFA	NMAS (mm)	D_f
1	35/50	5.5	16.23	68.69	9.5	2.91
2	35/50	6	15.69	78.77	9.5	2.91
3	35/50	6.5	15.24	89.04	9.5	2.91
4	50/70	5.5	16.23	68.69	9.5	2.91
5	50/70	6	15.69	78.77	9.5	2.91
6	50/70	6.5	15.24	89.04	9.5	2.91
7	70/100	5.5	16.23	68.69	9.5	2.91
8	70/100	6	15.69	78.77	9.5	2.91
9	70/100	6.5	15.24	89.04	9.5	2.91
10	35/50	6	16.4	82.31	22	2.63
11	35/50	6	14.3	97.2	16	2.83
12	35/50	6	14.1	99.2	16	2.78
13	50/70	6	16.4	82.31	22	2.63
14	50/70	6	14.3	97.2	16	2.83
15	50/70	6	14.1	99.2	16	2.78
16	70/100	6	16.4	82.31	22	2.63
17	70/100	6	14.3	97.2	16	2.83
18	70/100	6	14.1	99.2	16	2.78

The Hirsch model was used to predict the complex modulus and the phase angle data knowing the complex modulus of the corresponding binder and the volumetric properties of the mixtures.

In addition mixtures composed with different percentages of RAP (0, 20, 35, 50% used in the previous section) were used to validate the found relationship together with the corresponding bituminous blends produced in laboratory and subjected to RTFO aging and with the extracted bituminous blends from the corresponding mixtures.

In order to obtain information on the volumetric configuration of the aggregate grading curve, the Fractal Theory was chosen. In fact, it allows determining the fractal dimension (D_f) that is calculated

as the distribution in weight of the dimensions of the aggregate particles and it represents a synthetic indicator of the configuration assumed by the solid structure; such information cannot be directly evaluated from the aggregate grading curves of the mix.

In order to calculate the fractal dimension of an aggregate grading, the method based on the representation in terms of cumulated number of the elements (N_C) was adopted (Losa & Leandri, 2012; Losa et. al, 2013). For a generic aggregate grading fraction, retained by the sieve with dimension *d* and passing to the superior sieve *D*, with mass *M* and specific gravity γ, it is possible to define the equivalent average volume of the single aggregate which is equal to that of the sphere with diameter, G_i, and the same volume. According to these hypotheses, it is possible to determine the number of the aggregate particles *N*, composing the aggregate grading fraction *d-D*, by using the Equation 43:

$$N = \frac{M}{\gamma \frac{\pi}{6}} G_i^3 \quad [43]$$

Similarly, it is possible to determine the cumulated number N_C of aggregate particles that have the average dimension G_i and that are retained by the sieve *d*, which are expressed as:

$$N_C(G_i > d) = \sum \frac{M_i}{\gamma_i \frac{\pi}{6}} G_i^3 \quad [44]$$

where the subscript *i* refers to the i^{th} aggregate grading fraction. The average dimension G_i of the aggregates within the grading fraction *d-D* can be determined using Equation 45:

$$G_i = \frac{\ln(D) - \ln(d)}{\frac{1}{d} - \frac{1}{D}} \quad [45]$$

The linear regression between the logarithm of the particle cumulated number N_C and the logarithm of the equivalent sphere diameter, G_i, results in Equation 46:

$$\log N_c(G_i > d) = A + B \; log \; {G_i}^{-D_F} \quad [46]$$

where *A* and *B* are the regression coefficients and D_f represents the fractal dimension of the specific aggregate grading. All the characteristics, such as the binder percentage, the voids in mineral aggregate (VMA), the voids in aggregates filled with mastic (VFA), the nominal maximum aggregate size (NMAS) and the fractal dimension D_f of the analyzed mixtures are reported in Table 39.

4.3.2 2S2P1D model fitting and determination of the α parameter

The DSR test results on binders and the mixtures predictions obtained with the Hirsch model (Equation 8 and 9) were fitted with the 2S2P1D model (Equation 1). The parameters of the 2S2P1D model are reported in Table 40 for binders and in Table 41 for the corresponding mixtures.

Table 40. *2S2P1D parameters for asphalt binders*

Binder	E_∞(Pa)	E_0(Pa)	k	h	δ	τ_0	β	R^2
35/50	2.40E+09	0	0.27	0.66	5.91	1.05E-04	251	0.99
50/70	2.80E+09	0	0.22	0.57	2.80	1.60E-04	400	0.99
70/100	3.00E+09	0	0.25	0.58	2.86	8.34E-06	120	0.99

Table 41. *2S2P1D parameters for the different mixtures*

Mixture	E_∞(Pa)	E_0(Pa)	k	h	δ	τ_0	β	R^2
1	1.56E+10	2.35E+08	0.28	0.66	5.91	8.95E-02	26	0.99
2	1.56E+10	2.39E+08	0.26	0.66	5.91	9.95E-02	26	0.99
3	1.56E+10	2.40E+08	0.28	0.66	5.91	1.47E-01	13	0.99
4	1.29E+10	2.22E+08	0.22	0.57	2.80	1.10E-02	250	0.99
5	1.27E+10	2.25E+08	0.21	0.57	2.80	2.50E-02	420	0.99
6	1.30E+10	2.21E+08	0.21	0.56	2.80	1.60E-01	390	0.99
7	1.50E+10	1.96E+08	0.25	0.58	2.86	2.54E-03	350	0.99
8	1.50E+10	1.96E+08	0.25	0.58	2.86	2.89E-03	111	0.99
9	4.69E+10	1.60E+08	0.25	0.58	2.86	1.47E-01	108	0.99
10	1.56E+10	2.39E+08	0.28	0.66	5.91	1.83E-01	250	0.99
11	1.87E+10	2.39E+08	0.28	0.66	5.91	4.44E-02	255	0.99
12	1.90E+10	2.39E+08	0.28	0.66	5.91	3.44E-02	250	0.99
13	1.86E+10	2.35E+08	0.22	0.57	2.80	1.50E-02	300	0.99
14	1.56E+10	2.38E+08	0.22	0.57	2.80	1.30E-02	300	0.99
15	1.86E+10	2.22E+08	0.22	0.57	2.80	1.30E-02	300	0.99
16	1.67E+10	1.97E+08	0.25	0.58	2.86	1.08E-02	350	0.99
17	1.72E+10	1.97E+08	0.25	0.58	2.86	4.94E-03	62	0.99
18	1.87E+10	2.00E+08	0.25	0.58	2.86	2.94E-02	65	0.99

The transformation parameters of the SHStS relationship were found by correlating the characteristic time of binders to those of the corresponding mixtures. Six α parameters, listed in Table 42, were found: three of them correspond to the relationship between the characteristic time of the mixtures, composed by the same grading and having different binder percentages (mixes with an identification number between 1 and 9, and the corresponding binders); the other three correspond to the

relationship between the mixtures composed by different gradings but having the same binder percentages (mixes with an identification number between 10 and 18).

Table 42. *Parameters α*

D_f	Binder %	α
2.91	5.5	3.36
2.91	6	3.42
2.91	6.5	3.36
2.63	6	3.13
2.83	6	3.36
2.78	6	3.26

4.3.3 Multiple-regression analysis of parameter α

By a multiple-regression analysis of α parameters versus the binder percentage, *%b*, and the fractal dimension, D_f, the simple relationship reported in Equation 47 was determined:

$$\alpha = A_0 + A_1 \%b + A_2 D_f \quad [47]$$

Where A_0, A_1, A_2 are regression coefficients equal to -0.49, 10.53, 1.13 respectively.

The regression analyses have shown an adjusted R^2 of 0.98 and a standard error of 0.04. The residual plots represented in Figure 76 indicate a random pattern confirming that the linear model provides a good fit.

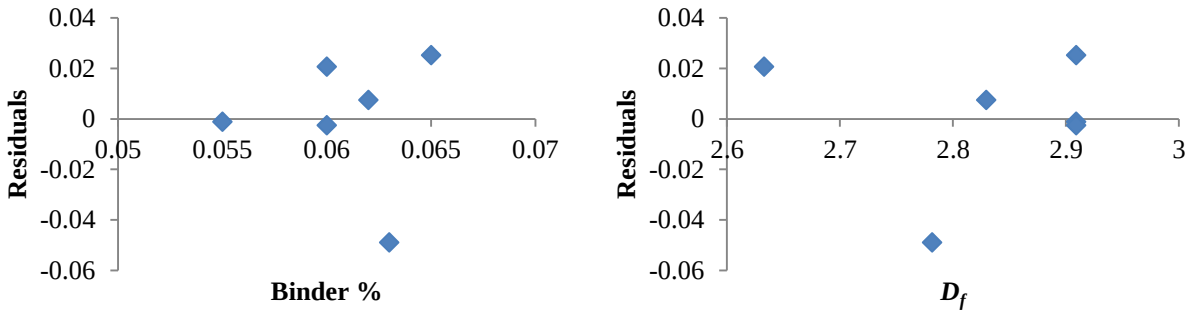

Fig. 76 *Residual plots.*

Furthermore, by using the F statistic test, the significance of the proposed model was checked and, by using the t-Student statistic test, the significance of the regression coefficients was checked. The values of *F* always resulted in greater values than the critical value *Fu* of the *F* function at one tail with *p* and *n-p-1* degrees of freedom, with a confidence level equal to 95% (where *n* is the number of

data and *p* is the number of variables used in the model). Similarly, the values of *t* always resulted greater than the critical value t_{n-p-1} of the t-student function at two tails, with *n-p-1* degrees of freedom, with a confidence level equal to 95% (where *t* is the ratio between each coefficient and the standard error referring to each coefficient, *n* is the number of data and *p* is the number of variables used in the model). Moreover, the *p-value* results lower than the significant level of 0.05, as shown in Tables 43 and 44, where all the *F* and *t* statistics are summarized respectively.

Table 43. *F statistic*

F	*Fu*	*p-value*
81.52	3.77	0.0024

Table 44. *t statistic*

	t	t_{n-p-1}	*p-value*
A_0	-9.71	±3.18	0.0028
A_1	6.71	±3.18	0.0067
A_2	10.85	±3.18	0.0016

Using Equation 47, the transformation parameter α, for the binder and mixture studied in the previous section 4.2, was determined. The fractal dimension is equal to 2.77 for the gradation curve used and the binder content is 0.05, therefore, α results equal to 3.16. The value obtained from fitting the experimental data, considering the bituminous blend produced in laboratory, is 3.66, while the value is 3.36 if considering the bituminous blends extracted from the mixtures.

Since, the results are very promising, even if complex moduli of the mixtures were generated using the Hirsch model, in future work, a dataset based on measured complex moduli will be generated in order to obtain regression coefficients more reliable for a wide range of mixtures.

4.4 Summary

In Chapter 4, the 2S2P1D model was studied in the different material phases (binder, mortar and mixture) as shown in Figure 77 and 78.

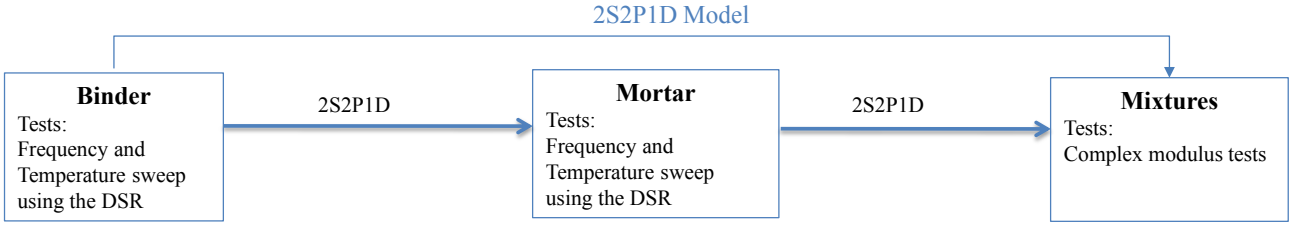

Fig. 77 *2S2P1D model between the different phases of the materials.*

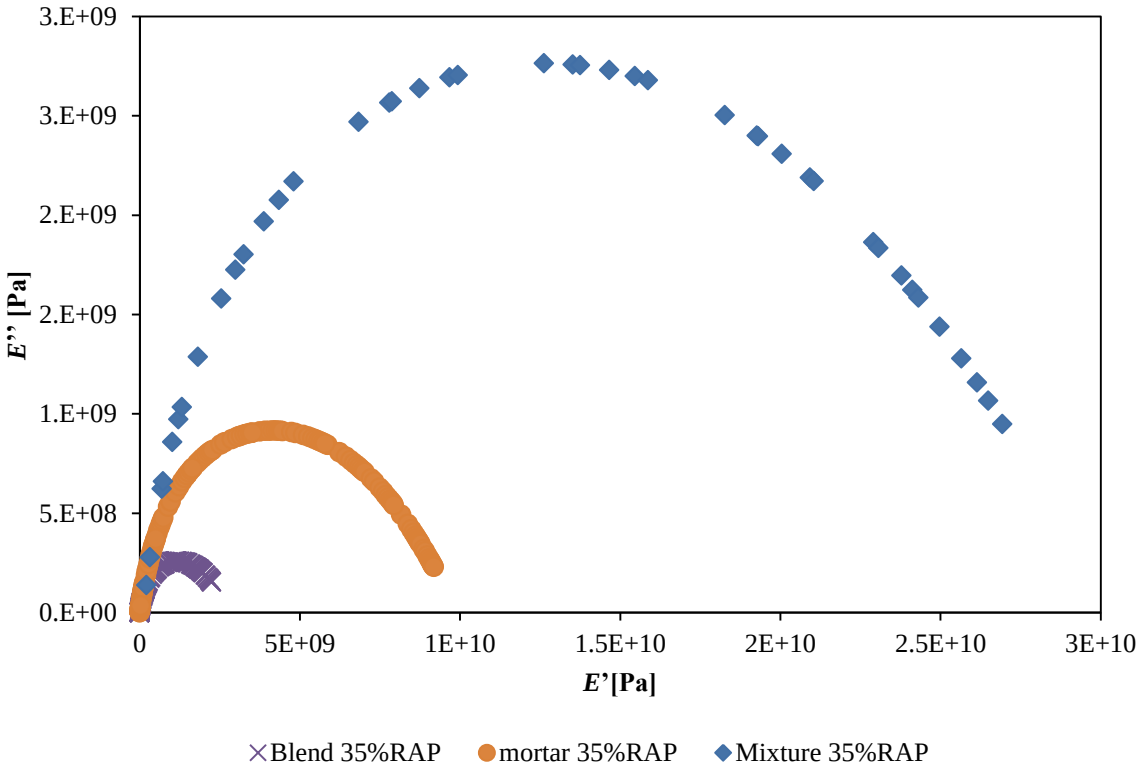

Fig. 78 *2S2P1D model for the different phases of the materials in the case of blend, mortar and mixture with 35%RAP.*

As shown in previous sections, the parameter that governs the SHStS transformation between the different materials' phases is the parameter α that links the characteristic times of the different phases. In particular, a simple relationship between the characteristic time of asphalt binder and asphalt mortar, that follows a linear trend in the log-log scale, was found. The intercept, which corresponds to the SHStS transformation parameter α, depends on the filler content according to a power function with two constants. It is hypothesized that these two constants are associated to the spatial distribution of the filler aggregates, as demonstrated in a different study on asphalt mixture. Therefore, using the SHStS transformation, the complex modulus of the mortar can be back-calculated from the complex modulus of the binder.

Moreover, it was found that characteristic time of the asphalt binder in the mortar depends on the recycled materials' properties and on their content according to an exponential function. A similar expression is valid also for the characteristic time of the corresponding mortar. This confirms previous findings of Mangiafico et al., 2013.

Then, a relationship between the characteristic time of the mortar and of the mixture was determined. This allows to calculate the characteristic time of the mixture knowing the characteristic time of the corresponding mortar, and by this way, using the 2S2P1D model and knowing the asymptotic value of

the mixture's moduli, the complex modulus of the mixture can be back-calculated. Another procedure that can be used to derive the complex modulus of the mixture consists in using the normalized moduli obtained for the mortar. Both procedures predict the measured value satisfactorily, with an RMSE% of 0.17 for the first procedure and with an RMSE% of 0.26 for the second procedure.

In addition, a relationship between the transformation parameter α, and the fractal dimension and the percentage of binder in the mixture was found. This allows to calculate the characteristic time of the mixture starting from the one of the binder and then, using the SHStS transformation, the complex modulus of the mixture can be back-calculated.

Therefore, all the different material phases are clearly connected to one each other, and this interrelation can be expressed by 2S2P1D model. So, starting from tests on asphalt binder or asphalt mortar, the complex modulus of the corresponding mixture can be back-calculated.

This is especially useful when RAP materials are investigated, since mortar composed with different proportions of SRAP materials can be used to back-calculate the complex modulus of the corresponding mixture. This allows to directly test the RAP binder as it is obtained from milling, avoiding any further type of treatment (solvent extraction, oxidation). Therefore, costly and time consuming tests on mixtures can be significantly reduced. For example, if the maximum percentage of RAP that can be added to a mixture without exceeding a reference stiffness needs to be determined, SRAP mortars in different proportions are produced, tested with DSR and then, using the 2S2P1D model and the found relationship, the complex modulus of the corresponding mixture with different proportions of RAP are back-calculated and the maximum percentage, corresponding to the limit of stiffness imposed, is determined. Finally, in order to confirm the prediction, only the mixture composed with that amount of RAP is produced and tested.

Chapter 5

5. Empirical models

In the following sections the empirical Hirsh and Witczak models are used to predict the complex moduli of the mixtures starting from the rheological properties measured on the bituminous blends produced in laboratory, extracted and recovered from the mixtures and from the rheological properties back-calculated using the Enhanced Nielsen model. In addition the Witczak model is re-calibrated in order to use the rheological properties of the mortars instead of those of binders to predict the complex moduli of the mixture.

5.1 Hirsch model

Using the Hirsch model reported in Equation 8 and 9 (Chapter 2), the complex modulus of the mixture can be back-calculated knowing the modulus of the aggregate (E_{agg}, that was assumed equal to 19 GPa=2750000 psi), the volumetric composition of the mixtures (VMA, VFA, the volume fraction of the aggregate, V_{agg} ,and of the binder, V_b) and the rheological properties of the binder (G_b*and δ). In Table 45 the volumetric properties of the different mixtures investigated are summarized.

Table 45. *Volumetric properties of the mixtures used as input in the Hirsch model.*

Mixture	VMA	VFA	V_{agg}	V_b
0% RAP	14.52	77.60	85.47	11.26
20% RAP	13.37	82.27	86.62	11.00
35% RAP	13.09	81.56	86.90	10.68
50% RAP	13.31	77.79	86.68	10.36

In Figure 79, the complex moduli of the mixture composed with 35%RAP, predicted by the Hirsch model, using the data of the bituminous blends produced in laboratory and subjected to RTFO aging, are plotted versus the measured values with the DTC-CY tests. As shown, the error is approximately 26%, while for the other mixtures the errors are similar, except for the 50%RAP, for which the error is around 36%.

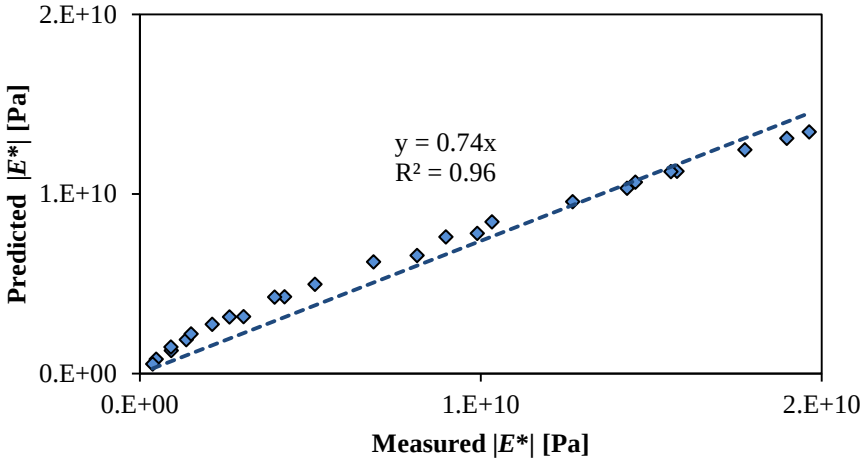

Fig. 79 *Predicted versus measured value of the complex modulus of the mixture with 35%RAP.*

In Figure 80, the phase angles predicted are plotted versus the measured ones. As shown, the error is smaller than the complex modulus, but the data are more dispersed especially at high temperature. A similar trend is obtained for the other mixtures, and the errors are in the range of 20-22%.

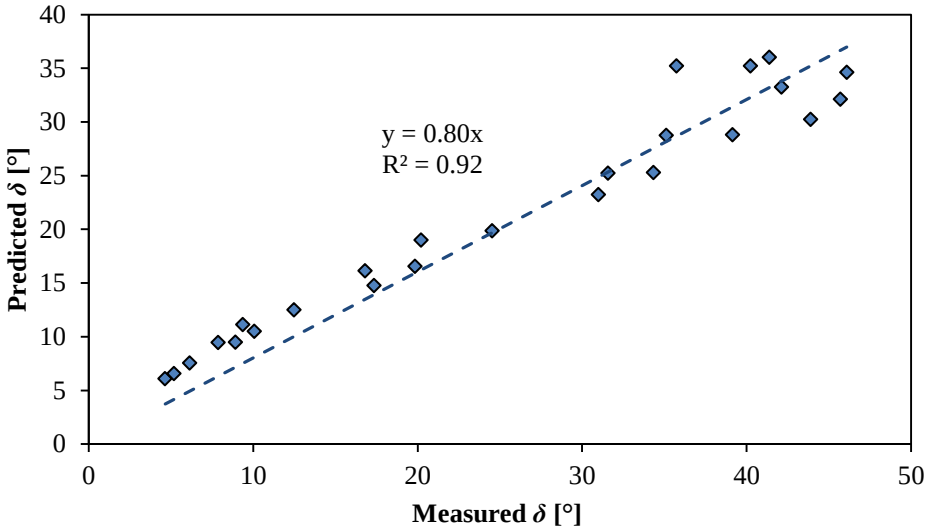

Fig. 80 *Predicted versus measured value of the phase angle of the mixture with 35%RAP.*

The Hirsch model was also fitted using the data of the bituminous blends back-calculated with the use of the enhanced Nielsen model, reported in Chapter 3. As shown in Figure 81, for the mixture with 35%RAP, the predicted data show worse agreement with the measured ones for the complex modulus, with an error of 47%. For the other mixtures (20 and 35%RAP) the errors are in the range of 35-40%.

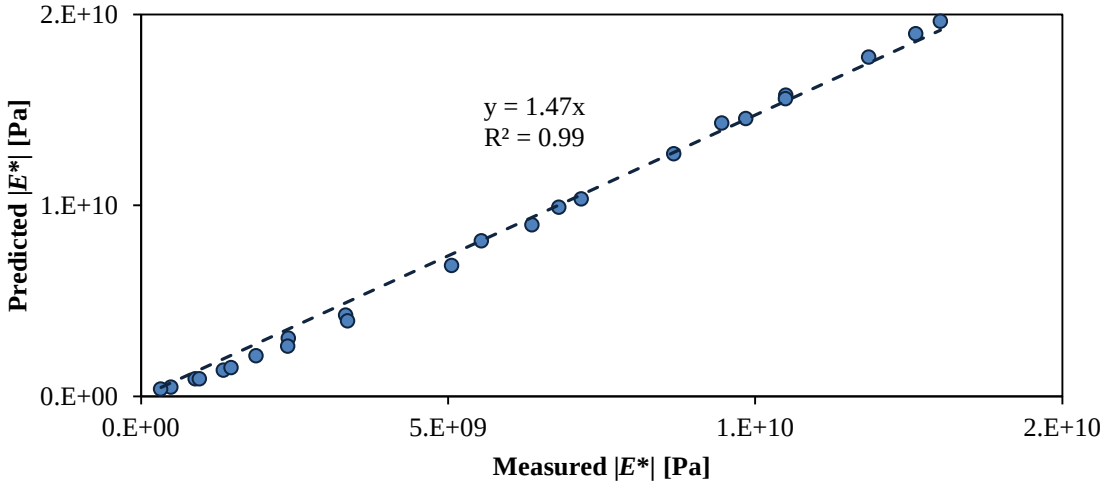

Fig. 81 *Predicted versus measured value of the complex modulus of the mixture with 35%RAP.*

Regarding the phase angles, the prediction shows a smaller error (14%) than the ones obtained with the bituminous blends produced in laboratory (Figure 82).

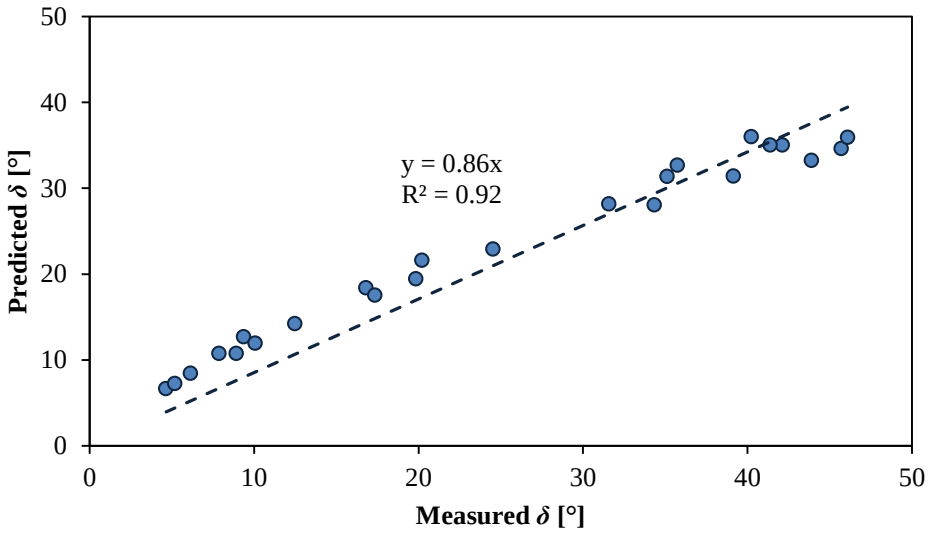

Fig. 82 *Predicted versus measured value of the phase angle of the mixture with 35%RAP.*

As a conclusion it can be postulated, that the Hirsch model cannot predict very well the measured data in both cases. In fact, the current available formulation of the Hirsch model, and the specific form proposed by Christensen et al. (2003), provides only a very simple assembly of the materials phases, which cannot capture the number of interactions occurring in a complex mixture system. This is exemplified by the contact volume parameter, *Pc*, which empirically combines the contribution of the volumetric properties into a single value, disregarding, for example, shape and distribution of a critical

material phase, such as air voids. This is also confirmed by the attempt of Zofka (2007) to propose an alternative expression of *Pc*, which is, however, tailored to the specific material investigated.

5.2 Witczak model

Using the Witczak model, described in Chapter 2 and reported in Equation 10, the complex modulus of the mixture can be calculated from the complex modulus and the phase angle of the bituminous blends produced in laboratory and from the data back-calculated with the Nielsen model. In order to fit the Witczak model, the following volumetric properties need to be known: ρ_{200}, that is the percentage passing #200 sieve, ρ_4 that is the cumulative percentage retained on #4 sieve, ρ_{38} that is the cumulative percentage retained on 3/8 in sieve, ρ_{34} that is the cumulative percentage retained on 3/4 in sieve, V_a that are the air voids (% by volume), and V_{beff} that is the effective binder content. All these information are summarized in Table 46.

Table 46. *Volumetric properties of the mixtures as input for Witczak model.*

Mixture	ρ_{200}	ρ_4	ρ_{38}	ρ_{34}	V_a	V_{beff}
0% RAP	6.2	48	11.9	0	16.46	56.98
20% RAP	5.6	45	15.34	1.82	13.38	56.03
35% RAP	8.5	48	11.20	3.09	12.40	54.89
50% RAP	8.5	48	11.01	2.18	15.25	53.45

Figure 83 reports the predicted values of the mixture's complex modulus determined with the Witczak model, using the rheological properties measured on bituminous blends produced in laboratory and RTFO aged, versus the measured ones for the mixture with 50%RAP. As shown, the error is only 7 %. Similar results were obtained for the other mixtures for which the errors are in the range of 7-9%. Therefore, the Witczak model predicts the measured values better than the Hirsch model for the studied mixtures.

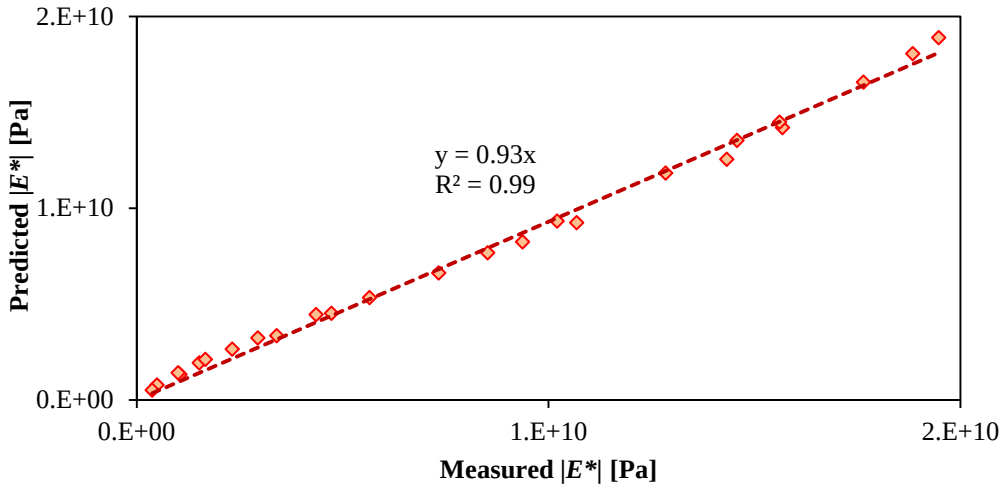

Fig. 83 *Predicted versus measured value of the complex modulus of the mixture with 50%RAP.*

In Figure 84, the predicted values, starting from the rheological properties of the bituminous blends back-calculated with the enhanced Nielsen model, versus the measured values are reported. As shown, the error is approximately the same (7%), but in this case, the predicted values overestimate the complex modulus at higher temperature.

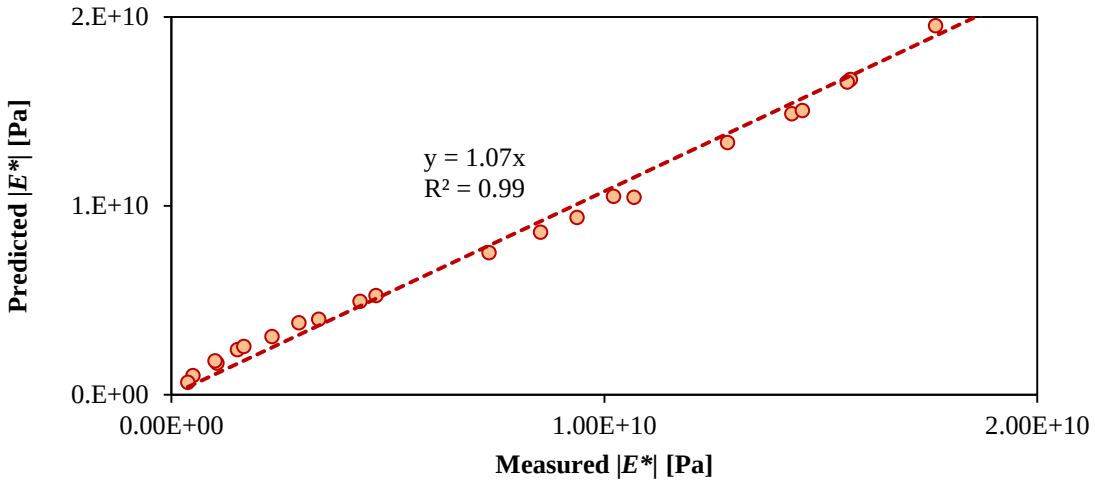

Fig. 84 *Predicted versus measured value of the complex modulus of the mixture with 50%RAP.*

Therefore, from tests on asphalt mortars, the complex modulus of the bituminous blends can be back-calculated using the Enhanced Nielsen model and then, using the Witczak model, the complex modulus of the corresponding mixture can be calculated knowing the volumetric properties of the mixture (Figure 85).

In the present work, the parameters of the Witczak model are fitted in order to connect directly the mortar and mixture phases (Figure 84).

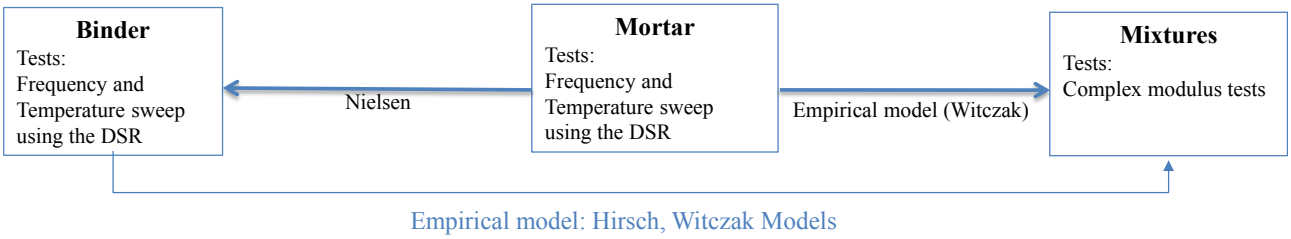

Fig. 85 *Prediction of the complex modulus of the mixture from tests on asphalt mortar using empirical models.*

Through non linear optimization, the initial parameters of the Witczak model, referred to the complex modulus and phase angle of the mortar (*a*, *b*, *c*, *d*, *e*) were optimized, until the minimum sum square error was reached. The model is given by Equation 48:

$$\log E^* = -a + b\,|G^*_{mortar}|(6.65 - 0.032\rho_{200} + 0.0027\,(\rho_{200})^2 + 0.011\rho_4 - 0.0001(\rho_4)^2 + 0.006\,\rho_{38} - 0.00014(\rho_{38})^2 - 0.08V_a - 1.06\left(\frac{V_{beff}}{V_{beff}+V_a}\right) + \frac{2.56+0.03\,V_a+0.71\left(\frac{V_{beff}}{V_{beff}+V_a}\right)+0.012\rho_{38}-0.0001(\rho_{38})^2-0.01\rho_{34}}{1+e^{(-c-d\,\log(|G_{bmortar}{}^*|)+e\,\log(\delta_{mortar}))}} \quad [48]$$

In order to find the parameters *a*, *b*, *c*, *d*, *e* all the mixtures composed with different percentages of RAP (0, 20, 35, 50%RAP) were analyzed. The found parameters are summarized in Table 47.

Table 47. *Calibrated parameters of the Witczak model.*

Parameter	Value
a	4.215
b	1.493
c	10.111
d	0.327
e	5.876

Plotting the predicted value of the complex modulus of the mixture, starting from the rheological data of the mortar, versus the measured one, the graph reported in Figure 86 is obtained. As shown, the regression coefficient R^2 is very high (0.95) and the slope is 0.98, therefore the model generally under-estimates the measured values by approximately 2% only.

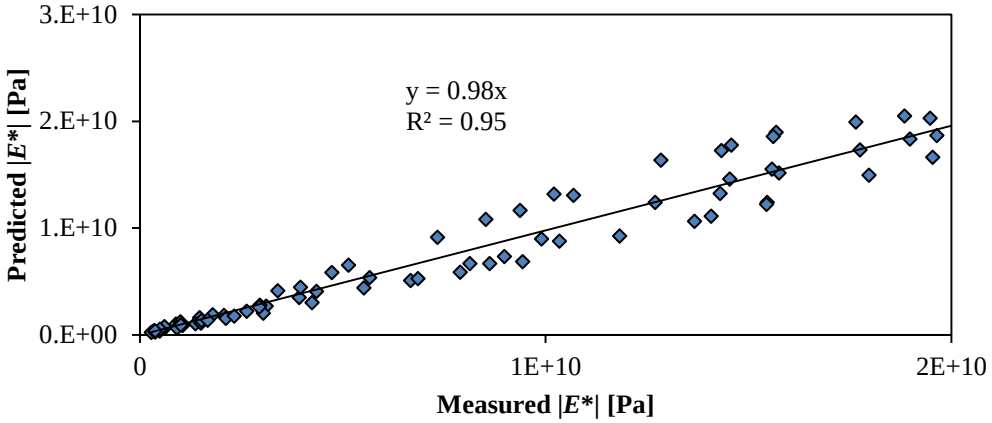

Fig. 86 *Predicted versus measured complex modulus of the mixture from rheological properties of mortars.*

In Figure 87, the residual plot (residuals versus the predicted values) is reported. Residuals are considered to have a horizontal band pattern.

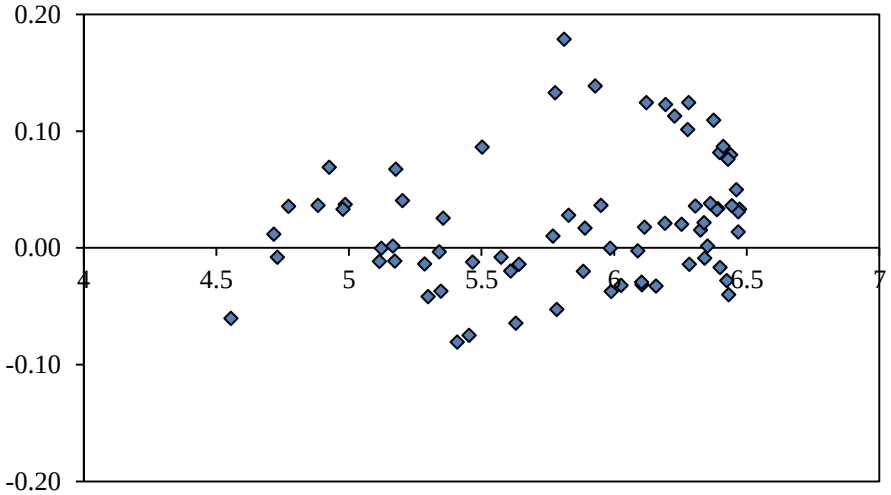

Fig. 87 *Residual plots of calibrated model.*

Therefore, the calibrated model seems to sufficiently predict the |*E**| of the investigated asphalt mixture, starting from tests on asphalt mortars.

5.3 Summary

In this chapter, the empirical Hirsch and Witczak models were investigated. Both models were fitted using the rheological properties of the bituminous blends produced in laboratory and subjected to RTFO aging, using the data of the bituminous blends extracted and recovered from the mixture and using the rheological properties of the blends back-calculated with the Enhanced Nielsen model. In Figure 88 the predicted versus measured values with the Hirsch and Witczak models are reported for all the mixtures. The predicted values, reported in Figure 88, were calculated using the results on

blends produced in laboratory. As shown, the Hirsch model under-estimates the measured values by 26%, while the Witczak overestimates the measured values of 2%. Therefore, the Witczak model is able to better predict the measured value for the examined mixtures. It is important to note, that these empirical models were determined on a database of mixtures, therefore, their performance varies with the type of mixtures and other volumetric properties.

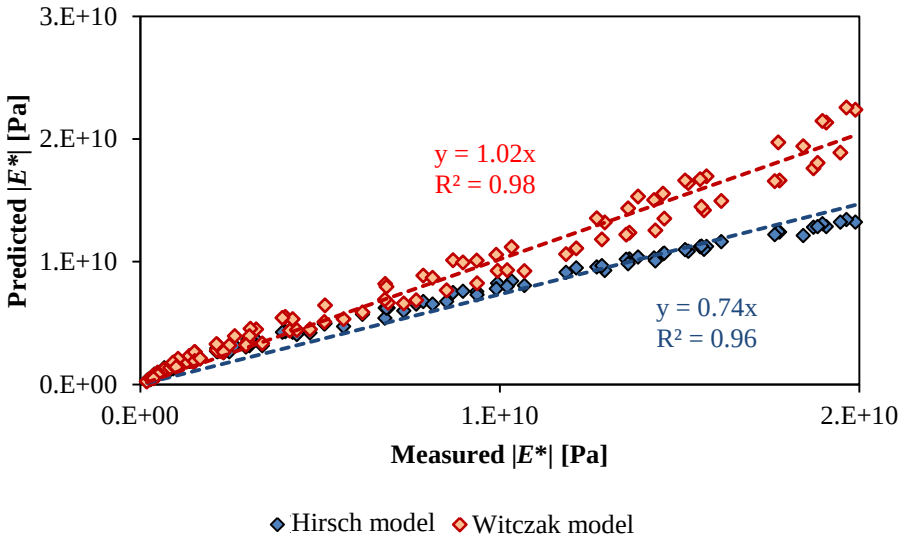

Fig. 88 *Predicted versus measured values with the Hirsch and Witczak models from the rheological properties of blends produced in laboratory.*

In Figure 89, the predicted versus the measured values with the Hirsch and Witczak models using the data of the binders extracted and recovered from the mixtures are reported. As shown, the Hirsch model underestimates the measured values by 23%, while the Witczak overestimates the measured values by 4%. Therefore, the errors are a slightly higher with respect to the previous case.

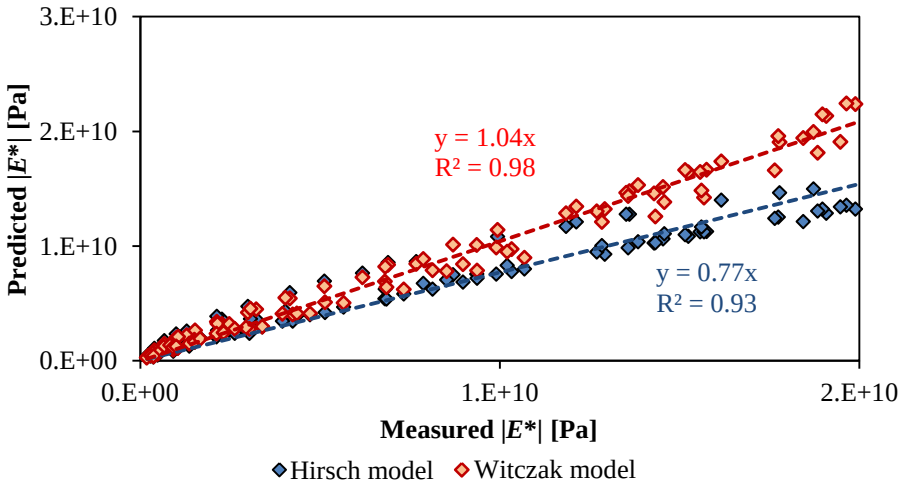

Fig. 89 *Predicted versus measured values with the Hirsch and Witczak models from the rheological properties of blends extracted and recovered.*

In Figure 90, the predicted versus measured values from the rheological properties of the bituminous blends back-calculated using the enhanced Nielsen model, are reported. As shown, the Witczak model over-estimates the measured values by 15%, while the Hirsch model underestimates the measured values by 28%. Therefore, the errors are slightly higher if compared to the previous predictions. However, the Witczak model can predict satisfactorily the measured values also considering the rheological properties of the blends determined with the enhanced Nielsen model.

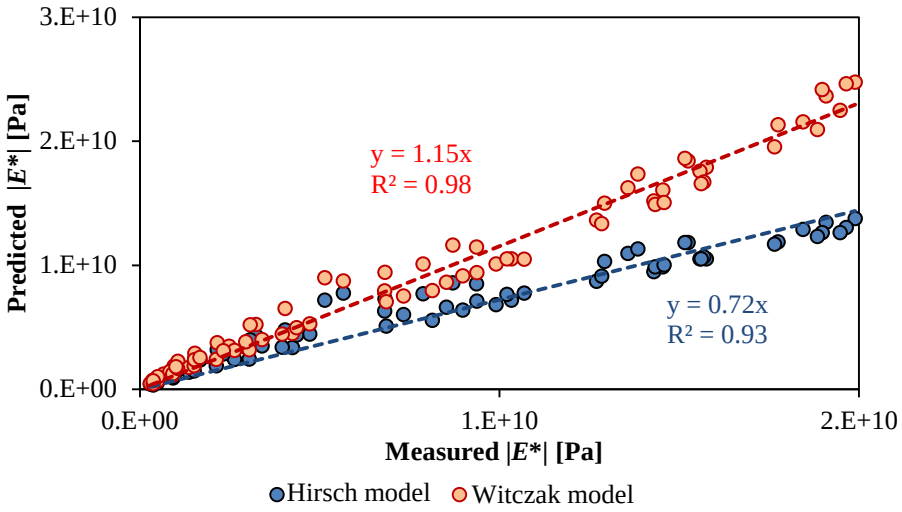

Fig. 90 *Predicted versus measured values with the Hirsch and Witczak models from the rheological properties of blends back-calculated by the enhanced Nielsen model.*

In addition, some parameters of the Witczak model were calibrated in order to use the rheological properties of the mortar instead of the binder. This allows to test directly the SRAP mortars and therefore the RAP binder as it is, avoiding the extraction and recovery method and avoiding the back-calculation with the enhanced Nielsen model. Using this method, an error of approximately 2% is observed.

Chapter 6

6. Conclusion

The present study focuses on an analytical forward and inverse formulation with the aim of predicting RAP-modified asphalt materials performance properties across the different material phases. This goal is achieved through the possibility of experimentally measuring the properties of binders, mortars and mixtures, while avoiding extraction and recovery of the RAP binder, and by rheological modeling the interrelation between the different material phases.

The following conclusions can be drawn:

1. A new procedure is proposed to back-calculate the rheological properties of the bituminous blends composed with RAP binder and of the RAP binder itself, based on the Nielsen model, specifically adapted, and on the Voigt and Arrhenius models. Validation is provided using different type of materials. The new procedure allows to avoid the extraction and recovery of the RAP binder that may alter the rheological properties of the aged binder producing binder hardening;
2. A procedure to calculate the Performance Grade (PG) of the bituminous blends and of the RAP binder from the Master curves, back-calculated with the Nielsen and Voigt model, is presented;
3. New procedure to determine the maximum amount of RAP that can be added to a mixture without compromising its fatigue performance were established;
4. The 2S2P1D model was implemented for multiscale modelling in order to link the different material's phases (binder, mortar, mixture). In particular, a relationship between the characteristic time of binder and that of asphalt mortar was found. It follows a linear trend in the log-log scale. The intercept, which corresponds to the SHStS transformation parameter, depends on the filler content according to a power function with two constants. It is hypothesized that these two constants are associated to the spatial distribution of the filler aggregates, as demonstrated in a different study on asphalt mixture. The SHStS transformation together with the simple power expression of the transformation parameter provide reasonably good predictions of the asphalt mortar complex modulus based on the experimentally measured binder data.
5. A relationship between the characteristic time of the mixtures and the one of the corresponding mortars was found. This allows to calculate the characteristic time of the

mixture knowing the characteristic time of the mortar, and to determine the moduli (storage and viscous moduli) of the mixture using the 2S2P1D model.

6. The transformation parameter, α, of the SHStS transformation between binder and mixture was found to depend on the binder content and on the fractal dimensions of the mixture.
7. The empirical Hirsch and Witczak models were used to determine the complex modulus of the mixture, starting from the rheological properties of the corresponding bituminous blends produced in laboratory and subjected to RTFO aging, of the extracted and recovered blends from the mixture and of the one back-calculated using the Enhanced Nielsen model. The Hirsch model was found to under-estimate the measured values, while the Witczak model slightly over-estimates the complex modulus. In addition, it was found that the Witczak model predicts better the experimental values (the errors are smaller and the regression coefficients are higher).
8. Some parameters of the Witczak model were calibrated in order to determine the complex modulus of the mixture, knowing the rheological properties of the corresponding mortar and the volumetric properties of the mixture.

Therefore, starting from mortar tests, in order to avoid the extraction and recovery of the RAP binder, different methods to back-calculate the complex modulus of the mixture can be used:

- passing directly from mortar to mixture using the Witczak model or the 2S2P1D model;
- passing from the back-calculated blends, with the Enhanced Nielsen model, to the mixture using the 2S2P1D model.

All these relationships will allow to reduce the amount of time consuming and costly tests of asphalt mixtures and will allow to test the RAP binder as it is after the milling process avoiding any further treatments.

In future works, new testing methods, new parameters and new limits directly on the mortars phase will be established. In addition, the effective blending between the fresh and RAP binder, that occurs during the mixing process and the diffusion mechanism of the fresh binder into the aged one, need to be further investigated and take into account. In order to achieve this aim, mortars composed at different temperatures and different time of mixing will be produced in order to verify the capability of the Nielsen model to back-calculate the effective rheological properties of the blends, capturing the effective blending that occurs in the mixture.

References

AASHTO MEPDG-1, "Mechanistic-Empirical Pavement Design Guide: A Manual of Practice." *American Association of State Highway and Transportation Officials*, 2008.

AASHTO M320-10UL, "Standard Method of Test for Performance Graded Asphalt Binder," *American Association of State Highway and Transportation Officials*, 2010.

AASHTO PP6 "Standard Practice for Grading or Verifying the Performance Grade of an Asphalt Binder" *American Association of State Highway and Transportation Officials*, 1994.

AASHTO TP101-12UL. Standard Method of Test for Estimating Fatigue Resistance of Asphalt Binders Using the Linear Amplitude Sweep. *American Association of State Highway and Transportation Officials*, 2010.

AASHTO T315-12-UL, "Standard Method of Test for Determining the Rheological Properties of Asphalt Binder Using a Dynamic Shear Rheometer (DSR)," *American Association of State Highway and Transportation Officials*, 2012.

AASHTO T164-14-UL, "Standard Test Method for Quantitative Extraction of Asphalt Binder from Hot Mix Asphalt (HMA)," *American Association of State Highway and Transportation Officials*, 2014.

Anderson, D., A., Tarris, J., P., Brock, J., D.," Dust Collector Fines and their Influence on Mixture Design*" Journal of the Association of Asphalt Paving Technologists*, Vol. 80, 1982, 363-397

Anderson, D.A., Christensen, D.W., Bahia, H.U., Dongre, R., Sharma, M.G., Antle, C.E., & Button, J. (1994). *Binder Characterization and Evaluation. Volume 3: Physical Characterization. Report SHRP A-369*, Strategic Highway Research Program, Washington, D.C.

Asphalt Institute. (1997). *Mix Design Methods for Asphalt*, 6th ed., MS-02. Asphalt Institute. Lexington, KY.

Arshadi, A., Tabatabee, H., A., Sefidmazgi, N., R., Bahia, H. U. (2014). Enhanced Finite Element Multi scaling Approach for prediction of Mechanical Response of Asphalt Mixture. 92th Transport Research Board Annual Meeting, Washington DC.

Bari &Witczak. Development of a new revised version of the Witczak Predictive Model for hot mix asphalt mixtures. *Journal of the Association of Asphalt Paving Technologist, Vol. 75, 2006,* 381-423.

Berryman, J. G. (1985). Measurement of spatial correlation functions using image processing techniques. *Journal of Applied Physics, 57(7), 2374–2384*. doi: 10.1063/1.334346

Burr, B., Davison, R., Jemison, H., Glover, C. and Bullin, J., "Asphalt Hardening in Extraction Solvents". *Transportation Research Record*, Vol. 1323, 1991, pp. 70-76.

Cannone Falchetto, A., Montepara, A., Tebaldi, G. and Marasteanu, M., "Microstructural and Rheological Investigation of Asphalt Mixtures Containing Recycled Asphalt Materials," *Construction and Building Materials*, Vol. 35, 2012, pp. 321-329.

Cannone Falchetto, A., Montepara, A., Tebaldi, G., & Marasteanu, M. (2013). Microstructural characterization of asphalt mixtures containing recycled asphalt materials. *Journal of Materials in Civil Engineering*, 25(1), 45-53. doi:10.1061/(ASCE)MT.1943-5533.0000544

Cannone Falchetto, A. and Moon, K. H., "Micromechanical–Analogical Modeling of Asphalt Binder and Asphalt Mixture Creep Stiffness Properties at Low Temperature," Road Materials and Pavement Design, Vol. 16(1), 2015, 111-137.

Christensen, R. M. "*Theory of Viscoelasticity- an Introduction"*, Academic Press, 1982, New York.

Christensen, R. M. "Viscoelastic Properties of Heterogeneous Media," *Journal of the Mechanics and Physics of Solids*, Vol. 17, 1969, pp.23-41.

Christensen, D., Pellinen, T. and Bonaquist, R. F., "Hirsch Model for Estimating the Modulus of Asphalt Concrete," *Journal of the Association of Asphalt Paving Technologists*, Vol. 72, 2003, pp. 97-121.

Davison, R. "Desing and use of Superior Aspahlt binders", *Research Report 1249-1F, The Texas A&M Univeristy*, 1994.

Delaporte, B., Di Benedetto, H., Chaverot, P. and Gauthier, G., "Linear Viscoelastic Properties of Bituminous Materials Including New Products Made with Ultrafine Particles," *Road Materials and Pavement Design*, 10(1), 2009, 7–38.

Di Benedetto, H., Sauzeat, C., Bilodeau, K., Buannic, M., Mangiafico, S., Nguyen, Q., T., Pouget, S., Tapsoba, N., Van Rompu, J., "General overview of the time-temperature superposition principle validity for materials containing bituminous binder", International Journal of Roads and airport, ISSN 2036-2595, 2010.

Di Benedetto, H., Olard, F., Sauzéat, C. and Delaporte, B., "Linear Viscoelastic Behavior of Bituminous Materials: from Binders to Mixes," *Road Materials and Pavement Design*, Vol. 5, 2004, pp. 163-202.

Dukatz and Anderson, 1980; "The Effect Of Various Fillers On The Mechanical Behavior Of Asphalt And Asphalt Concrete," *Journal of the Association of Asphalt Paving Technologists*, Vol.49, 1980, pp. 530-549.

Einstein, A., "Eine Neuebestimmung der molekuldimensionen," *Annalen der Physik*, Vol. 19, 1906, 289-306.

EN 1097-4, "Tests for Mechanical And Physical Properties Of Aggregates - Part 4: Determination Of The Voids Of Dry Compacted Filler," *European Committee for Standardization*, 2008.

EN 1097-7, "Tests for Mechanical And Physical Properties Of Aggregates - Part 7: Determination Of The Particle Density Of Filler," *European Committee for Standardization*, 2008.

EN 1426 "Bitumen and bituminous binders. Determination of needle penetration." *European Committee for Standardization*, 2007

EN 1427 "Bitumen and bituminous binders. Determination of the softening point. Ring and Ball method." *European Committee for Standardization*, 2007

EN 12607-1, "Bitumen and bituminous binders. Determination of the resistance to hardening under influence of heat and air. RTFOT method." *European Committee for Standardization*, 2007.

EN 12694-4 "Bituminous mixtures. Test methods for hot mix asphalt. Bitumen recovery: Fractionating column" *European Committee for Standardization*, 2005.

EN 12697-2 "Bituminous mixtures. Test methods for hot mix asphalt. Determination of particle size distribution" *European Committee for Standardization*, 2015.

EN 12697-3 "Bituminous mixtures. Test methods for hot mix asphalt. Bitumen recovery: Rotary evaporator" *European Committee for Standardization*, 2013.

EN 12697-5 "Bituminous mixtures. Test methods for hot mix asphalt. Determination of the maximum density." *European Committee for Standardization*, 2009.

EN 12697-6 "Bituminous mixtures. Test methods for hot mix asphalt. Determination of bulk density of bituminous specimens." *European Committee for Standardization*, 2012.

EN 12697-26 "Bituminous mixtures. Test methods for hot mix asphalt. Stiffness." *European Committee for Standardization*, 2012.

EN 13108-8 "Bituminous mixtures. Material specifications. Reclaimed asphalt. *European Committee for Standardization*, 2016.

EN 14769,"Bitumen and bituminous binders. Accelerated long-term ageing conditioning by a Pressure Ageing Vessel (PAV) ." *European Committee for Standardization*, 2012.

Farrar, M., Sui, C., Salmans, S., Qin, Q. "Determining the Low. Temperature Rheological Properties of Asphalt Binder using a Dynamic Shear Rheometer (DSR)." *Technical paper prepared for Federal Highway Administration*, 2015

Hansen, K. R. and Copeland, A., "Annual Asphalt Pavement Industry Survey on Recycled Materials and Warm-Mix Asphalt Usage: 2009–2013," *4th Annual Asphalt Pavement Industry Survey*, 2014, National Asphalt Pavement Association (NAPA).

Hashin, Z., "The Elastic Moduli of Heterogeneous Materials," *Journal of Applied Mechanics*, Vol. 29(1), 1962, pp. 143-150.

Hashin, Z., "Complex moduli of viscoelastic composites. General theory and application to particulate composites," *International Journal of Solids and Structure*, Vol. 6, 1970, pp. 539-552.

Hintz C., Velasquez R., Johnson C., Bahia H., U. Modification and Validation of the Linear Amplitude Sweep Test for Binder Fatigue Specification. *Transport Research Record*. Washington, DC. Vol. 2207. pp. 99-106. 2011.

Holtz,K, Eighmy,T.T,"Scanning European Advances in the Use of Recycled Materials in Highway Construction" Public Roads, Vol. 64, No.1, July/August 2000.

Johnson C. M. Estimating Asphalt Binder Fatigue Resistance using an Accelerated Test Method. PhD Thesis. University of Wisconsin-Madison, Madison, 2010.

Kennedy, T. W., Tam, W. O. and Solaimanian, M., "Optimizing Use of Reclaimed Asphalt Pavement with the Superpave System," *Journal of the Association of Asphalt Paving Technologists*, Vol. 67, 1998, pp. 311-325.

Kondrath, E. (2009).Reclaimed Asphalt Pavement in Hot Mix Asphalt. New Jersey *Department of Transportation.*

Lakes, R., "Viscoelastic materials," Cambridge University Press, 2009, New York.

Landel, R. and Nielsen, L., "Mechanical Properties of Polymers and Composites," *CRC Press, Boca Raton*, 1993.

Leandri P, Riccardi C, Losa M (2015) A new approach to estimating rheological properties of the rap binder at intermediate temperatures. Road Mater Pav Design16(1): 280-299.doi:10.1080/14680629.2015.1029695

Levenberg, K. A method for the solution of certain nonlinear problems in least squares, Quart. Appl. Math. 164168. 1944.

Lewis, T.B., and Nielsen L.E., "Dynamic mechanical properties of particulate-filled composites." *Journal of Applied Polymer Science*, Volume 14, 1970, pp. 1449-1471.

Lewis, T.B., and Nielsen L.E. (1970). Generalized Equation for the Elastic Moduli of Composite Materials. *In Journal of Applied Physics, Volume 41*, pp. 4626-4627.

Liao, M. C., Airey, G., and Chen, J. S., "Mechanical Properties of Filler-Asphalt Mastic," *International Journal of Pavement Research and Technology*.Vol.6(5).576, 2013.

Losa, M., Leandri, P. (2012). A comprehensive model to predict acoustic absorption factor of porous mixes. *Materials and Structures*. Vol. 45, Issue N° 6, June 2012, ISSN 1359-5997, pp. 923-940.

Losa, M., Leandri, P., Licitra, G. (2013). Mixture Design Optimization of Low Noise Pavements. *Transportation Research Record: Journal of the Transportation Research Board*. No. 2372, Washington, D.C., ISSN 0361-1981, DOI 10.3141/2372-04, pp. 25-33.

Ma, T., Mahmoud, E., Bahia, H., U. Estimation of RAP binder Low-Temperature Properties without Extraction. *Transportation Research Record: Journal of the Transportation Research Board*. No.2179, Washington, D.C., 2010, DOI: 10.3141/2179-07

Ma, T., Bahia, H., U., Mahmoud, E., Hajj, E. "Estimating Allowable RAP in Asphalt Mixes to meet Target Low Temperature PG Requirements" *Jounral of the Association of Asphalt Pavement Technologists*. Vol 79, 2010, pp. 473-496.

Ma, T., and Huang, X., "Recycling Law of Aged Asphalt based on Composite Theory of Material," *Journal of Southeast University*, Vol. 38(3), 2008, pp. 520−524.

Ma, T., and Zhang, D. Y., "Research on Influence and Modification of Extraction and Recovery Experiments for SBS Modified Asphalt," *Journal of Southeast University*, Vol. 40(5), 2008, pp. 511−523.

Mangiafico, S., Di Benedetto, H., Sauzéat, C. and Olard, F., "Influence of Reclaimed Asphalt Pavement Content on Complex Modulus of Asphalt Binder Blends and Corresponding Mixes: Experimental Results and Modellin," *Road Materials and Pavement Design*, Vol. 14(1), 2013, pp. 132-148.

Mangiafico, S., Di Benedetto, H., Sauzéat, C. and Olard, F., Pouget, S., & Planque, L. "New method to obtain viscoelastic properties of bitumen blends from pure and reclaimed asphalt pavement binder constituents", *Road Materials and Pavement Design*, 15:2, 312-329, 2014, DOI: 10.1080/14680629.2013.870639

Marquardt, D. W. An algorithm for least squares estimation of nonlinear parameters. *Journal of the Society for Industrial and Applied Mathematics*, 11(2):431-441, 1963.

Martono, W., Bahia, H., U., "Considering Pavement Temperature and Structure in Defining Asphalt Binder Fatigue", Proceedings of ASCE 18th Engineering Mechanics Conference, Virginia, 2007.

McGraw, J., Johnson, E., Johnson, G., Dai, S., Linell, D. and Watson, M., "Incorporation of Recycled Asphalt Shingles in Hot-Mixed Asphalt Pavement Mixtures," *Final Report MN/RC 2010-08*, 2010, Minnesota Department of Transportation.

Milton, G. W., "Bounds on the Electromagnetic, Elastic, and Other Properties of Two-component Composites," Physical Review Letters, Vol. 46(8), 1981, pp. 542-545.

Moon, K. H., Cannone Falchetto, A. & Hu, J. W. (2014). Investigation of Asphalt Binder and Asphalt Mixture Low Temperature Creep Properties Using Semi Mechanical and Analogical Models, *Construction and Building Materials*, 53, 568–583. DOI:10.1016/j.conbuildmat.2013.12.022.

MS-2 Asphalt Mix Design Methods, Asphalt Institute, 2015. ISBN: 9781934154700.

NCHRP 452 (2001). Recommended Use of Reclaimed Asphalt Pavement in the Superpave Mix Design Method: Technician's Manual. *National Academy Press Washington, D.C.*

NCHRP 459 (2001). Characterization of Modified Asphalt Binders in Superpave Mix Design. *National Academy Press Washington, D.C.*

Nielsen L.E., "Generalized Equation for the Elastic Moduli of Composite Materials," *Journal of Applied Physics*, Volume 41, 1970, pp. 4626-4627.

Nielsen, L. E. ;Landel, R.F. (1994). Mechanical properties of Polymers and composites.

Olard, F. (2003). *Comportement thermomécanique des enrobés bitumineux à basses températures. Relations entre les propriétés du liant et de l'enrobé* (PhD Thesis). Université de Lyon, Lyon.

Olard, F., & Di Benedetto, H. (2003). General "2S2P1D" model and relation between the linear viscoelastic behaviour of bituminous binders and mixes. *Road Materials Pavement Design 4(2)*, 185-224. doi:10.1080/14680629.2003.9689946

Pouget, S., Sauzéat, C., Di Benedetto, H., & Olard, F. (2010) From the behavior of constituent materials to the calculation and design of orthotropic bridge structures. *Road Material and Pavement Design, 11, Special Issue EATA 2010*, 111-144. doi:10.1080/14680629.2010.9690329

Peterson, R. Soleymani, H., Anderson, R. and McDaniel, R., "Recovery and Testing of RAP Binders from Recycled Asphalt Pavements," *Journal of the Association ofAsphalt Paving Technologies*, Vol. 69, 2000, pp. 72-91.

Rad, F. Y., Sefidmazgi, N. R. and Bahia, H., "Application of Diffusion Mechanism to Study Degree of Blending Between Fresh and RAP Binder in Dynamic Shear Rheometer," *Transportation Research Record*, Vol.2444, 2014, pp. 71-77.

Radenberg, M.; Wistuba, M.; Hauser, E. Einsatz von Rejuvenatoren bei der Wiederherstellung von Asphalt. Forschungsprojekt (Rejuvenatoren) Nr. FE 07.0250/2011/LRB, ongoing research project,

Federal Ministry for Transport, Building and Urban Development, Ruhr-Universität Bochum (Lehrstuhl für Verkehrswegebau), Technische Universität Braunschweig (Institut für Straßenwesen) and Basalt-Actien-Gesellschaft (BAG), Germany, 2012.

Riccardi C., Cannone Falchetto A., Leandri L., Losa M. and Wistuba M. "A novel back-calculation approach for determining the rheological properties of rap binder", *International Journal of Road Materials and Pavement Design* (in press,2016).

Riccardi C., Cannone Falchetto A., Losa M. and Wistuba M. "Estimation of the High Temperature Properties of Reclaimed Asphalt Pavement Binder without Extraction". *8th International Conference on Maintenance and Rehabilitation of Pavements (MAIREPAV8)*, July 27–29, 2016b, Singapore.

Riccardi C., Cannone Falchetto A., Losa M. and Wistuba M. "Back-calculation method for determining the maximum rap content in stone matrix asphalt mixtures with good fatigue performance based on asphalt mortar tests*", Construction and Building Materials, Elsevier*, 2016c

Riccardi C., Leandri, P., Losa, M. "Determining the allowable content of RAP in HMA with regard to fatigue resistance" *8th RILEM International Conference on Mechanisms of cracking and debonding in Pavements*, June 7-9, 2016d, Nantes, France.

Riccardi C., Cannone Falchetto A., Losa M. and Wistuba M. "Development of simple relationship between asphalt binder and mastic based on rheological tests", *International Journal of Road Materials and Pavement Design*, Taylor & Francis, 2016e, http://dx.doi.org/10.1080/14680629.2016.1230514

Riccardi C., Leandri, P., Losa, M. "Determining the allowable content of RAP in HMA using the blending charts and RAP mortar properties", *6th International Conference Bituminous mixture and pavements*, June 10-12, 2015, Tessaloniki, Greece.

Riccardi C., Cannone Falchetto A., Losa M. and Wistuba M., "Rheological modeling of asphalt binder and asphalt mortar containing recycled asphalt material", *Materials and Structures, Srpinger*. DOI: 10.1617/s11527-015-0779-z, 2015b

Sayegh, G. (1965). Variation des modules de quelques bitumes pur seten robes bitumen eux (Dissertation) Université de Paris [In French].

Shashidar, N. and Romero, P. 1998. Factors affecting the Stiffening Potential of Mineral Fillers. *Transport Research Record*, Vol. 1638, 1998, pp. 94-100.

Shashidar, N., Needham, S., P., Chollar, B., H and Romero, P. 1999. Prediction of the performance of mineral fillers in SMA. *Journal of the Association of Asphalt Paving Technologists*, Vol. 68, 1999, pp. 222-251.

Stroup-Gardiner, M., and Nelson, J., "Use of Normal Propyl Bromide Solvents for Extraction and Recovery of Asphalt Cements."*Report 00-06*, 2014, National Asphalt Pavement Association (NAPA).

Sui,C., Farrar, M. J., Tuminello, W. H. and Turner, T. F., "New Tecnique for measuring Low-Temperature Properties of Asphalt binders with Small amounts of Materials". *Transport Research Record* 2179, 2010, pp. 23-29.

Tiouajni, S., Di Benedetto, H., Sauzéat, C., & Pouget, S. (2011). Approximation of linear viscoelastic model by generalized Kelvin Voigt or generalized Maxwell Models: Application to bituminous materials. *Road Materials and Pavement Design, 12(4), 897-930*. doi:10.1080/14680629.2011.9713899

Torquato, S. (2002). *Random heterogeneous materials*. New York: Springer.

Underwood, B., S., Kim, Y., R. (2013). Microstructural Investigation of Asphalt Concrete for performing multiscale experimental studies. *International Journal of Pavement Engineering*, 2013. Vol. 14 (5) pp. 498-516.

Wistuba, M. The German segmented steel roller compaction method – state-of-the-art report. *International Journal of Pavement Engineering*, 2016. Vol. 17, Issue 1: aspahtl compaction, Taylor and Francis.

Wistuba, M.; Hauser, E.; Walther, A. Untersuchungen an mit Rejuvenatoren modifizierten Asphalten und Ermittlung des Nutzungszeitraumes. F&E-Projekt (MaxRecycling) ongoing research project, Federal State authority of Lower Saxony for Road Building and Transportation, Institut für Straßenwesen - Braunschweig Pavement Engineering Centre, Technische Universität Braunschweig, Germany, 2012.

ANNEX 1

The parameters of the master curves of the different materials, reported in Chapter 3, at a reference temperature of 20°C, are summarized in the following tables.

- **Artificially RAP source:**

  Master curves of the complex modulus of binders

	G^*_e [Pa]	G^*_g [Pa]	f_c [Hz]	m_e [-]	K [-]	R^2 [-]
70/100 fresh binder	0	$5 \cdot 10^8$	35.88	1.05	0.245	1.00
50/70 RTFO+2PAV (artificially aged binder)	0	$1 \cdot 10^9$	0.17	0.93	0.126	1.00
Blend 70/100+22% artificially aged binder	0	$7 \cdot 10^8$	34.63	1.08	0.180	1.00
Blend 70/100+41% artificially aged binder	0	$1 \cdot 10^9$	1.332	1.06	0.156	1.00

Master curves of the phase angle of binders

	δ_m [°]	f_d [Hz]	R_d [-]	m_d [-]	R^2 [-]
70/100 fresh binder	83.86	0.0020	20.95	28.91	0.998
50/70 RTFO+2PAV	57.27	0.000002	8.51	3.34	0.996
Blend 70/100+22% artificially aged binder	77.53	0.00029	10.01	6.07	0.997
Blend 70/100+41% artificially aged binder	71.28	0.00010	10.90	6.02	0.998

Master curves of the complex modulus of mortars

	G^*_e [Pa]	G^*_g [Pa]	f_c [Hz]	m_e [-]	K [-]	R^2 [-]
BSRAP *Vp*20	$5 \cdot 10^4$	$1 \cdot 10^9$	21.04	1.05	0.240	1.00
BSRAP *Vp*35	$1 \cdot 10^5$	$1.3 \cdot 10^9$	21.07	1.02	0.261	1.00
BSRAP *Vp*50	$2 \cdot 10^5$	$2 \cdot 10^9$	25.95	0.93	0.309	1.00
SRAP *Vp*35	$4 \cdot 10^5$	$1.2 \cdot 10^9$	12.01	0.94	0.243	1.00
SRAP *Vp*50	$3 \cdot 10^6$	$3 \cdot 10^9$	0.58	0.97	0.180	1.00

Master curves of the phase angle of mortars

	δ_m [°]	f_d [Hz]	R_d [-]	m_d [-]	R^2 [-]
BSRAP *Vp*20	81.92	0.0020	17.68	22.22	0.999
BSRAP *Vp*35	82.44	0.0020	26.90	53.10	0.999
BSRAP *Vp*50	76.93	0.0097	8.59	8.62	0.999
SRAP *Vp*35	76.42	0.00038	36.41	77.45	0.997
SRAP *Vp*50	67.73	0.000005	20.55	22.10	0.986

- **Italian RAP source:**

Master curves of the complex modulus of binders

	G^*_e [Pa]	G^*_g [Pa]	f_c [Hz]	m_e [-]	K [-]	R^2 [-]
90H+10S	0	$8 \cdot 10^8$	23.69	1.08	0.191	1.00
80H+20S	0	$6 \cdot 10^8$	62.7	1.02	0.204	1.00
70H+30S	0	$6 \cdot 10^8$	109.5	0.99	0.208	1.00

Master curves of the phase angle of binders

	δ_m [°]	f_d [Hz]	R_d [-]	m_d [-]	R^2 [-]
90H+10S	80.62	0.0018	8.76	5.15	0.995
80H+20S	77.55	0.00605	6.62	3.41	0.994
70H+30S	77.53	0.00029	10.01	6.07	0.997

Master curves of the complex modulus of mortars

		G^*_e [Pa]	G^*_g [Pa]	f_c [Hz]	m_e [-]	K [-]	R^2 [-]
90H+10S	**BSRAP *Vp*20**	$3 \cdot 10^3$	$1 \cdot 10^9$	21.34	1.01	0.205	1.00
	BSRAP *Vp*40	$3 \cdot 10^4$	$2 \cdot 10^9$	2.63	1.15	0.170	1.00
	BSRAP *Vp*60	$4 \cdot 10^4$	$2.3 \cdot 10^9$	19.27	0.79	0.243	1.00
	SRAP *Vp*20	$3.5 \cdot 10^3$	$1.7 \cdot 10^9$	15.28	1.12	0.163	1.00
	SRAP *Vp*40	$4 \cdot 10^4$	$2.6 \cdot 10^9$	7.02	1.06	0.169	1.00
	SRAP *Vp*60	$5 \cdot 10^4$	$2.8 \cdot 10^9$	4.06	0.75	0.235	1.00
80H+20S	**BSRAP *Vp*20**	$2 \cdot 10^3$	$1 \cdot 10^9$	7.70	1.08	0.180	1.00
	BSRAP *Vp*40	$1 \cdot 10^4$	$1.8 \cdot 10^9$	18.50	0.99	0.212	1.00
	BSRAP *Vp*60	$2 \cdot 10^4$	$3 \cdot 10^9$	11.16	0.85	0.191	1.00
	SRAP *Vp*20	$3 \cdot 10^3$	$1.5 \cdot 10^9$	1.30	1.15	0.162	1.00
	SRAP *Vp*40	$2.5 \cdot 10^4$	$2.5 \cdot 10^9$	1.41	1.05	0.173	1.00
	SRAP *Vp*60	$3 \cdot 10^4$	$2.8 \cdot 10^9$	1.89	0.78	0.232	1.00
70H+30S	**BSRAP *Vp*20**	$1.2 \cdot 10^3$	$1.4 \cdot 10^9$	24.74	1.03	0.187	1.00
	BSRAP *Vp*40	$1.6 \cdot 10^3$	$1.8 \cdot 10^9$	62.23	0.94	0.233	1.00
	BSRAP *Vp*60	$1.8 \cdot 10^3$	$1.7 \cdot 10^9$	52.60	0.75	0.240	1.00
	SRAP *Vp*20	$5.54 \cdot 10^3$	$1.7 \cdot 10^9$	0.73	1.24	0.15	1.00
	SRAP *Vp*40	$2 \cdot 10^4$	$2.1 \cdot 10^9$	3.62	0.98	0.19	1.00
	SRAP *Vp*60	$3 \cdot 10^4$	$2.2 \cdot 10^9$	3.82	0.73	0.23	1.00

Master curves of the phase angle of mortars

		δ_m [°]	f_d [Hz]	R_d [-]	m_d [-]	R^2 [-]
90H+10S	**BSRAP *Vp*20**	78.63	0.00066	11.60	7.82	0.996
	BSRAP *Vp*40	76.62	0.00085	15.28	14.34	0.997
	BSRAP *Vp*60	63.44	0.00323	9.18	7.38	0.990
	SRAP *Vp*20	73.04	0.00026	8.89	4.94	0.997
	SRAP *Vp*40	69.83	0.00010	13.89	10.38	0.998
	SRAP *Vp*60	54.22	0.00109	4.95	3.14	0.995
80H+20S	**BSRAP *Vp*20**	78.83	0.00037	11.22	6.98	0.997
	BSRAP *Vp*40	75.89	0.00136	12.97	10.89	0.997
	BSRAP *Vp*60	59.60	0.01102	5.27	3.09	0.994
	SRAP *Vp*20	76.33	0.00018	10.69	6.25	0.997
	SRAP *Vp*40	71.02	0.00016	14.80	11.36	0.998
	SRAP *Vp*60	55.70	0.00121	5.60	3.55	0.996
70H+30S	**BSRAP *Vp*20**	77.88	0.00059	21.85	24.22	0.995
	BSRAP *Vp*40	74.18	0.00472	12.25	10.49	0.997
	BSRAP *Vp*60	58.48	0.02465	4.84	2.82	0.987
	SRAP *Vp*20	76.24	0.00015	11.96	6.89	0.997
	SRAP *Vp*40	70.86	0.00021	14.69	11.65	0.998
	SRAP *Vp*60	53.61	0.00485	3.63	1.95	0.980

- **English RAP source:**

Master curves of the complex modulus of binders

	G^*_e [Pa]	G^*_g [Pa]	f_c [Hz]	m_e [-]	K [-]	R^2 [-]
50/70 fresh binder	0	$4 \cdot 10^8$	61.75	1.00	0.263	1.00
Blend 50/70+30%RAP	0	$1.6 \cdot 10^9$	0.15	1.64	0.147	1.00
Blend 50/70+60%RAP	0	$1.8 \cdot 10^9$	0.053	2.69	0.114	1.00
Extracted RAP binder	0	$8 \cdot 10^8$	0.25	1.28	0.160	1.00

Master curves of the phase angle of binders

	δ_m [°]	f_d [Hz]	R_d [-]	m_d [-]	R^2 [-]
50/70 fresh binder	87.23	0.0022	3.74	2.45	0.994
Blend 50/70+30%RAP	75.45	0.0011	6.82	4.54	0.998
Blend 50/70+60%RAP	40.25	3.0130	3.52	3.14	0.987
Extracted RAP binder	40.4	0.2951	1.04	0.70	0.989

Master curves of the complex modulus of mortars

	G^*_e [Pa]	G^*_g [Pa]	f_c [Hz]	m_e [-]	K [-]	R^2 [-]
BSRAP *Vp*20	$4 \cdot 10^3$	$1.8 \cdot 10^9$	1.22	1.08	0.18	1.00
BSRAP *Vp*35	$5 \cdot 10^3$	$2 \cdot 10^9$	0.58	1.02	0.202	1.00
BSRAP *Vp*50	$8 \cdot 10^3$	$2 \cdot 10^9$	2.25	1.03	0.249	1.00
SRAP *Vp*35	$4 \cdot 10^4$	$2 \cdot 10^9$	0.57	1.02	0.201	1.00
SRAP *Vp*50	$5 \cdot 10^4$	$2.2 \cdot 10^9$	0.70	0.82	0.249	1.00

Master curves of the phase angle of mortars

	δ_m [°]	f_d [Hz]	R_d [-]	m_d [-]	R^2 [-]
BSRAP *Vp*20	74.66	0.00019	11.22	7.83	0.999
BSRAP *Vp*35	70.41	0.00036	7.09	4.41	0.998
BSRAP *Vp*50	72.93	0.0047	5.57	4.36	0.993
SRAP *Vp*35	70.42	0.00036	7.09	4.41	0.998
SRAP *Vp*50	62.97	0.00022	6.62	4.44	0.997

- **German RAP source:**

Master curves of the complex modulus of binders

	G^*_e [Pa]	G^*_g [Pa]	f_c [Hz]	m_e [-]	K [-]	R^2 [-]
50/70 fresh binder	0	$1 \cdot 10^9$	7.18	1.10	0.167	1.00
Blend 50/70+20%RAP	0	$1 \cdot 10^9$	4.28	1.08	0.168	1.00
Blend 50/70+35%RAP	0	$1 \cdot 10^9$	3.53	1.07	0.166	1.00
Blend 50/70+50%RAP	0	$1 \cdot 10^9$	1.05	1.09	0.157	1.00
Extracted RAP binder	0	$1 \cdot 10^9$	0.19	1.12	0.195	1.00

Master curves of the phase angle of binders

	δ_m [°]	f_d [Hz]	R_d [-]	m_d [-]	R^2 [-]
50/70 fresh binder	88.95	0.0000035	376.85	4177.81	1.00
Blend 50/70+20%RAP	87.60	0.0000034	375.11	4493.77	0.998
Blend 50/70+35%RAP	89.95	0.0000008	376.85	4170.82	0.998
Blend 50/70+50%RAP	88.95	0.0000005	376.85	4170.81	0.997
Extracted RAP binder	86.60	0.0000003	14.27	7.41	0.994

Master curves of the complex modulus of mortars

	G^*_e [Pa]	G^*_g [Pa]	f_c [Hz]	m_e [-]	K [-]	R^2 [-]
BSRAP 20%RAP	$4 \cdot 10^3$	$2 \cdot 10^9$	26.84	0.95	0.19	1.00
BSRAP 35%RAP	$5 \cdot 10^3$	$3.7 \cdot 10^9$	11.67	0.99	0.18	1.00
BSRAP 50%RAP	$8 \cdot 10^3$	$4.8 \cdot 10^9$	1.939	1.03	0.17	1.00
SRAP 20%RAP	$4.5 \cdot 10^3$	$2 \cdot 10^9$	4.196	1.03	0.19	1.00
SRAP 35%RAP	$4 \cdot 10^4$	$2.5 \cdot 10^9$	2.35	0.95	0.208	1.00
SRAP 50%RAP	$5 \cdot 10^4$	$2.7 \cdot 10^9$	1.80	0.81	0.236	1.00

Master curves of the phase angle of mortars

	δ_m [°]	f_d [Hz]	R_d [-]	m_d [-]	R^2 [-]
BSRAP 20%RAP	65.28	0.0159	10.27	8.40	0.997
BSRAP 35%RAP	57.38	0.7799	3.01	2.38	0.995
BSRAP 50%RAP	67.37	0.00074	333.97	6314.23	0.998
SRAP 20%RAP	87.39	0.000002	338.17	5215.73	0.998
SRAP 35%RAP	72.71	0.000059	319.16	5089.11	0.994
SRAP 50%RAP	61.91	0.00037	8.10	5.88	0.993